Asymptotic Analysis of Interference in Cognitive Radio Networks

by

Yaobin Wen

Thesis submitted to the
Faculty of Graduate and Postdoctoral Studies
In partial fulfillment of the requirements
For a doctoral degree in
Electrical and Computer Engineering

School of Electrical Engineering and Computer Science

Faculty of Engineering

University of Ottawa

Abstract

The aggregate interference distribution in cognitive radio networks is studied in a rigorous and analytical way using the popular Poisson point process model. While a number of results are available for this model for non-cognitive radio networks, cognitive radio networks present extra levels of difficulties for the analysis, mainly due to the exclusion region around the primary receiver, which are typically addressed via various ad-hoc approximations (e.g., based on the interference cumulants) or via the large-deviation analysis. Unlike the previous studies, we do not use here ad-hoc approximations but rather obtain the asymptotic interference distribution in a systematic and rigorous way, which also has a guaranteed level of accuracy at the distribution tail. This is in contrast to the large deviation analysis, which provides only the (exponential) order of scaling but not the outage probability itself. Unlike the cumulant-based analysis, our approach provides a guaranteed level of accuracy at the distribution tail. Additionally, our analysis provides a number of novel insights. In particular, we demonstrate that there is a critical transition point below which the outage probability decays only polynomially but above which it decays super-exponentially. This provides a solid analytical foundation to the earlier empirical observations in the literature and also reveals what are the typical ways outage events occur in different regimes. The analysis is further extended to include interference cancelation and fading (from a broad class of distributions). The outage probability is shown to scale down exponentially in the number of canceled nearest interferers in the below-critical region and does not change significantly in the above-critical one. The proposed asymptotic expressions are shown to be accurate in the non-asymptotic regimes as well.

Acknowledgments

I would like to express my deep gratitude to my thesis supervisors, Prof. Sergey Loyka and Prof. Abbas Yongacoglu, for their great help, support, understanding and supervising this research work. Their patience and extensive guidance helped me fulfill this thesis proposal smoothly.

Thanks to Prof. Halim Yanikomeroglu, Prof. Yongyi Mao, Prof. Florence Danilo-Lemoine, Prof. Peter Galko and Prof. Claude D'Amours who provided the fundamental knowledge for my research.

Thanks to my colleagues in wireless communication lab, Georgy Levin and Wei Yu, who provided help during my studies.

Finally, I acknowledge the constant support and encouragement from my family and friends throughout my study.

Contents

List of Abbreviations

4G	fourth generation
CCDF	complementary cumulative distribution function
CDF	cumulative distribution function
CDMA	Code Division Multiple Access
CF	characteristic function
CGF	cumulant generating function
CLT	central limit theorem
CR	cognitive radio
DSA	dynamic spectrum access
FCC	Federal Communication Commission
FR	forbidden (exclusion) region
INR	interference-to-noise ratio
IP	internet protocol
LDP	large deviations principle
MAC	media access control
MGF	moment generating function
OFDM	Orthogonal Frequency Division Multiplexing
PAPR	peak to average power ratio
pdf	probability density function
PU	primary user

QoS	quality-of-service
SDR	software defined radio
SINR	signal to interference plus noise ratio
SIR	signal-to-interference ratio
SS	spread-spectrum
SU	secondary user
TDCS	transform domain communication system
UHF	ultra high frequency
VHF	very high frequency
WDCS	wavelet domain communication system

List of Symbols

Symbol	Explanation	page where the symbol is defined
D	$= I_{th}/P_0$, an interference-to-noise (INR) threshold value.	25
d	$= D/D_{\max}$	26
D_1	The INR from the boundary of the disk with radius R_1.	33
d_1	$= D/D_1$	33
$D_{\max}$	$= I_{\max}/P_0$, the maximum INR caused by a single node.	26
g	The propagation path gain.	24
g_a	The average propagation path gain.	24
g_l	The large scale (shadowing) fading gain.	24
g_s	The small scale (multipath) fading gain.	24
$\hat{\theta}$	A solution of the saddle-point equation.	32
$H_r(x)$	Hermite polynomial of degree r.	46
I_{ag}	The aggregate interference power.	25
I_{ai}	The interference power from i-th SU in non-fading channels.	24
I_i	The interference power from i-th SU without order.	24
I_k	k-th nearest node's interference power.	59

I_{li}	The interference power coming from i-th SU under large-scale fading channels.	72
I_{si}	The interference power coming from i-th SU under small-scale fading channels.	70
I_{th}	The threshold of the aggregate interference power.	25
λ	The node density of the SU network	21
$I_{\max}$	The maximum interference power caused by a single node.	26
N_0	$= \pi\lambda R_0^2$.	29
$\mathcal{N}(0,1)$	The normal distribution with zero mean and unit variance.	46
$N_{\max}$	The average number of nodes in the disk of radius $R_{\max}$.	33
N_r	The average number of nodes in the ring between the circles of radii $R_{\max}$ and R_s.	33
N_s	The average number of nodes in FR.	33
ν	The path loss exponent.	24
$o(\cdot)$	The small o function, $y = o(x)$ if $\lim_{D\to\infty} y/x = 0$	26
P_0	The receiver own noise power.	24
P_{con}	The outage probability of the conventional network.	26
$\phi(x)$	The pdf of $\mathcal{N}(0,1)$, $\phi(x) = \exp(-x^2/2)/\sqrt{2\pi}$.	46
P_{out}	The outage probability of the CR network.	26
$P_{out,1}$	$= \Pr\{I_1 > I_{th}\}$.	29
$P_{out,k}$	$= \Pr\{I_k > DP_0\}$.	59
P_t	The transmitter power.	24
$Q(x)$	$= 1/\sqrt{2\pi}\int_x^\infty \exp(-u^2/2)\,du$, the standard Q-function	32
R_0	A SU at the distance R_0 from the receiver induces the interference equal to the receiver noise level.	22
R_1	The average number of nodes in the disk of radius R_1 is one.	22
r_i	The distance between the i-th SU and the PU.	24

$R_{\max}$	The maximum distance from the PU receiver to a SU (no SU nodes are located outside of this area).	22
R_s	The radius of the forbidden region.	22
σ	The standard deviation of $\ln x$ in natural units, where x is a log-normal random variable.	72

Chapter 1

Introduction

Cognitive Radio (CR) is an intelligent wireless communication system. It is aware of the dynamic environment and capable of self-adjustment, i.e., it learns the changes in the surrounding environment and adapts its operating parameters in real time, such as transmit-power, carrier-frequency, and modulation strategy. It makes wireless communication more reliable and the utilization of the radio spectrum more efficient [1]. It is being considered as one of the key candidate technologies for beyond fourth generation (4G) wireless systems.

As higher data rate services are required in wireless communications over a limited spectrum, there is a need for higher-efficiency spectrum utilization. *Spectrum policy task force report* [2] released by Federal Communications Commission (FCC) shows that rigid spectrum policy makes utilization of the licensed spectrum very low, i.e., the licensed spectrum is not used most of the time. To overcome the overcrowded and underutilized spectrum problem and to use spectrum more efficiently, CR allows the secondary users (SU) to share currently allocated spectrum without harming the primary user's (PU) service quality.

1.1 Motivation

Due to the uncertainty in the number of SUs and their locations, the PU performance may be seriously affected by the aggregate interference induced by the SUs in the PU receiver. Therefore, its accurate modeling is important to design cognitive radio networks and also to estimate their potential benefits.

There is extensive literature dealing with aggregate interference modeling of conventional (non-CR) networks [3]. The most popular elements of those models are a Poisson point process (to model the interferers' spatial locations) [4, 5] and the standard propagation path loss models (e.g., path loss exponent and fading). Based on that, Sousa and Silvester [6] studied the aggregate interference power obtaining its characteristic function (CF) and concluding that it is an α-stable random variable. Except for some special cases, the closed-form probability density function (pdf) is not available. Using the multivariate Lepage series representation, Ilow and Hatzinakos [7] obtained the CF of the aggregate interference including the log-normal and Rayleigh fading effects and concluding that the aggregate interference is a spherically symmetric α-stable random vector.

The benefits of interference cancelation of various forms in wireless networks have been investigated in [8–10]. Unlike previous studies, which were mainly based on the CF approach, [9] studied the tail of the aggregate interference distribution directly and found that, at the low outage regime, the aggregate interference is dominated by the nearest interferer, and this also holds under various fading models and interference cancelation mechanisms. Based on the direct asymptotic analysis, compact and accurate closed-form expressions for the outage probability were obtained and a number of insights were pointed out. The beneficial impact of optimum combining using the standard array processing techniques (e.g., an MMSE spatial filter) has been studied

in [10]. While in some special cases the aggregate interference distribution of a large wireless network approaches Gaussian, it is far from being accurate in general [11].

The studies above are limited to conventional (non-CR) networks. Cognitive radio networks present additional difficulties for the analysis due to the presence of the forbidden (exclusion) region around the PU receiver where no SUs are allowed to transmit (to ensure the PU's proper quality-of-service (QoS)), so that the distribution of the aggregate interference is not α-stable any more. Consequently, the above-mentioned models/results can not be used as they are fundamentally based on the α-stable nature of the problem. Furthermore, the asymptotic analysis of the interference distribution tail (low outage region) does not apply either, since the forbidden region has a major impact on the tail. These difficulties are addressed in the literature in mainly two typical ways: via various ad-hoc approximations (e.g., using the interference distribution cumulants found from its CF) [12, 13] or via the large deviation analysis [14]. Additionally, numerical simulations provide a wealth of empirical observations [15]. Since a direct analysis of the interference distribution is challenging while the characteristic function is much more amenable to the analysis, from which its cumulants can be found, this approach was adopted in [12] and [13] to obtain approximations of the interference distribution based on the Edgeworth expansion and truncated stable distributions, respectively. While this approach predicts the main body of the distribution well, its accuracy deteriorates significantly at the distribution tail, i.e., at the practically-important low-outage regime (high QoS for the PU). This happens because a limited number of cumulants (typically two) can not represent the tail well. On the other hand, the use of the large deviation analysis allows one to predict the (exponential) rate of decay of the distribution tail but not the distribution itself (as all constants and slowly-varying functions are neglected in the analysis; in particular, the results are independent of the node density) so that "more

refined estimates of the actual probability are needed" [14]. This is accomplished in the thesis.

To overcome the above-mentioned difficulties, we develop a direct approach to outage probability analysis based on the heavy tail and saddle-point approximation theories. The advantage of this combined approach is that the distribution tail can be found in an explicit closed-form with a guaranteed level of percentage accuracy, to the best of our knowledge, for the first time. Additionally, this analysis provides a number of insights and the expressions are also accurate in the non-asymptotic regime (in fact, some of them are accurate over the whole range), and it can also be extended to include the impacts of interference cancelation and fading (from a broad class of distributions), also in combination with each other. Important geometrical and system parameters affecting critically the outage probability are clearly identified.

We have studied a similar CR scenario in [16, 17] based on the concept of typical outage events and using ad-hoc approximations in different regimes, which were validated via Monte-Carlo simulations but not via a rigorous analysis. Unlike [16, 17], the thesis gives a rigorous analytical evaluation of the asymptotic outage probability (summarized in Theorems 1-4, Corollaries 1-3 and Proposition 4), from which the typical outage events of [16,17] follow as a consequence and do not require any ad-hoc assumptions or approximations.

1.2 Contributions

The main contributions of this thesis can be summarized as follows:

- In the literature, there are mainly two typical ways to study aggregate interference in CR networks: via various ad-hoc approximations or via the large deviation analysis. In this thesis, we develop a direct approach to the outage probability analysis based on the heavy tail and saddle-point approximation theories. The advantage of this combined approach is that the distribution tail can be found in an explicit closed-form with a guaranteed level of percentage accuracy. Additionally, this analysis provides a number of insights and the expressions are also accurate in the non-asymptotic regime.

- Based on asymptotic technique, saddle point theory and the typical outage event, the outage region can be divided into three parts: high-outage regime, heavy tail regime and super-exponential tail regime. Using the present approach, we demonstrate that there is a critical point below which the outage probability decays polynomially (i.e., slowly) but above which it decays super-exponentially (i.e., very fast), as a function of the threshold interference-to-noise ratio (INR), thus revealing a qualitative transition around this point. This provides a rigorous analytical foundation for the earlier empirical observations in the literature [15], and is also in agreement with a similar phenomenon observed in statistical physics [18]. The analysis also reveals the outage-forming mechanism that is responsible for such behavior: the polynomial (heavy tail) decay is due to a dominant contribution of the nearest active interferer (this also holds under interference cancelation and fading) and the super-exponential decay is due to the aggregate effect of many interferers, none of which is able to cause an outage alone. The main analytical tools are the heavy tail distribution theory

for the below-critical region and the saddle-point approximation theory for the above-critical one.

- While increasing the forbidden region gives more protection to the PU receiver (by reducing the interference), it also reduces the spectral efficiency of the SUs by allowing fewer of them to transmit. A compromise solution is to decrease the forbidden region and to implement some form of interference cancelation in the PU receiver to keep its quality-of-service at an acceptable level. This becomes a feasible solution when the PU is offered some incentives [19] to implement interference cancelation such as a reduced license fee. This configuration is studied in Chapter 4 (to the best of our knowledge, for the first time) by extending the analysis above. The nearest active node is shown to provide the dominant contribution to the outage probability in this case as well, which scales down exponentially in the number of canceled nodes thus demonstrating significant potential of this approach, at the below-critical level. On the contrary, this approach gives little improvement in the above-critical region.

- The obtained results are extended in Chapter 5 to include the effect of fading from a broad class of fading distributions whose tails decay faster than polynomially, which includes all popular models, e.g., Rayleigh, Rice, Nakagami, log-normal, Weibull, also in combination with each other and with interference cancelation. In particular, Rayleigh fading is shown to have a negligible impact on the outage probability in the below-critical region and significantly increases it in the above-critical region, while the log-normal fading induces a slight increase in the former and a significantly higher increase in the latter region. Similarly to non-CR networks [3], it is the random CR network geometry that dominates the outage probability in the below-critical region.

1.3 Thesis organization

The outline of this thesis is as follows:

- Chapter 2 reviews the literature in cognitive radio, the distribution of aggregate interference in wireless networks, and the outage probability.

- Chapter 3 analyzes the distribution of aggregate interference and the outage probability in CR networks for non-fading scenario. Based on the typical outage event, the outage region can be divided into three parts: high-outage regime, heavy tail regime, and super-exponential tail regime. Rigorous analysis is given based on asymptotic technique and saddle point theory. Theorem 1 and 2 provide the conditions for heavy tail regime and super-exponential tail regime separately. The rigorous foundation has been established for earlier empirical observations in the literature.

- Chapter 4 studies the outage probability in CR networks under interference cancelation for non-fading scenario. Due to spectrum trading, PUs may be willing to implement interference cancelation in their side with small forbidden region for SU network. With this implementation, SUs' spectrum efficiency increases significantly. Rigorous analysis is given based on asymptotic technique. From Theorem 3, when $(k-1)$ nearest (to the PU receiver) interferers located outside the FR are canceled, the outage probability is still dominated by the nearest active (k-th) node. By implementing interference cancelation, the outage probability decreases significantly at PU side with the same system parameters, so SUs can gain some spectrum efficiency without more harm on PU side.

- Chapter 5 studies the outage probability in CR networks with fading and interference cancelation. Rigorous analysis is given based on asymptotic approaches.

Theorem 4 and Proposition 4 show that when $(k-1)$ nearest nodes are canceled, the outage probability is dominated by the nearest active (k-th) node. A broad class of fading distributions is considered in the analysis. Rayleigh and log-normal fading scenarios are specifically studied and simulated. Extensive simulation results show that the approximation is accurate over the whole INR range with different system parameters.

- Chapter 6 concludes this thesis by reviewing the main contributions along with new future research directions for the distribution of aggregate interference in CR networks.

1.4 Publications

The related publications are listed as follows:

- Y.Wen, S. Loyka, and A. Yongacoglu, "Asymptotic analysis of interference in cognitive radio networks," IEEE Journal on Selected Areas in Communications, vol. 30, no. 10, Nov. 2012.
- Y.Wen, S. Loyka, and A. Yongacoglu, "On Outage Probability in Cognitive Radio Networks," in 2012 IEEE International Conference on Communications (ICC), Jun. 2012.
- Y.Wen, S. Loyka, and A. Yongacoglu, "The impact of fading on the outage probability in cognitive radio networks," in 2010 IEEE 72nd Vehicular Technology Conference: VTC2010-Fall, Sept. 2010.
- Y.Wen, S. Loyka, and A. Yongacoglu, "On distribution of aggregate interference in cognitive radio networks," in 25th Biennial Symposium on Communications (QBSC), pp. 265-268, May. 2010.

Chapter 2

Literature Review

In this chapter, we review the literature on wireless networks, cognitive radio networks, and aggregate interference in wireless networks.

2.1 Wireless networks

In a typical scenario, a wireless network contains a number of nodes, which communicate with each other over a wireless channel. Some wireless networks have a centralized control and only last hop being wireless, such as cellular networks and mobile IP. The others do not have a centralized control and all links are wireless, such as ad hoc networks.

The capacity limit of large wireless networks is important to the design of networks and protocols, but it is hard to determine it, so that the capacity scaling laws of large wireless networks were studied instead of it. Gupta and Kumar [20] found that the throughput of each node decreases with a rate of the square root of the number of nodes under certain circumstances (the nodes are optimally placed in a disk of unit area; traffic patterns are optimally assigned; each transmission range is optimally

chosen.). Xie and Kumar [21] studied the capacity scaling law with fewer assumptions and considered both high and low attenuation cases. Both papers considered the scaling law (how the capacity scales when the number of the nodes n in the network goes to infinity). However, the capacity with finite n is more relevant for network design. Leveque and Telatar [22] derived the information theoretic upper bounds on the capacity of large extended ad hoc wireless networks, and concluded that the rate per communication link (source - destination) tends to zero as the number of nodes gets large.

The relationship of the node's mobility and the capacity of large networks is another interesting topic because most of the wireless communication devices are mobile. Grossglauser and Tse [23] found that node's mobility increases the capacity of ad hoc wireless networks without a delay constraint. On the other hand, Jafar [24] showed that too much mobility limits the capacity of wireless ad hoc networks due to channel uncertainty, network homogeneity and loss of degrees of freedom.

Cooperative communication combats fading by using space diversity and multiuser diversity [25]. Laneman, Tse and Wornell [26] studied cooperative diversity in wireless networks. Several cooperative strategies are considered, such as fixed relaying schemes, selection relaying schemes and incremental relaying schemes. Performance analysis in term of outage probability was given.

Stochastic geometry of wireless networks is another important issue for wireless networks [27]. Haenggi et al [28] gave a survey on some techniques based on stochastic geometry and random graphs to study the capacity, the connectivity, the outage probability and other fundamental limits of wireless networks.

2.2 Cognitive radio networks

CR network is a specific wireless network which is aware of the environment and capable of self-adjustment, and improves spectrum utilization efficiency.

Since CR has been introduced in 1999 [29], it rapidly became very popular. Many books and papers studying cognitive radio published in the last few years. *Cognitive wireless communication networks* [30] discusses the physical and Media Access Control (MAC) layer of CR networks in theory and design. *Cognitive radio networks* [31] studies the physical, MAC and routing layer of CR networks, and crosslayer design is also considered. *Cognitive Radio, software defined radio, and adaptive wireless systems* [32] discusses the cognitive radio, software defined radio (SDR), and adaptive radio concepts from several aspects, such as CR architecture, spectrum sensing, application of CR and so on. There are also some IEEE special issues on CR. *Special issue on adaptive, spectrum agile, and cognitive wireless networks* of Journal on Selected Areas in Communications (JSAC) [33] is focused on the spectrum sensing and resource allocation of CR networks. *Special issue on cognitive radio: Theory and applications* of JSAC [34] is focused on spectrum sensing and sharing, physical, MAC layer and game theory application of CR networks. *Special issue on signal processing and networking for dynamic spectrum access* of Journal of Selected Topics in Signal Processing (JSTSP) [35] is focused on spectrum sensing, spectrum management, and fundamental capacity limits of dynamic spectrum access (DSA). *Special issue on cognitive radio technology* of Signal Processing Magazine (SPM) [36] is focused on the fundamental information theoretic limits, modulation, anti-jamming code and game theory application of CR networks. On the other hand, the first cognitive radio wireless regional area network standard, IEEE 802.22, was released in November 2008. In that standard, TV channels 5-13 in the VHF band and 14-51 in the UHF band can

be used for fixed broadband access systems [37, 38]. From the discussion above, we conclude that cognitive radio is an important and hot topic in wireless communication field.

The research field of CR can be classified into a few aspects: spectrum awareness (spectrum sensing), fundamental information and communication theoretic limits, modulation techniques, resource allocation and so on.

One of most importance features of CR networks is awareness of the dynamic environment. Spectrum awareness is a key to the dynamic use of spectrum. It can be obtained by using geometric location database, beacon signals or spectrum sensing. Yucek and Arslan [39] gave a survey of spectrum sensing algorithms for CR applications. There are several spectrum sensing methods for CR [30–32, 39, 40]:

- Energy detector based sensing (radiometer or periodogram) [41–44]. Due to low computational and implementation complexities, it is the most popular way of spectrum sensing.

- Waveform based sensing [43]. It uses known patterns of PU's signal, such as preambles, pilot signals and spreading sequences.

- Cyclostationarity based sensing [45, 46]. It uses the periodicity in PU's signal or the statistics of PU's signal.

- Matched filtering sensing [44, 47]. It uses match filter to detect PU's signal and requires perfect knowledge of PU's signal.

On the other hand, cooperative sensing [48,49] and multiband sensing [50,51] decrease the probabilities of miss detection and false alarm, and mitigate the hidden PU problem. Ghasemi and Sousa [52] discussed the details of spectrum sensing requirements, challenges and design trade-offs.

The information theoretic limit of CR networks is another important research topic. Devroye et al [53] studied achievable rates in CR channels. Theoretic limits of 2×2 cognitive radio channels are found for both causal and non-causal cases. Devroye et al [54] also studied capacity region, the scaling laws and aggregate interference of CR networks. Fundamental information theoretic limits are derived based on four approaches: interference avoiding, interference controlling, opportunistic interference cancelation and asymmetric transmitter side information. Jovicic and Viswanath [55] derived the capacity of the CR channel for "low-interference" region under two constraints: PUs have no rate degradation, and use a single user decoder.

There are two classes of modulation techniques uses in CR systems [56]: multi carrier [57] and single carrier modulations. In multi carrier CR systems, Orthogonal Frequency Division Multiplexing (OFDM) is the strong candidate due to the spectrum access flexibility, and its limitations are high sidelobe and peak to average power ratio (PAPR). Wavelet packet based CR system is another multi carrier CR system which provide higher sidelobe suppression when comparing with regular OFDM. Transform domain communication system (TDCS) is a single carrier system, and it shapes its signal to share the spectrum with PUs, i.e., adapts its waveform to avoid the interference to PUs. Wavelet domain communication system (WDCS) is another single carrier system, where the Fourier transform operation in TDCS is replaced by wavelet transformation.

How to share the spectrum resource among the CR users is important for both PU's and SU's networks. Game theory is a useful tool which models the competition and cooperation among users as a spectrum sharing game [58–60]. The game theory model consists of a set of players, a space of the strategies for each player and utility function. In a noncooperative spectrum sharing game, each user only maximize its own utility function. One of the popular solutions is an algorithm to find Nash equilibrium.

Since CR network's behavior is similar to that of a society, many economic models can be implemented to solve the spectrum sharing problem. For example, Niyato and Hossain [19] introduced a market equilibrium based approach for spectrum trading. On the other hand, [61] and [62] studied spectrum trading using contract-theoretic model and agent-based model separately.

There are some other interesting research fields, such as cognitive femtocell [63], artificial intelligence [64] and so on. CR network is a very active and popular topic in academic and industrial fields.

2.3 Aggregate interference in wireless networks

How to model the multi-user interference is a fundamental issue for wireless networks. The simplest way is treating the interference as a Gaussian noise, but Gaussian noise model does not accurately represent the reality in many cases, so it is important to find more accurate statistical models for non-Gaussian impulsive noise. Those models can be divided into two groups: empirical models and statistical physical models [65]. The most popular statistical-physical model is the $\alpha-$stable noise model.

Definition: A random variable X is said to have a stable distribution if for any positive numbers A and B, there is a positive number C and a real number D, such that $AX_1 + BX_2 \overset{d}{=} CX + D$, where X_1 and X_2 are independent copies of X, and where "$\overset{d}{=}$" denotes equality in distribution [66].

A stable distribution can be characterized by its CF:

$$\mathbf{E}(e^{jt\mathbf{X}}) = \begin{cases} \exp\left(jt\mu - \gamma|t|^{\alpha}(1 - j\beta\mathrm{sgn}(t)\tan(\pi\alpha/2))\right) & \alpha \neq 1 \\ \exp\left(jt\mu - \gamma|t|(1 + j\beta\mathrm{sgn}(t)\frac{2}{\pi}\ln|t|)\right) & \alpha = 1, \end{cases} \tag{2.1}$$

where $\mathrm{sgn}(t)$ is the sign of t; $\alpha \in (0, 2]$ is the index of stability; $\beta \in [-1, 1]$ is the skew

parameter; μ is the drift; γ is the dispersion parameter. It has been well developed by finance mathematicians [67], but the only known stable distributions with closed-form density functions are the Gaussian, the Levy, and the Cauchy distribution.

When $\alpha = 2$, the distribution reduces to a Gaussian one with the variance $\sigma^2 = 2\gamma$ and the mean μ; the skewness parameter β has no effect. The CF of Gaussian distribution is

$$\mathbf{E}(e^{jt\mathbf{X}}) = \exp\left(jt\mu - \gamma t^2\right). \tag{2.2}$$

and the PDF is

$$f(\mathbf{X}) = \frac{1}{\sqrt{2\pi}\sigma} \exp\left(\frac{(x-\mu)^2}{2\sigma^2}\right). \tag{2.3}$$

When $\alpha = 1/2$ and $\beta = 1$, the distribution reduces to a Levy distribution. The CF of Levy distribution is

$$\mathbf{E}(e^{jt\mathbf{X}}) = \exp\left(jt\mu - \gamma\sqrt{-2jt}\right). \tag{2.4}$$

and the PDF is

$$f(\mathbf{X}) = \frac{\gamma \exp\left(\frac{-\gamma^2}{2(x-\mu)}\right)}{\sqrt{2\pi}(x-\mu)^{3/2}}. \tag{2.5}$$

when $\alpha = 1$ and $\beta = 0$, the distribution reduces to a Cauchy distribution. The CF of Cauchy distribution is

$$\mathbf{E}(e^{jt\mathbf{X}}) = \exp\left(jt\mu - \gamma|t|\right). \tag{2.6}$$

and the PDF is

$$f(\mathbf{X}) = \frac{1}{\pi\gamma\left[1 + \left(\frac{x-\mu}{\gamma}\right)^2\right]}. \tag{2.7}$$

Gaussian distribution is a special $\alpha -$ stable distribution with parameter $\alpha = 2$.

When $\alpha < 2$, $\alpha-$stable distribution has a heavy tail which decays much slower than that of Gaussian distribution [66].

The aggregate interference of conventional (i.e., non-CR) wireless networks has been studied for a few decades. Based on Poisson point process model and average path loss propagation model, Sousa and Silvester [6] studied the aggregate interference power. They obtained its CF and concluded that the aggregate interference power is an $\alpha-$stable random variable. Sousa [68] extended that model and studied the aggregate interference as a random vector at the output of receiver correlators, and concluded that the aggregate interference is a symmetric $\alpha-$stable random vector. Only in some special cases, the closed-form pdf was derived from its CF.

Using the multivariate Lepage series representation, Ilow and Hatzinakos [7] obtained the CF of the aggregate interference according to a Poisson point process of node locations in the plane/volume, including the log-normal and Rayleigh fading effects, and concluded that the aggregate interference is a spherically symmetric $\alpha-$stable random vector whose CF is:

$$\mathbf{E}(e^{jt\mathbf{Y}}) = \exp\left(\gamma\|\mathbf{t}\|^{\alpha}\right). \tag{2.8}$$

Chan and Hanly [69] calculated the outage probability in a CDMA network based on the Poisson point process, the average path loss and fading models. By using Campbell's theorem, the cumulants of the aggregate interference power were found. The outage probability is approximated by Poisson-Gaussian and Edgeworth expansion. A Chernoff bound on the outage probability was provided. In the thesis, we will use their Edgeworth expansion approximation (see (3.44)). The detail about the Edgeworth expansion can be found in Appendix C.1.

Yang and Petropulu [70] studied the correlated interference in a Poisson field with

average path loss model. They concluded that the distribution of aggregate correlated interference is $\alpha-$ stable only for some special cases.

Weber and et al [8, 71, 72] studied the transmission capacity of wireless Ad Hoc networks. In [71], they studied the transmission capacity of spread-spectrum (SS) wireless Ad Hoc networks with outage constraints based on the Poisson point process. The upper and lower bounds on transmission capacity were derived. The work in [72] extended the results in [71] by considering the effect of fading, channel inversion power control and threshold-based scheduling on the capacity. In [8], they studied the transmission capacity with successive interference cancelation in wireless Ad Hoc networks. The Poisson point process and the average path loss models were considered. The closed-form expressions of transmission capacity under successive interference cancelation were derived for a given number of canceled nodes and the cancelation effectiveness.

Mordachev and Loyka [9] studied the tradeoff of the outage probability and the node density in wireless networks also based on the Poisson point process and the average path loss, and including different fading models and interference cancelation mechanisms as well. By studying the tail of the aggregate interference distribution, they found that, at the low outage region, the aggregate interference is dominated by the nearest one, i.e.,

$$\lim_{D\to\infty}\frac{\Pr\left\{\sum_i P_{ai}>x\right\}}{\Pr\left\{P_{a1}>x\right\}}=1 \tag{2.9}$$

where P_{ai} is the i_{th} near interference power. So that the outage probability can be approximated as in [9],

$$P_{out}\approx\begin{cases}1, & D\le D_1\\ \overline{N}_0 D^{-2/\nu}, & D>D_1\end{cases} \tag{2.10}$$

where $\overline{N}_0 = \pi\lambda R_0^2$ is the average number of nodes in the disk of the radius $R_0 = P_0^{-1/\nu}$, where P_0 is the noise power; ν is the path loss exponent; D is the threshold interference to noise ratio. The disk of R_0 was termed "potential interference zone" in [9]), and outside the circle of the radius R_0, the interference level is below the noise level. $D_1 = \overline{N}_0^{\nu/2} = (\pi\lambda)^{\nu/2} / P_0$ is a critical value which separates the high and low outage probability regions. It corresponds to on average one SU being in the disk of the radius R_1.

Ghasemi and Sousa [12] studied the aggregate interference in cognitive radio networks based on the Poisson point process, the average path loss and different fading models. Using Campbell's theorem, the CF and cumulants of the aggregate interference power were obtained, and the approximations of the outage probability are derived based on the cumulants. The effect of cooperative sensing on the distribution of the aggregate interference power for i.i.d. fading channels has also been studied. Since their approximations of the outage probability are based on the cumulants, its accuracy deteriorates significantly at the distribution tail which is important for real system designs. It is also difficult to get insights rather the complicated formulas.

Ganesh and Torrisi [14] studied the aggregate interference in a large wireless network using large deviations principle (LDP) based on Poisson point process model and random transmission powers. They found exponential rate functions for different assumptions on the distribution of transmission powers. Unfortunately, the exponential rate function is not sufficient to evaluate the outage probability, even in the large deviation region, so that "more refined estimates of the actual probability are needed" [14]. Their model can be extended to CR networks since their model consider a forbidden region in the discussion section of their paper. From Theorem 12 of [14],

we have

$$P_\varepsilon = \Pr\{V_\varepsilon > z\} = \Pr\left\{V > \frac{z}{\varepsilon}\right\} = P_{out}\left\{\frac{z}{\varepsilon}\right\} \sim \exp\left(-\frac{c\ R^\nu z}{\varepsilon}\right)$$
$$P_{out}\{y\} \approx c_1\ \exp\left(-c\ R^\nu y\right) \tag{2.11}$$

where $c,\ c_1$ are undetermined constants; $y = z/\varepsilon$ is the threshold of the aggregate interference power; ε and R are defined as in [14]. In our notation, R is equivalent to the radius of the forbidden region introduced in Section 3.1.2. The detail of the comparison between LDP and our approach is given in Section 3.3. With LDP, the order of scaling is derived, and some important insights also may be found, but it can not be used in the practical design, as P_{out} itself is not known (due to unknown $c,\ c_1$). Our approach gives a more refined estimation of the actual outage probability.

Salbaroli and Zanella [73] analyzed aggregate interference in a Poisson finite field, and average path loss and log-normal fading are considered. They derived the distribution of channel gain and any moment of the aggregate interference on a finite area.

Haenggi and Ganti [3] reviewed the interference in large wireless networks considering different nodes spatial distribution models (lattice models, homogeneous and cluster Poisson models, and general motion-invariant models) and path loss models (singular and non-singular models). Based on those models, the distribution of the interference and SIR are derived, outage probabilities are analyzed, and the asymptotic behavior of the interference distribution is studied.

Chapter 3

Aggregate Interference and Outage Probability Analysis

In the chapter, we study the outage at the primary user's receiver causing by the aggregate interference generated by secondary users' transmitters for non-fading scenarios. The system model and the definition of the outage probability are given. Rigorous analysis is given based on asymptotic technique and saddle point theory. Theorem 1 and 2 provide the conditions for heavy tail regime and super-exponential tail regime separately. The rigorous foundation has been established for earlier empirical observations in the literature.

3.1 System model

3.1.1 Node spatial distribution model: Poisson point process

Poisson point process is the most popular spatial distribution model to model the distribution of users in wireless networks [3, 4]. It is simple and fits well with the reality in many cases.

The Poisson distribution

A random variable χ has the Poisson distribution $P(\mu)$ if its possible values are positive integers and if

$$P(\chi = n) = \pi_n(\mu) = \frac{\mu^n \exp(-\mu)}{n!} \tag{3.1}$$

for $n \geq 0$. Here μ can take any value in $\mu > 0$, and is the mean of the distribution $P(\mu)$, $\mu = E(\chi) = \sum_{n=0}^{\infty} n\pi_n(\mu)$ [5].

The Poisson point process

The Poisson point process is characterized by two basic properties [4, 5]: One is that the number of nodes falling into a region $S = \boldsymbol{R}^d$ has a Poisson distribution with mean $\mu(S) = \int_S \lambda(x)dx$, where dx stands for $dx_1 dx_2 \cdots dx_d$; $\lambda(x)$ is the node density function. The probability of exactly k nodes falling into the region S is:

$$P(k, S) = \frac{(\mu(S))^k \exp(-\mu(S))}{k!}. \tag{3.2}$$

The other is that, the number of nodes in the region S is independent with that in any other disjoint region.

The homogeneous Poisson point process is a Poisson point process whose node density is fixed, i.e., the node density $\lambda(x)$ is a constant λ. The probability of exactly k nodes falling into the region S is:

$$P(k, S) = \frac{(\lambda S_a)^k \exp(-\lambda S_a)}{k!}, \tag{3.3}$$

where S_a is the area or volume of the region S.

In this thesis, we use the homogeneous Poisson point process as the node spatial distribution model, following earlier work in [6] - [18].

3.1.2 Geometry and protocol of the CR network

Let us consider a cognitive radio network which contains a primary user's receiver and many secondary users' transmitters (nodes) on a plane. The PU is located at the origin. The SUs are randomly located according to a Poisson point process of the density $\lambda[\texttt{nodes/m}^2]$. Interference coming from the SU nodes outside the circle of a certain radius $R_{\max}$ is assumed to be negligible (alternatively, no SUs are located outside of this circle, which models a realistic finite-size network). The interference coming from a node outside of the circle of radius R_0 is below the noise level at the PU receiver. The average number of nodes in the disk of the radius R_1 is one. We follow IEEE 802.22 standard, and consider a geolocation CR protocol, i.e., all the devices in the network are equipped with satellite-based geolocation technology (GPS, Galileo, etc.), and the base station has a database which contains the location data of the primary devices [37]. Based on geolocation database, all SUs which are inside of a forbidden region (FR) (also known as exclusion region), i.e., the circle of the radius R_s centered on the PU, stop their transmissions so that some protection to the PU receiver is provided. The geometry of the CR network is illustrated in Fig. 3.1.

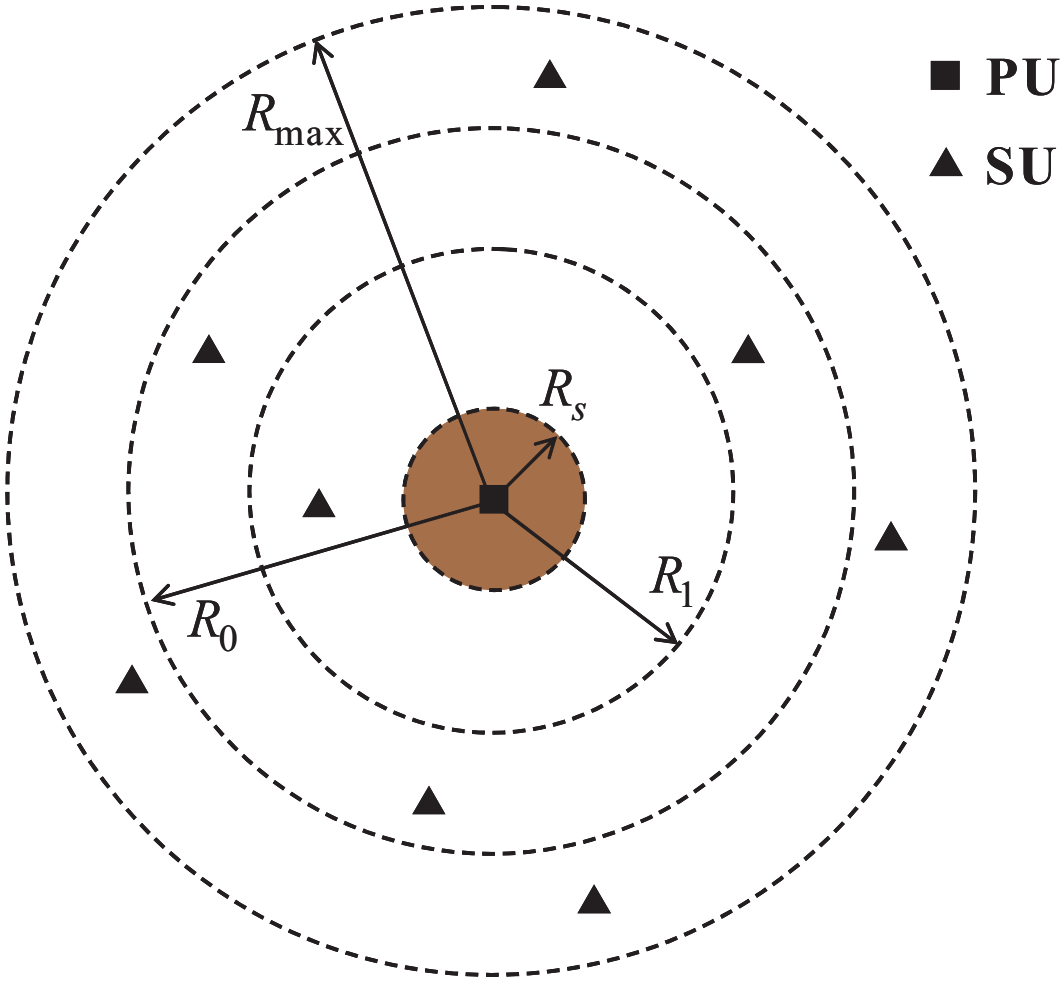

Fig. 3.1 The geometry of the CR network. Interference coming from the SU nodes outside the circle of the radius $R_{\max}$ is negligible. The interference coming from a node outside of the circle of radius R_0 is below the noise level at the PU receiver. The average number of nodes in the disk of the radius R_1 is one. All SUs inside the circle of the radius R_s centered on the PU, the forbidden region (FR), stop their transmissions.

3.1.3 Propagation model

We assume that the desired signal, interferences and noise are independent. The total received power at the PU receiver can be expressed as:

$$P_{PU} = P_d + \sum_{i=1}^{N} I_i + P_0 \tag{3.4}$$

where P_d is the desired signal power; I_i is the interference signal power coming from i-th node; P_0 is the noise power; N is a Poisson random variable which denotes the number of nodes in the ring between circles of the radii R_s and $R_{\max}$, i.e., the potential interference zone where all active interferers are located. The power at the receiver antenna input coming from a transmitter of power P_t is given by the standard link budget equation [74],

$$P_r = P_t G_t G_r g \tag{3.5}$$

where G_t and G_r are the transmitter and receiver antenna gains; g is the propagation path gain, $g = g_a g_l g_s$, where g_a is the average path gain, g_l is the large scale (shadowing) fading gain, and g_s is the small scale (multipath) fading gain; $g_a = a_\nu r^{-\nu}$, where ν is the path loss exponent, r is the distance between the transmitter and receiver, and a_ν is a constant independent of r. For simplicity, we assume the transmitter and receiver antennas are isotropic with unity gain, and all SUs transmit at the same constant power level P_s, so that the power at the receiver antenna input coming from a SU $P_r = P_s g$. In the non-fading scenario, the i-th SU generates the interference power $I_{ai} = P_s a_\nu r_i^{-\nu}$ at the PU receiver, where r_i is the distance between the i-th SU and the PU. Without loss of generality, we normalize $P_s a_\nu = 1$, so $I_{ai} = r_i^{-\nu}$.

In this chapter, we study the non-fading scenarios which correspond to $g_l = g_s = 1$, and fading will be introduced in Chapter 5.

3.2 Outage probability

When the signal to interference plus noise ratio (SINR) is less than a certain threshold η, there is a significant performance degradation in a wireless link and it is considered to be in outage. This is equivalent, under the adopted channel model, to the aggregate interference power $I_{ag} = \sum_i I_i$ exceeding the threshold $I_{th} = P_d/\eta - P_0$, so that the outage probability is

$$P_{out} = \Pr\{\text{SINR} < \eta\} = \Pr\{I_{ag} > I_{th}\} \tag{3.6}$$

Defining the interference-to-noise ratio (INR) as

$$\gamma = \sum_{i=1}^{N} I_i/P_0, \tag{3.7}$$

its threshold value is $D = I_{th}/P_0$, so that the outage probability can be expressed as

$$P_{out} = \Pr\{\gamma > D\} = 1 - F(D) \tag{3.8}$$

where $F(D)$ is the cumulative distribution function (CDF) of the INR. Under the adopted channel model, P_{out} also serves as a complementary CDF (CCDF) of the aggregate interference I_{ag}.

The outage probability is an important performance metric for wireless system design. It can be related with other performance metrics, such as frame error rate.

3.3 Asymptotic results

In this section, we present our main contributions in Theorem 1 and 2, and Corollaries 1, 2, which are further extended to the non-asymptotic regime in the next section, and to the case of interference cancelation and fading in the following chapters.

Since the CR protocol forces all SU nodes inside the forbidden region of the radius R_s to cease their transmissions, the interference generated by a single node can not exceed $I_{\max} = R_s^{-\nu}$, i.e., the value coming from an active SU node at the closest possible distance, so that the maximum INR caused by a single node is $D_{\max} = I_{\max}/P_0$. Let us compare the CR network with the forbidden region of the radius R_s and a corresponding conventional (non-CR) network, which is identical to the CR one except that there is no forbidden region (i.e., $R_s = 0$). The relationship of their respective outage probabilities P_{out} and P_{con} in the asymptotic (low-outage) regime and when $D < D_{\max}$ is characterized as follows.

Theorem 1: Let $d = D/D_{\max} \leq a < 1$ be the normalized threshold INR bounded away from unity, and $D \to \infty$. The CR outage probability P_{out} is then asymptotically proportional to the conventional one P_{con} (for which $R_s = 0$):

$$P_{out} = \Pr\{I_{ag} > DP_0\} = (1 - d^{2/\nu})P_{con} \cdot (1 + o(1)) \tag{3.9}$$

where $a \in (0, 1)$ is an arbitrary fixed number; $o(\cdot)$ is the small o function[1].

[1] $y = o(x)$ if $\lim_{D\to\infty} y/x = 0$ [75].

Proof:

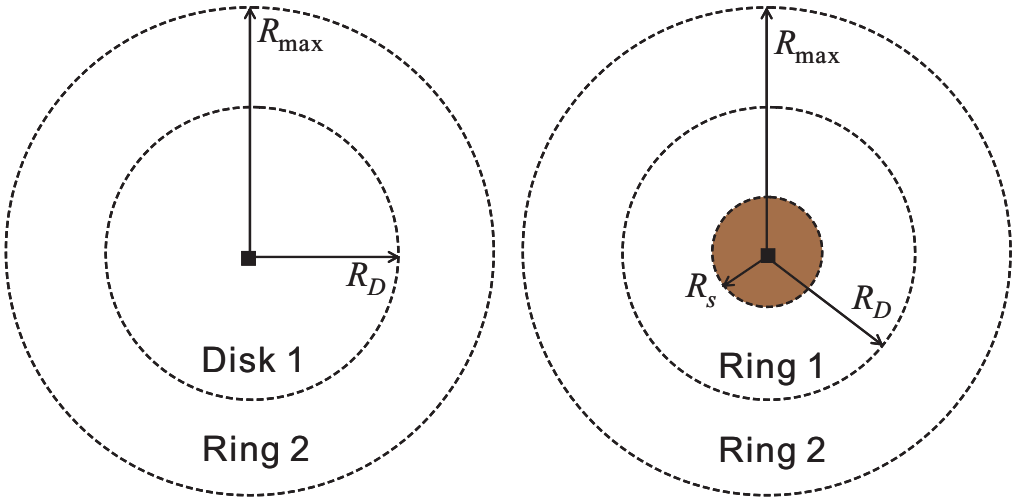

(a) conventional network (b) cognitive radio network

Fig. 3.2 Geometry of conventional (no forbidden region) and CR wireless networks. Disk 1 and Ring 1 are active interference zones (presence of a single node there causes an outage event), while Ring 2 is a potential interference zone (several nodes there are required to cause an outage event).

Let n_D be the number of nodes in disk 1 of the radius R_D in Fig. 3.2.a, and n_1 be the number of nodes in ring 1 which is between the circles of radii R_s and R_D in Fig. 3.2.b. Let ring 2 be the ring between the circles of radii R_D and $R_{\max}$ in Fig. 3.2. Define the following probabilities:

$$P_1 = \Pr\{n_D \geq 1\},\ P_3 = \Pr\{n_1 \geq 1\}$$
$$P_2 = \Pr\left\{\sum_{i \subseteq \text{ring } 2} I_i > DP_0\right\}$$

The conventional outage probability can be now expressed as:

$$P_{con} = P_1 + (1 - P_1)P_2$$

From the Poisson point process,

$$P_1 = 1 - \exp(-\lambda\pi R_D^2),$$

and from Theorem 1 in [9], as $D \to \infty$,

$$(1 - P_1)P_2/P_1 = o(1) \tag{3.10}$$

The CR outage probability can be expressed as:

$$P_{out} = P_3 + (1 - P_3)P_2$$

Since $D = d \cdot D_{\max}$, one obtains

$$P_3 = 1 - \exp[-\lambda\pi R_D^2(1 - d^{2/\nu})].$$

When $d < 1$ and $D \to \infty$, the limit of the ratio of P_{out} and P_{con} can be evaluated as follows:

$$\begin{aligned} \lim_{D\to\infty} \frac{P_{out}}{P_{con}} &= \lim_{D\to\infty} \frac{P_3 + (1 - P_3)P_2}{P_1 + (1 - P_1)P_2} \\ &= \lim_{D\to\infty} \frac{\frac{P_3}{P_1} + \frac{(1-P_3)P_2(1-P_1)}{P_1(1-P_1)}}{1 + \frac{(1-P_1)P_2}{P_1}} \\ &= (1 - d^{2/\nu}) \end{aligned} \tag{3.11}$$

from which (3.9) follows. ■

From Theorem 1 and the corresponding result for the conventional network in [9], it follows that the aggregate interference tail is dominated by the nearest node when

$d < 1$, which is formalized below.

Corollary 1: Let $P_{out,1} = \Pr\{I_1 > I_{th}\}$ be the probability that the nearest node interference exceeds the threshold (thus causing an outage event). The lower bound

$$P_{out} \geq P_{out,1}$$

holds for any D and is tight at low ($D \to 0$) as well as high INR, when $d < 1$ and $D \to \infty$,

$$\begin{aligned} P_{out} &= P_{out,1}(1 + o(1)) && (3.12) \\ &= (1 - d^{2/\nu}) N_0 D^{-2/\nu}(1 + o(1)) && (3.13) \end{aligned}$$

where $N_0 = \pi\lambda R_0^2$ is the average number of nodes in the disk of radius R_0.

Proof:

From [[9] Theorem 1], when $D \to \infty$,

$$P_{con} = N_0 D^{-2/\nu} \cdot (1 + o(1)) \tag{3.14}$$

where $N_0 = \pi\lambda R_0^2$. When $d < 1$ and $D \to \infty$, one obtains from (3.9) and (3.14),

$$P_{out} = N_0 (D^{-2/\nu} - D_{\max}^{-2/\nu}) \cdot (1 + o(1)) \tag{3.15}$$

where $D_{\max} = D/d$. On the other hand, using the Poisson point process probabilities when $d < 1$,

$$P_{out,1} = N_0 (D^{-2/\nu} - D_{\max}^{-2/\nu}). \tag{3.16}$$

Comparing (3.15) and (3.16), when $d > 1$ and $D \to \infty$, $P_{out} = P_{out,1} \cdot (1 + o(1))$.

When $D \to 0$, P_{out} and $P_{out,1}$ both achieve one.

So the bound $P_{out} \geq P_{out,1}$ is achievable at both low and high INR. ■

It follows from Corollary 1 that the lower bound $P_{out} \geq P_{out,1}$ is tight at high INR as well as at low (since $P_{out,1} \to 1$ as $D \to 0$). In fact, this corollary says that a typical (dominant) outage event occurs when the nearest node interference exceeds the threshold rather than the combined interference from many distant nodes doing so. This insight has a dramatic consequence for the interference cancelation considered in Chapter 4. It is clear from the $(1+o(1))$ term in (3.9) and (3.13) that they provide low relative (%) error and thus can be used as accurate approximations (without $o(1)$ term) for finite but large D (low-outage or high quality-of-service region) when $D < D_{\max}$, as we demonstrate below in Section 3.4. Note that (3.13) gives the tail behavior of P_{out} with a guaranteed accuracy level (vanishing % error as $D \to \infty$) as an explicit function of geometrical and system parameters.

While Theorem 1 holds for the $D < D_{\max}$ case, the opposite case of $D > D_{\max}$ is also of considerable practical interest for CR networks. In fact, while the outage probability decreases only polynomially with D in the first case (i.e., comparatively slowly), Corollary 2 below shows that it decreases super-exponentially in the latter case (i.e., very fast), thus revealing a remarkable qualitative transition around the $D = D_{\max}$ point. To better understand why this happens, observe that $d < 1$ in Theorem 1 implies $D < D_{\max}$, so that single-node interference can exceed the threshold D and cause an outage event. Corollary 1 further demonstrates that this is a typical outage event. On the other hand, when $D > D_{\max}$, the single-node interference can not exceed the threshold so that a combined effect of several nodes is required. Let $n = \lceil D/D_{\max} \rceil$, where $\lceil x \rceil = \min\{n \in \mathbb{Z} \mid n \geq x\}$ is a ceiling function. The outage occurs when the combination of at least n nodes' interference exceeds the

threshold. When $D_{\max} < \infty$ and $D \to \infty$, we have $n \to \infty$, so that some form of the central limit theorem (CLT) should apply to the combined interference, which results in the Gaussian approximation being a main candidate and an exponential scaling follows. As is well-known, this applies around the mean of the distribution but quickly deteriorates as one moves to the distribution tail, i.e., the region we are interested in (that is the low-outage region), when n is not sufficiently large. To overcome this problem, we use the saddle-point theory (also known as the tilted Edgeworth expansion), which suggest tilting the original distribution in such a way that the point of interest is always around the mean (akin to the importance sampling technique) [76]. An immediate effect is that the relative rather than absolute error becomes small, which has a dramatic positive consequence for the distribution tail [77]. The background of the tilted Edgeworth expansion is given in Appendix C.

A summary of the saddlepoint approximation theory is given in the following Lemma, which is instrumental for further analysis.

Lemma 1: Let $Y_1, \cdots, Y_n$ be independent and identically distributed (i.i.d) random variables with the Moment Generation Function (MGF) $M_Y(\theta) = E[\exp(\theta Y)]$, and $\sup\{\theta : M_Y(\theta) < \infty\} = \tau_2$; $S_n = \sum_{i=1}^{n} Y_i$ is a compound sum, where n is a Poisson random variable with mean υ. Its MGF is

$$M_c(\theta) = E\left[\exp(\theta S_n)\right] = \exp\left\{\upsilon\left[M_Y(\theta) - 1\right]\right\} \tag{3.17}$$

where the subscript c stands for compound. When $M_Y(\theta)$ is finite for $\theta < \tau_2$ with $\tau_2 > 0$, and $M_Y(\theta) \to \infty$ for $\theta \to \tau_2$, the probability of S_n exceeding a threshold s is

$$\Pr(S_n > s) = Q(z_2 + z_2^{-1}\ln(z_3/z_2))\left\{1 + O[\rho_{c4}(\hat{\theta})]\right\} \tag{3.18}$$

where $Q(x) = 1/\sqrt{2\pi}\int_x^\infty \exp(-u^2/2)\,du$ is the standard Q-function; O is the big-O function[2], $\hat{\theta}$ is a saddle point which is a solution of the stationarity condition $\upsilon M_Y'(\theta) = s$;

$$\begin{aligned}\rho_{ck}(\hat{\theta}) &= \frac{\upsilon M_Y^{(k)}(\hat{\theta})}{[\upsilon M_Y''(\hat{\theta})]^{k/2}},\\ z_2 &= \mathrm{sgn}(\hat{\theta})(2\hat{\theta}s - 2\upsilon(M_Y(\hat{\theta})-1))^{1/2},\\ z_3 &= \hat{\theta}\sqrt{\upsilon M_Y''(\hat{\theta})},\end{aligned}$$

and $\mathrm{sgn}(x) = 1$ for $x \geq 0$ and -1 otherwise.

Proof: see [[76], Ch.7]. ■

Based on this Lemma, one obtains a rigorous result supporting the intuitive discussion above.

Theorem 2: When $D_{\max} < \infty$ and $D \to \infty$, which implies $D > D_{\max}$, the CR outage probability can be expressed as:

$$P_{out} = Q\left(z_2 + z_2^{-1}\ln(z_3/z_2)\right)(1 + o(1)) \tag{3.19}$$

where

$$z_2 = \mathrm{sgn}(\hat{\theta})\left(2\hat{\theta}d_1 - \frac{4}{\nu}\int_{N_{\max}^{-\nu/2}}^{N_s^{-\nu/2}} \exp(\hat{\theta}x)\; x^{-1-2/\nu}dx - 2N_r\right)^{1/2}, \tag{3.20}$$

$$z_3 = \hat{\theta}\left(\frac{2}{\nu}\int_{N_{\max}^{-\nu/2}}^{N_s^{-\nu/2}} \exp(\hat{\theta}x)\; x^{1-2/\nu}dx\right)^{1/2}, \tag{3.21}$$

[2] $y(x) = O(g(x))$ if $|y(x)/g(x)| \leq C < \infty$ as $x \to \infty$, where C is a constant [75, 78].

and $d_1 = D/D_1$ is the normalized threshold INR,

$$D_1 = 1/R_1^{\nu} P_0 = (\pi\lambda)^{\nu/2}/P_0,$$

and R_1 is the radius of the disk with on average one node in it (so that D_1 is the INR from the boundary of that disk[3]); $N_r = \pi\lambda(R_{\max}^2 - R_s^2)$ is the average number of nodes in the ring between the circles of radii $R_{\max}$ and R_s; $N_s = \pi\lambda R_s^2$ is the average number of nodes in the forbidden region of the radius R_s; $N_{\max} = \pi\lambda R_{\max}^2$ is the average number of nodes in the disk of radius $R_{\max}$, and $\hat{\theta}$ is the solution of the following saddle-point equation[4]

$$d_1 = \frac{2}{\nu} \int_{N_{\max}^{-\nu/2}}^{N_s^{-\nu/2}} \exp(\hat{\theta}x)\; x^{-2/\nu} dx \tag{3.22}$$

An asymptotic analytical solution for the saddle-point $\hat{\theta}$ is

$$\hat{\theta} = N_s^{\nu/2} \left(\ln w + \ln\ln w\right) + o(\ln\ln w) \tag{3.23}$$

where $w = \nu N_s^{\nu/2-1} d_1/2$, and

$$z_2 = \operatorname{sgn}(\hat{\theta}) \left\{2d_1(\hat{\theta} - N_s^{\nu/2})\right\}^{1/2} (1 + o(1)), \tag{3.24}$$

$$z_3 = \hat{\theta}\sqrt{d_1 N_s^{-\nu/2}}\,(1 + o(1)). \tag{3.25}$$

[3] it is also a critical value which separates the high and low outage probability regions in non-CR networks [9].

[4] Unfortunately, this is an integral equation for which an analytical solution is not known. Since it involves a finite-interval integral, it can be solved efficiently using any known numerical technique [79]. Alternatively, (3.23), (3.24) and (3.25) give a closed-form asymptotic solution.

Proof: see the Appendix A.1. ■

Note that Theorem 2 includes two parts: part I is the asymptotic outage probability in (3.19)-(3.21) while the saddle-point is evaluated via (3.22) (e.g., numerically); part II also makes use of (3.19) but also adds to it the asymptotic expansions in (3.23)-(3.25). While the Gaussian or Edgeworth expansion [11, 12] can provide a small absolute error (and thus non-negligible % error), the saddle point approximation above gives a small relative (%) error as shown by the $(1 + o(1))$ term in (3.19), so that only the latter is accurate at the distribution tail [77]. The next section shows that (3.19) can be used as an accurate approximation (without $o(1)$ term) for finite but large D when $D > D_{\max}$, and that the saddlepoint approach reduces the approximation error significantly compared to the Gaussian or Edgeworth approximations. The following Corollary shows that, unlike the outage probability in (3.13) which decays only polynomially in D (heavy tail), that in (3.19) decays super-exponentially, i.e., much faster.

Corollary 2: When $D_{\max} < \infty$ and $D \to \infty$, the outage probability in (3.19) decays as

$$P_{out} = \exp\{-N_s^{\nu/2} d_1 \ln d_1 (1 + o(1))\} \tag{3.26}$$

Proof:

From (3.24) and (3.25),

$$z_2 = (2d_1\hat{\theta})^{1/2} (1 + o(1)),$$

and

$$z_2^{-1}\ln(z_3/z_2) = o(z_2).$$

so that, from (3.19)

$$P_{out} = Q\left(z_2\left(1+o\left(1\right)\right)\right).$$

Since

$$Q(x) = \frac{1}{\sqrt{2\pi}x}\exp\left(-x^2/2\right)\left(1+o\left(1\right)\right),$$

$$\begin{aligned} P_{out} &= Q\left(z_2\left(1+o\left(1\right)\right)\right) \\ &= \frac{1}{\sqrt{2\pi}z_2}\exp\left(-z_2^2/2\left(1+o\left(1\right)\right)\right) \\ &= \exp\left(-z_2^2/2\left(1+o\left(1\right)\right)\right) \\ &= \exp\left(-d_1\hat{\theta}\left(1+o\left(1\right)\right)\right) \\ &= \exp\left(-N_s^{\nu/2}d_1\ln d_1\left(1+o\left(1\right)\right)\right) \end{aligned} \tag{3.27}$$

■

This qualitative transition in the behavior of P_{out} around the $D = D_{\max}$ point is in agreement with the earlier empirical observations in the literature [15].

A similar result has been obtained earlier in [14] via the large deviation analysis. In our notations, it can be expressed as (see Theorems 12 in [14]):

$$P_{out} = c\cdot\exp\left(-b\cdot d_1\ln\left(d_1\right)\left(1+o(1)\right)\right) \tag{3.28}$$

where c and b are undetermined constants[5]. Comparing this to (3.26), one observes that the latter includes the relevant constant and thus can be used to estimate P_{out},

[5]The large deviation analysis does not capture them. In fact, c can also be a function of d_1: $c = o(d_1\ln d_1)$.

unlike the former. Unfortunately, the $(1+o(1))$ term appears in the exponent and thus creates a significant uncertainty[6] (see also below). The following Corollary eliminates this uncertainty via an upper bound, leaving vanishing multiplicative uncertainty only.

Corollary 3: When $D_{\max} < \infty$ and $D \to \infty$, the outage probability in (3.19) can be upper bounded as

$$P_{out} \leq \frac{1}{2} \exp\left\{-N_s^{\nu/2} d_1 \left(\ln d_1 + a_1\right)\right\} \left(1 + o\left(1\right)\right), \tag{3.29}$$

where $a_1 = \frac{\nu}{2} \ln N_s - \ln(2N_{\max}/\nu) - (N_{\max}/N_s)^{1+2/\nu} + N_r N_s^{-\nu/2} d_1^{-1}$.

Proof:

Let us consider the integral $\int_a^b \exp(\hat{\theta}x)\ x^{-p} dx$ in (A.5). It can be upper bounded as

$$\frac{d_1}{p} = \int_a^b \frac{\exp(\hat{\theta}x)}{x^p} dx \leq \frac{\int_a^b \exp(\hat{\theta}x) dx}{a^p} \leq \frac{\exp(\hat{\theta}b)}{a^p \hat{\theta}} \left[1 - \exp\left(-\hat{\theta}(b-a)\right)\right] \tag{3.30}$$

similarly,

$$\frac{d_1}{p} \geq \frac{\exp(\hat{\theta}b)}{b^p \hat{\theta}} \left[1 - \exp\left(-\hat{\theta}(b-a)\right)\right] \tag{3.31}$$

Using the standard tools of asymptotic analysis (see e.g., [75]), when x is large, the lower bound for x in the equation $e^x/x = \mu$ is $x \geq \ln \mu$, so that the lower bound for $\hat{\theta}$ is

$$\hat{\theta} \geq N_s^{\nu/2} (\ln d_1 + a_2) \tag{3.32}$$

[6]It can be shown that $d_1^p = e^{o(d_1 \ln d_1)}\ \forall p < \infty$ or $d_1^{d_1^\alpha} = e^{o(d_1 \ln d_1)}, 0 < \alpha < 1$, i.e., unbounded polynomial or super-polynomial may be present in front of the exponent in (3.26) and (3.28).

where

$$a_2 = p\ln a - \ln b - \ln p = \frac{\nu}{2}\ln N_s - \ln(2N_{\max}/\nu)$$

When $D \to \infty$, then $\hat{\theta} \to \infty$, which implies that $\hat{\theta} > 0$ for sufficiently large D, so that

$$z_2^2 \le 2\hat{\theta}d_1 + 2N_r, \quad z_3^2 \ge pa^{1-p}\hat{\theta}\exp(\hat{\theta}b)[1-\exp(-\hat{\theta}(b-a))] = \hat{\theta}^2 d_1(1+o(1))$$

and also $z_3 \ge z_2 > 0$. Therefore, $z_2^{-1}\ln(z_3/z_2) \ge 0$ and

$$z_1 = z_2 + z_2^{-1}\ln(z_3/z_2) \ge z_2.$$

On the other hand, when $\hat{\theta} > 0$,

$$z_2^2 \ge 2\hat{\theta}d_1 + 2N_r - \frac{2p\exp(\hat{\theta}b)}{a^{1+p}\hat{\theta}}[1-\exp(-\hat{\theta}(b-a))] \tag{3.33}$$

and using (3.31) and (3.33), one obtain

$$z_2^2 \ge 2\hat{\theta}d_1 + 2N_r - \frac{2d_1 b^p}{a^{1+p}} \tag{3.34}$$

Using these facts, the outage probability in (3.19) can now be bounded as

$$\begin{aligned}
P_{out} &= Q(z_1)(1+o(1)) \\
&\le \frac{1}{2}\exp(-z_1^2/2)(1+o(1)) \\
&\le \frac{1}{2}\exp(-z_2^2/2)(1+o(1)) \\
&\le \frac{1}{2}\exp\left\{-d_1\left(N_s^{\nu/2}(\ln d_1 + a_2) - \frac{N_{\max}^{1+2/\nu}}{N_s} + \frac{N_r}{d_1}\right)\right\}(1+o(1)) \\
&= \frac{1}{2}\exp\left\{-N_s^{\nu/2}d_1(\ln d_1 + a_1)\right\}(1+o(1))
\end{aligned} \tag{3.35}$$

■

Further comparison of (3.26) and (3.28) to (3.19) shows that the latter eliminates any exponential uncertainty and provides low % error when estimating P_{out} (provided that a numerical solution is used for (3.22)), which is also supported by the simulation study below. To understand the implications of the $o(1)$ term better, consider the relative error ε in (3.19):

$$\varepsilon = \frac{P_{out} - \tilde{P}_{out}}{P_{out}} = o(1) \tag{3.36}$$

where $\tilde{P}_{out}$ is the right-hand side of (3.19) without the $o(1)$ term, i.e., used as an approximation. It follows that $\varepsilon \to 0$ as $D \to \infty$, i.e., % error $\to 0$. On the other hand, when $\tilde{P}_{out}$ is the right-hand side of (3.26) or (3.28) without the $o(1)$ term, one obtains

$$\varepsilon = \exp\left(o\left(d_1 \ln d_1\right)\right) \tag{3.37}$$

so that % error may be unbounded ($\to \infty$) as the examples in footnote 6 demonstrate. Therefore, the saddle-point asymptotic in Theorem 2 is the best as the $(1+o(1))$ term enters multiplicatives rather than exponentially, providing small % error.

3.4 Non-asymptotic outage probability

The asymptotic results in Theorems 1, 2 and Corollary 1 can be used as approximations (without $o(1)$ terms) for finite but large D under certain conditions, which we summarize below based on the concept of typical outage events by considering three typical cases.

3.4.1 Case 1: $D < D_{\max}$ and $D_1 < D_{\max}$.

From Theorem 1 and Corollary 1, for finite but large D and $D < D_{\max}$, $P_{out} \approx P_{out,1}$. The key question is: "When is D sufficiently large so that the approximation is accurate?" From [9], the nearest interferer approximation is accurate in the conventional network when $D > D_1$ (i.e., the low-outage regime), where $D_1 = (\pi\lambda)^{\nu/2}/P_0$ is a critical value which separates the high and low outage probability regions, and is the INR coming from the boundary of the disk (centered on the PU) with on average one node in it. As Theorem 1 links P_{out} and P_{con}, the corresponding condition also applies to the former, so that large D means $D_{\max} > D > D_1$, the aggregate interference is dominated by the nearest node one and $P_{out} \approx P_{out,1}$. This is possible when $D_1 < D_{\max}$, which implies $R_s < R_1$, i.e., a small forbidden region. The 1st constraint $D_1 < D$ can be further removed by observing that $P_{out,1} \leq P_{out}$ $\forall D$ (since one way for an outage to occur is when the nearest node interference exceeds the threshold) and that $P_{out,1} \to 1$ as $D \to 0$ so that $P_{out,1} \approx P_{out}$ in this high-outage regime; finally, $P_{out} \approx P_{out,1}$ $\forall D < D_{\max}$. Fig. 3.3 shows the outage probability for Case 1. When $D < D_{\max}$ (heavy tail or below-critical regime), it is well approximated by the nearest node one $P_{out,1}$. Note that the standard Edgeworth expansion (e.g., as in [12]) is significantly less accurate in this case. On the other hand, since the nearest node interference can not exceed $D_{\max}$, the above approximation breaks down when $D > D_{\max}$ (super-exponential or above-critical regime). These observation have been validated via extensive Monte-Carlo simulations for a wide range of system parameters, of which Fig. 3.3 is only a sample. More simulation results are given in Section 3.5.

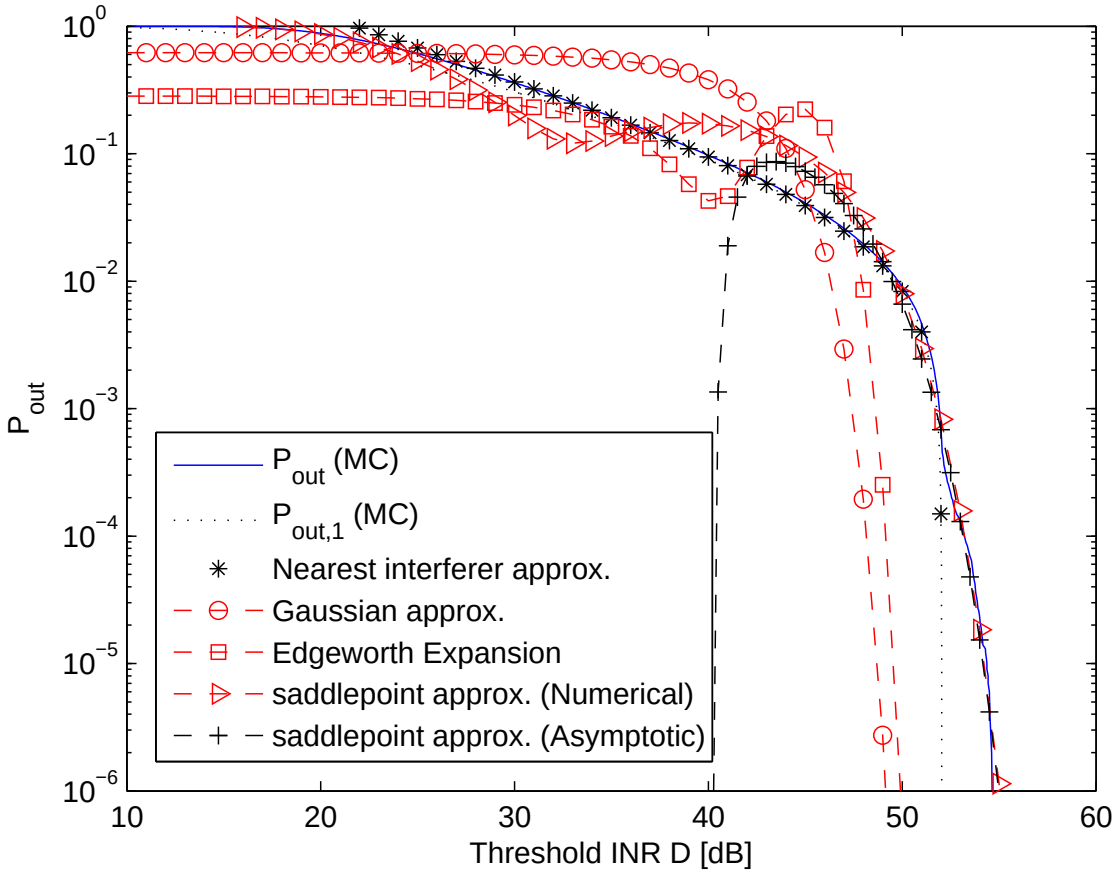

Fig. 3.3 Outage probability for $D_{\max} > D_1$ ($R_s < R_1$ or small forbidden region). The simulation parameters are $\nu = 4$, $R_s = 10m$, $R_1 = 56m$, $R_0 = 200m$, $R_{\max} = 10^3 m$, $\lambda = 10^{-4}$ [nodes/m^2], $D_1 = 22$dB, $D_{\max} = 52$dB. MC denotes Monte-Carlo simulations (5×10^6 runs).

3.4.2 Case 2: $D > D_{\max}$ and $D_1 < D_{\max}$.

When $D_1 < D_{\max}$ (which implies $R_s < R_1$, i.e., a small forbidden region) and $D > D_{\max}$, a single node contribution can not cause an outage so that combined contribution of a few nodes is required. On the other hand, the number n of nodes contributing to a typical outage event is not sufficiently large for a practically-important outage range (say $P_{out} > 10^{-6}$), so that Gaussian or Edgeworth approximations are not accurate, as Fig. 3.3 shows. However, as explained above, the saddlepoint method tilts the original distribution and makes the relative (%) error small so that its accuracy is much better at the tail. Fig. 3.3 shows the saddlepoint approximation for $R_s < R_1$. When $D > D_{\max}$, its accuracy is remarkably good. On the other hand, when $D < D_{\max}$, the saddlepoint approximation is not accurate since the aggregate interference is dominated by the nearest node one and the CLT-type argument is not expected to work well in this case, so that Theorems 1 and 2 are essentially complementary to each other, providing a combined accurate approximation of P_{out} for the whole INR range via three typical regimes, which are summarized below:

$\diamond$ *High-outage regime*: $D < D_1$ so that $P_{out} \approx 1$. Nearest node dominates.

$\diamond$ *Below-critical (heavy tail) regime*: $D_1 < D < D_{\max}$ so that $P_{out} \approx P_{out,1} \approx (1 - d^{2/\nu})N_0 D^{-2/\nu}$. Nearest node dominates.

$\diamond$ *Above-critical (super-exponential tail) regime*: $D > D_{\max}$ so that P_{out} is as in (3.19) and (3.26). Several nodes contribute to typical outage events.

These regimes are illustrated in Fig. 3.4. It is interesting to observe that these regimes are also inline with the corresponding observations in [18] which identify different modes of convergence for truncated Levy flights.

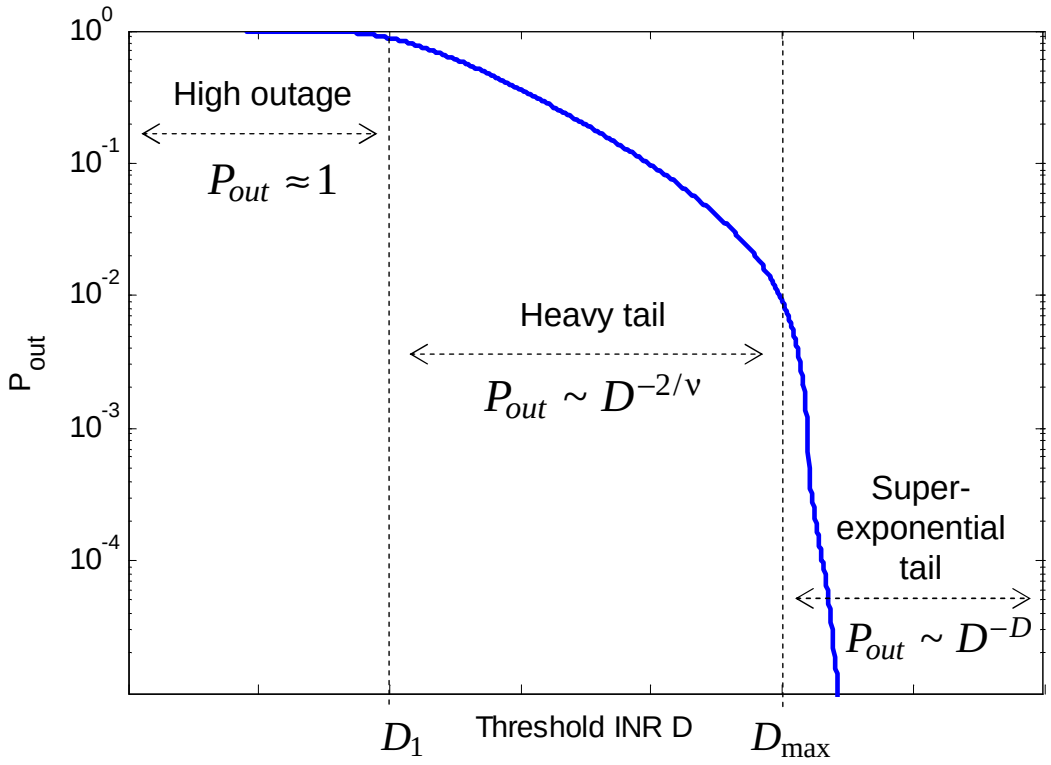

Fig. 3.4 Three different regimes in the outage probability vs. INR behavior when $D_1 < D_{\max}$. If $D_1 > D_{\max}$, the heavy-tail regime disappears.

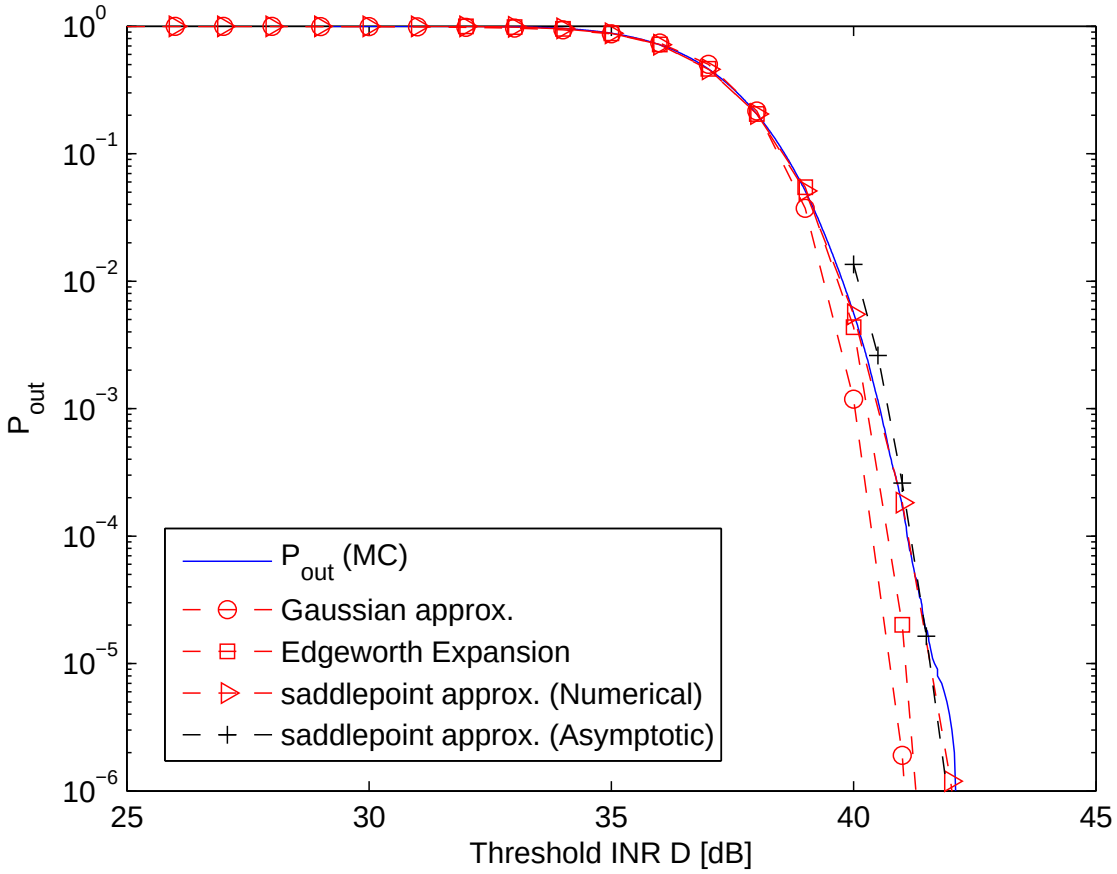

Fig. 3.5 Outage probability for $D_1 > D_{\max}$ ($R_s > R_1$, i.e., large forbidden region). The simulation parameters are $\nu = 4$, $R_s = 32m$, $R_1 = 18m$, $R_0 = 200m$, $R_{\max} = 10^3 m$, $\lambda = 10^{-3}[\text{nodes/m}^2]$, $D_1 = 42\text{dB}$, $D_{\max} = 32\text{dB}$. MC denotes Monte-Carlo simulations (10^6 runs).

3.4.3 Case 3: $D_1 > D_{\max}$.

When $D_1 > D_{\max}$, which implies $R_s > R_1$, i.e., a large forbidden region, n is large in the low outage range, i.e., a typical outage event is when the combination of interference from many nodes exceeds the threshold, and the aggregate interference is closely approximated by a Gaussian random variable, $\sum_{i=1}^{N} I_i \sim \mathcal{N}$ [15, 17]. As Fig. 3.5 demonstrates, the Gaussian and Edgeworth approximations are accurate with $1-$ 2 dB gap at the tail, and the saddlepoint approximation is the most accurate one with 0.1 dB gap at the tail. The closed-form expression of the saddlepoint approximation is less accurate than the numerical one, since the former was based on the asymptotic expansions in (3.23) - (3.25).

3.5 Simulation details and results

In this section, simulation details and more results will be demonstrated.

3.5.1 Simulation details

We use Matlab to run the Monte Carlo (MC) simulations. The sample code is given in Appendix B.1. We use the system model given in Chapter 3.1. In all simulations, we generate random geometry of the CR network based on Poisson point process for each run, and the parameters given in the figure captions. We fixed $R_{\max} = 1000m$, and the noise power after normalization is 200^{-4}, so $R_0 = 200^{4/\nu}$. The path loss ν, the radius of the forbidden region R_s and the density of active SU nodes λ are variables for different cases. The results are based on 10^6 runs.

In [12], the authors derived the cumulants of the aggregate interference for $\nu > 2$ and $R_{\max} \to \infty$. In this thesis, we introduce a simpler way to obtain the cumulants including $\nu = 2$ scenario, and $R_{\max}$ can be finite as well. The PDF of the interference

I coming from a single node (without ordering) is:

$$f_I(I) = \begin{cases} \frac{2}{\nu}\frac{I^{-1-2/\nu}}{R_{\max}^2 - R_s^2} & R_{\max}^{-\nu} \leq I \leq R_s^{-\nu} \\ 0 & \text{otherwise} \end{cases} \tag{3.38}$$

From the system model, $I_{ag} = \sum_{i=1}^{N} I_i$, where N is Poisson random variable, and independent of each I_i. The MGF of I_{ag} is

$$M_{I_{ag}}(\theta) = E\left[\exp(\theta I_{ag})\right] = \exp\left\{\upsilon\left[M_I\left(\theta\right) - 1\right]\right\} \tag{3.39}$$

where $\upsilon = \lambda\pi\left(R_{\max}^2 - R_s^2\right)$ is the mean of N.

The cumulant generating function (CGF) is defined as:

$$G_x(\theta) = \ln(M_x(\theta)) = \ln(E(\exp(\theta x))).$$

The n_{th} cumulant can be extracted from the CGF via differentiation at zero of $G_x(\theta)$,

$$\kappa_n = G_x^{(n)}(0).$$

So that the n_{th} cumulant of I_{ag} is

$$\kappa_n = G_{I_{ag}}^{(n)}(0) = \upsilon M_I^{(n)}(0). \tag{3.40}$$

From (3.38),

$$M_I\left(\theta\right) = \frac{2}{\nu(R_{\max}^2 - R_s^2)} \int_{R_{\max}^{-\nu}}^{R_s^{-\nu}} \exp(\theta I)\ I^{-1-2/\nu} dI,$$

and

$$M_I^{(n)}(\theta) = \frac{2}{\nu(R_{\max}^2 - R_s^2)} \int_{R_{\max}^{-\nu}}^{R_s^{-\nu}} \exp(\theta I)\ I^{n-1-2/\nu} dI.$$

So that,

$$M_I^{(n)}(0) = \begin{cases} \frac{2(R_s^{2-n\nu} - R_{\max}^{2-n\nu})}{(n\nu-2)(R_{\max}^2 - R_s^2)} & \nu > 0 \text{ and } \nu \neq \frac{2}{n} \\ \frac{2(\ln R_{\max} - \ln R_s)}{R_{\max}^2 - R_s^2} & \nu = \frac{2}{n} \end{cases} \tag{3.41}$$

and

$$\kappa_n = \begin{cases} \frac{2\pi\lambda(R_s^{2-n\nu} - R_{\max}^{2-n\nu})}{n\nu-2} & \nu > 0 \text{ and } \nu \neq \frac{2}{n} \\ 2\pi\lambda(\ln R_{\max} - \ln R_s) & \nu = \frac{2}{n}. \end{cases} \tag{3.42}$$

The results are consistent with eq. (40) in [12].

We may use the first two cumulants to generate Gaussian approximation for I_{ag}. The outage probability can be approximated as:

$$P_{out} = \Pr\{\gamma > D\} \approx Q\left(\frac{DP_0 - \kappa_1}{\sqrt{\kappa_2}}\right) \tag{3.43}$$

For Edgeworth expansion, detail can be found in Appendix C. We use the approximation in [69] and [12].

$$P_{out} = \Pr\{\gamma > D\} \approx Q(z) + \phi(z)\frac{\kappa_3}{3!\kappa_2^{3/2}} H_2(z) \tag{3.44}$$

where $z = \frac{DP_0 - \kappa_1}{\sqrt{\kappa_2}}$; $\phi(x) = \exp(-x^2/2)/\sqrt{2\pi}$ is the pdf of $\mathcal{N}(0,1)$, $H_r(x)$ is the Hermite polynomial of degree r, and $H_2(x) = x^2 - 1$.

In all figures, $P_{out}(MC)$ curve is generated by the Monte Carlo simulation results of the outage probability causing by aggregate interference; $P_1(MC)$ curve is generated by the Monte Carlo simulation results of the outage probability causing by the nearest interference; Nearest interferer approx curve is generated based on (3.12); Gaussian approx curve is generated based on (3.43); Edgeworth Expansion curve is generated

based on (3.44); saddlepoint approximation (Numerical) curve is generated based on the numerical solution in (3.19)-(3.21) while the saddle-point is evaluated via (3.22) using Mathcad; saddlepoint approximation (Asymptotic) curve is generated based on the asymptotic expansions in (3.23)-(3.25).

3.5.2 Simulation results

First, let us study the outage probability with different path losses.

Fig. 3.3 and 3.6-3.10 show the outage probability with path loss ν from 8 to 2 for $D_1 < D_{\max}$ scenarios. For other simulation parameters, $R_s = 10m$, $R_1 = 56m$, $\lambda = 10^{-4}$ [nodes/m^2]. As shown in Fig. 3.3 with $\nu = 4$, there are clear as three regions which are described in 3.4 for $\nu = 8$ and $\nu = 6$ cases. We emphasize them here:

$\diamond$ *High-outage regime*: $D < D_1$ so that $P_{out} \approx 1$. Nearest node dominates.

$\diamond$ *Below-critical (heavy tail) regime*: $D_1 < D < D_{\max}$ so that $P_{out} \approx P_{out,1} \approx (1 - d^{2/\nu})N_0 D^{-2/\nu}$. Nearest node dominates.

$\diamond$ *Above-critical (super-exponential tail) regime*: $D > D_{\max}$ so that P_{out} is as in (3.19) and (3.26). Several nodes contribute to typical outage events.

For $\nu = 2$ scenario, the convergence from P_{out} to $P_{out,1}$ is quite slower than that in larger ν scenarios. The reason is that when ν is small, nearest node dominating happens in very low outage region. $I = R^{-\nu}$, so the difference between the nearest node interference and the second or third nearest node interference is not as big as the large ν scenarios in heavy tail regime. On the other hand, the gap between D_1 and $D_{\max}$ is smaller, so the room for convergence is smaller. If we let $D_{\max} \to \infty$, i.e., no forbidden region, P_{out} will converge to $P_{out,1}$ in the low outage region for sure. Please see Fig. 3.11.

Our approximations also apply for $\nu < 2$ scenarios, and their behaviors are similar to that of $\nu = 2$ scenario. This can be observed from the analytic expressions and

simulations.

In heavy tail region, with larger ν, P_{out} decays more slowly, since $P_{out} \sim D^{-2/\nu}$. We observe this behavior also in simulations. In super-exponential tail regime, the saddle point approximation (numerical solution) is the most accurate one among all approximations.

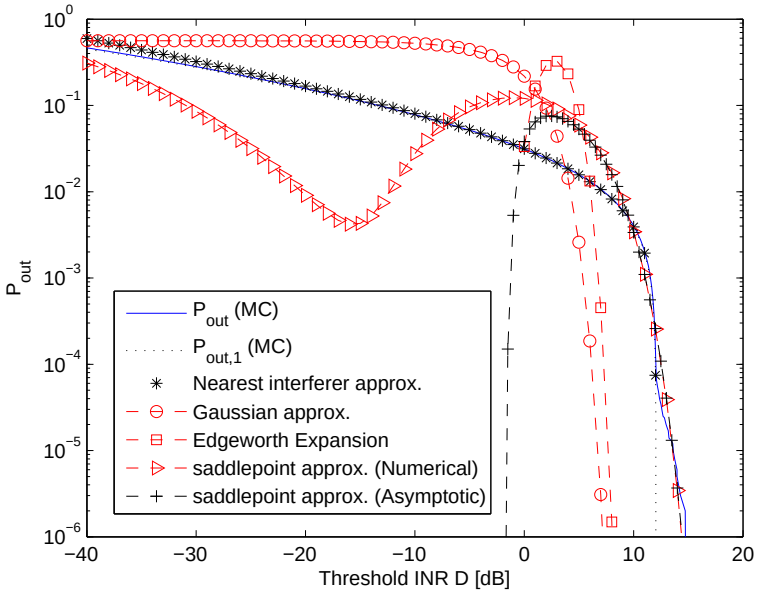

Fig. 3.6 Outage probability for $D_{\max} > D_1$ ($R_s < R_1$ or small forbidden region). The simulation parameters are $\nu = 8$, $R_s = 10m$, $R_1 = 56m$, $R_{\max} = 10^3 m$, $\lambda = 10^{-4}$ [nodes/m^2], $D_1 = -48$dB, $D_{\max} = 12$dB.

In Figures with $R_s < R_1$, the curves of Edgeworth expansion and saddle-point approx (numerical solutions) show ups and downs. It comes from the approximate nature of this expansions, which do not have to be monotonically-decreasing as a true CCDF always is (for example, Taylor expansion of exp(-x) oscillates while the function itself is clearly monotonic). Edgeworth expansion we use is from (3.44) where the second term introduces the oscillations in this case. Similar reasoning applies to the saddlepoint approximation when the saddle point $\hat{\theta} \to 0$, and then changes the

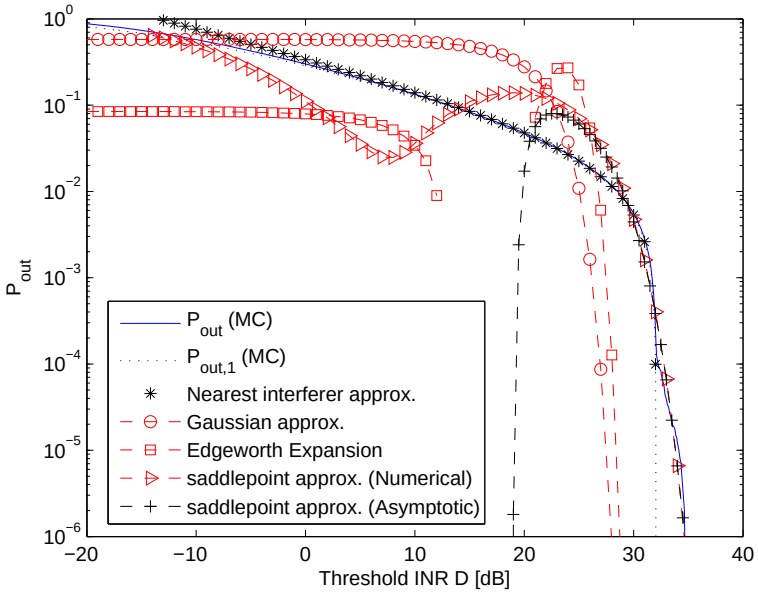

Fig. 3.7 Outage probability for $D_{\max} > D_1$ ($R_s < R_1$ or small forbidden region). The simulation parameters are $\nu = 6$, $R_s = 10m$, $R_1 = 56m$, $R_{\max} = 10^3 m$, $\lambda = 10^{-4}$ [nodes/m^2], $D_1 = -13$dB, $D_{\max} = 32$dB.

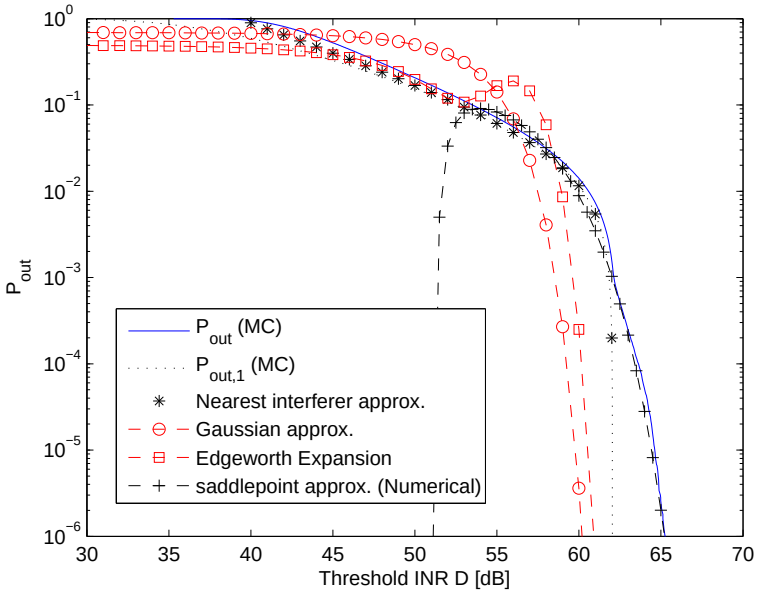

Fig. 3.8 Outage probability for $D_{\max} > D_1$ ($R_s < R_1$ or small forbidden region). The simulation parameters are $\nu = 3$, $R_s = 10m$, $R_1 = 56m$, $R_{\max} = 10^3 m$, $\lambda = 10^{-4}$ [nodes/m^2], $D_1 = 39$dB, $D_{\max} = 62$dB.

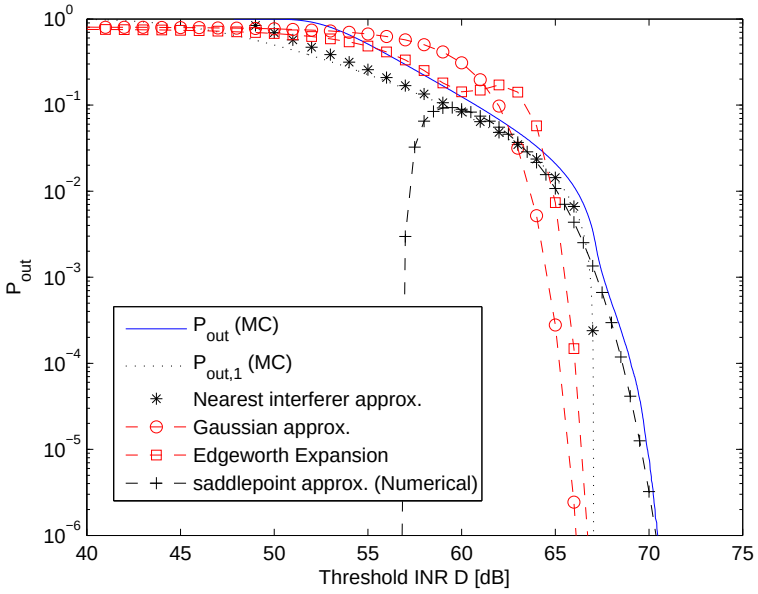

Fig. 3.9 Outage probability for $D_{\max} > D_1$ ($R_s < R_1$ or small forbidden region). The simulation parameters are $\nu = 2.5$, $R_s = 10m$, $R_1 = 56m$, $R_{\max} = 10^3 m$, $\lambda = 10^{-4}$ [nodes/m^2], $D_1 = 48$dB, $D_{\max} = 67$dB.

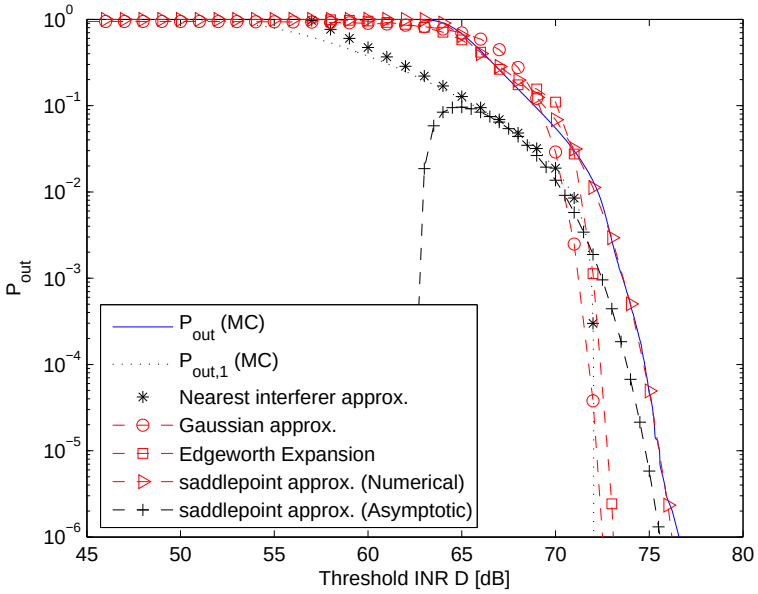

Fig. 3.10 Outage probability for $D_{\max} > D_1$ ($R_s < R_1$ or small forbidden region). The simulation parameters are $\nu = 2$, $R_s = 10m$, $R_1 = 56m$, $R_{\max} = 10^3 m$, $\lambda = 10^{-4}$ [nodes/m^2], $D_1 = 57$dB, $D_{\max} = 72$dB.

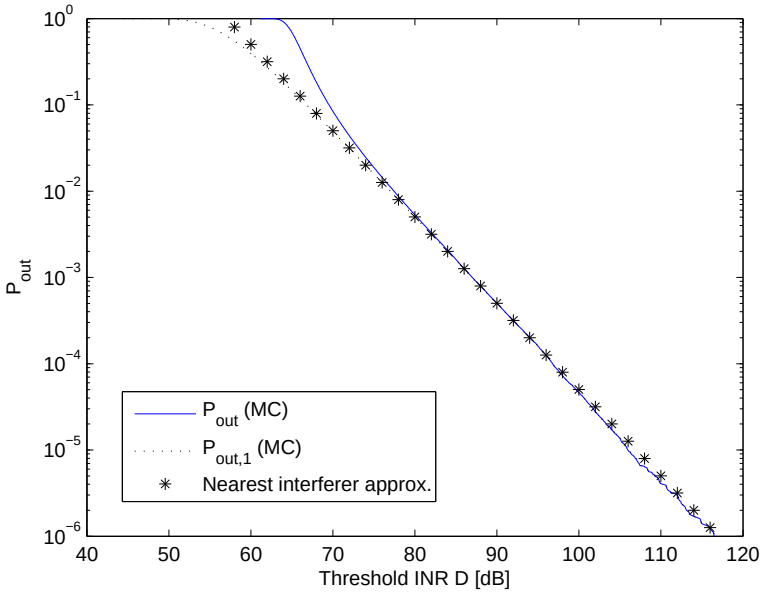

Fig. 3.11 Outage probability under interference cancelation without forbidden region. The simulation parameters are $\nu = 2$, $R_{\max} = 10^3 m$, $\lambda = 10^{-4}$ [nodes/m^2],$D_1 = 57$dB .

sign. In addition to this, the oscillation region corresponds to very small values of $\hat{\theta}$ so that the numerical solution of the non-linear equation in (3.22) is not so accurate, while this never happens in the smaller outage region, where $\hat{\theta}$ is not very small.

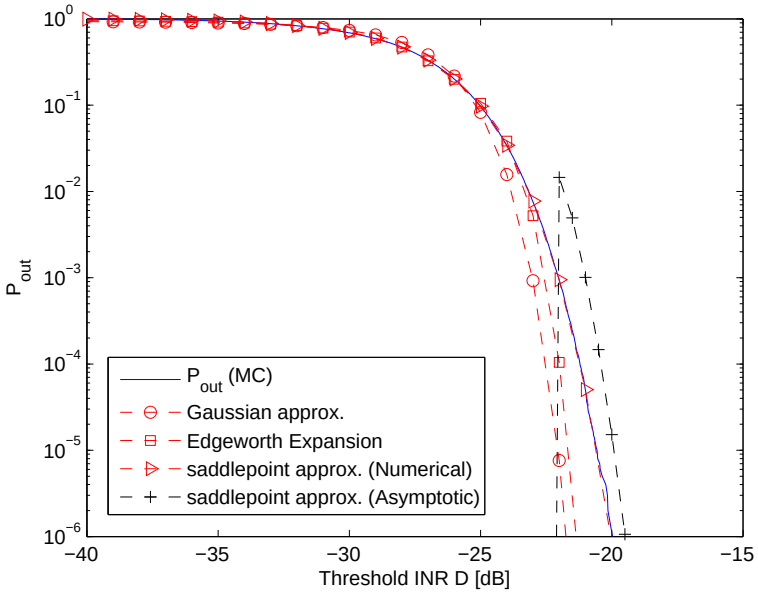

Fig. 3.12 Outage probability for $D_1 > D_{\max}$ ($R_s > R_1$, i.e., large forbidden region). The simulation parameters are $\nu = 8$, $R_s = 32m$, $R_1 = 18m$, $R_{\max} = 10^3 m$, $\lambda = 10^{-3}[\text{nodes/m}^2]$, $D_1 = -8\text{dB}$, $D_{\max} = -28\text{dB}$.

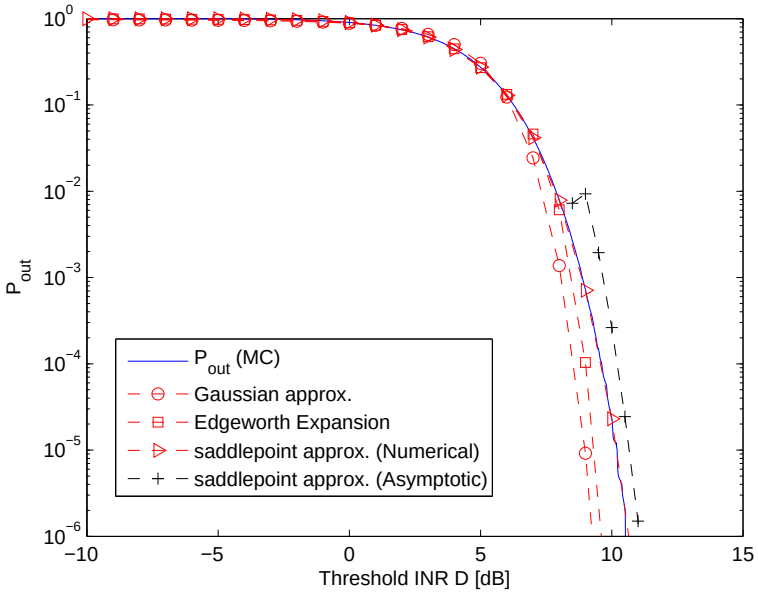

Fig. 3.13 Outage probability for $D_1 > D_{\max}$ ($R_s > R_1$, i.e., large forbidden region). The simulation parameters are $\nu = 6$, $R_s = 32m$, $R_1 = 18m$, $R_{\max} = 10^3 m$, $\lambda = 10^{-3}[\text{nodes/m}^2]$, $D_1 = 17\text{dB}$, $D_{\max} = 2\text{dB}$.

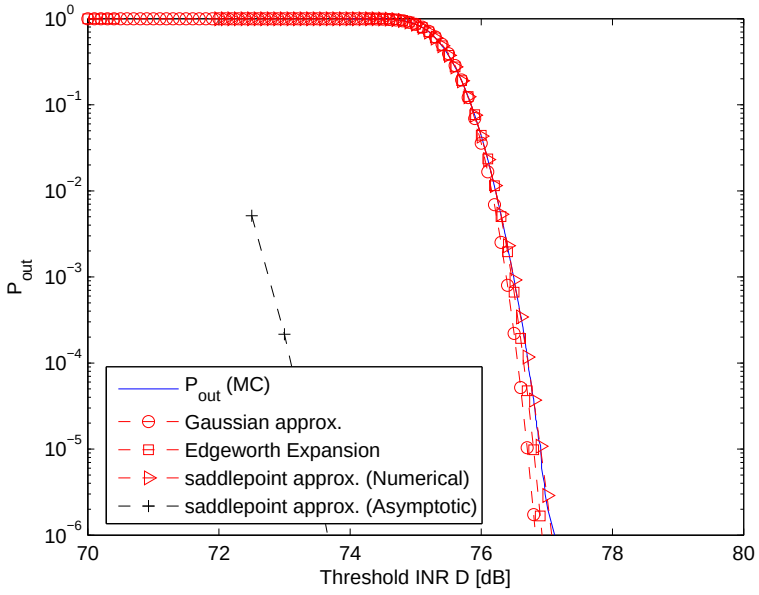

Fig. 3.14 Outage probability for $D_1 > D_{\max}$ ($R_s > R_1$, i.e., large forbidden region). The simulation parameters are $\nu = 2$, $R_s = 32m$, $R_1 = 18m$, $R_{\max} = 10^3 m$, $\lambda = 10^{-3}$[nodes/m^2], $D_1 = 67$dB, $D_{\max} = 62$dB.

Fig. 3.5 and 3.12-3.14 show the outage probability with path loss ν from 8 to 2 for $D_1 > D_{\max}$ scenarios. For other simulation parameters, $R_s = 32m$, $R_1 = 18m$, $\lambda = 10^{-4}$ [nodes/m^2]. As shown in Fig. 3.3 with $\nu = 4$, there are clear two regions which are described in 3.4: high-outage regime and super-exponential tail regime. From the figures, we found that with larger ν, P_{out} decays more slowly. The reason can be found in (3.26) from Corollary 2, and $P_{out} \sim \exp\{-N_s^{\nu/2} d_1 \ln d_1\}$. On the other hand, with larger ν, Gaussian approximation and Edgeworth Expansion are less accurate. The saddle point approximation (numerical solution) is the most accurate one among all approximations.

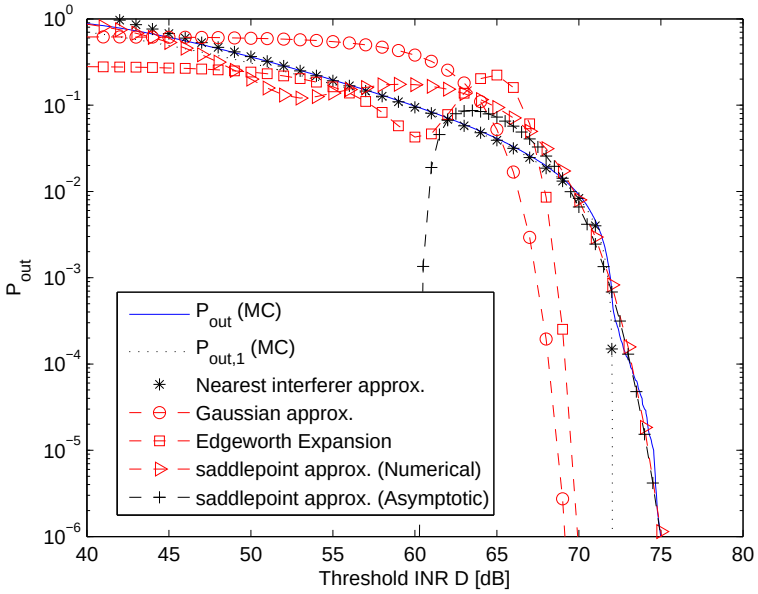

Fig. 3.15 Outage probability for $D_{\max} > D_1$ ($R_s < R_1$ or small forbidden region). The simulation parameters are $\nu = 4$, $R_s = 3m$, $R_1 = 18m$, $R_{\max} = 10^3 m$, $\lambda = 10^{-3}$ [nodes/m^2], $D_1 = 42$dB, $D_{\max} = 72$dB.

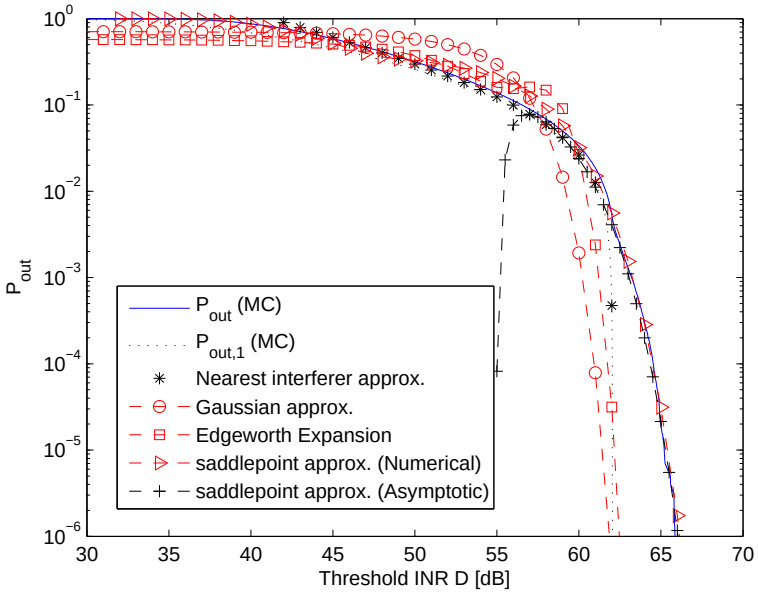

Fig. 3.16 Outage probability for $D_{\max} > D_1$ ($R_s < R_1$ or small forbidden region). The simulation parameters are $\nu = 4$, $R_s = 6m$, $R_1 = 18m$, $R_{\max} = 10^3 m$, $\lambda = 10^{-3}$ [nodes/m^2], $D_1 = 42$dB, $D_{\max} = 62$dB.

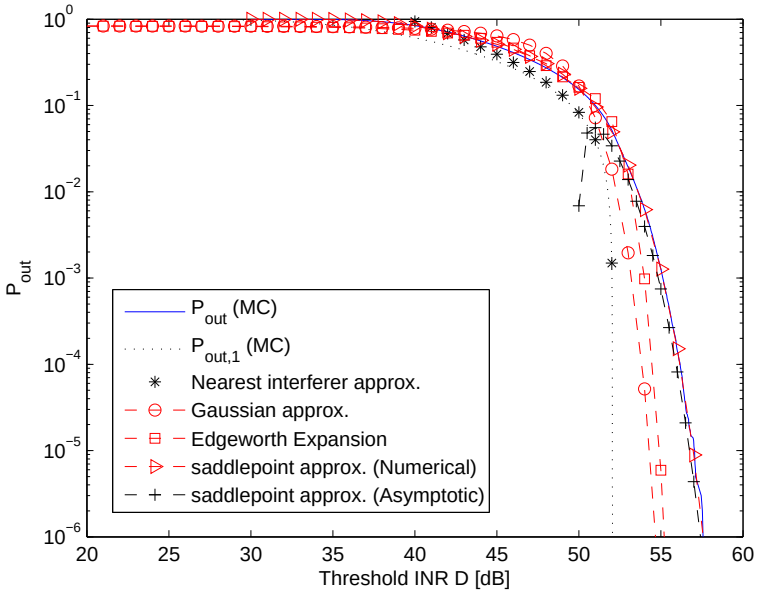

Fig. 3.17 Outage probability for $D_{\max} > D_1$ ($R_s < R_1$ or small forbidden region). The simulation parameters are $\nu = 4$, $R_s = 10m$, $R_1 = 18m$, $R_{\max} = 10^3 m$, $\lambda = 10^{-3}$ [nodes/m^2], $D_1 = 42$dB, $D_{\max} = 52$dB.

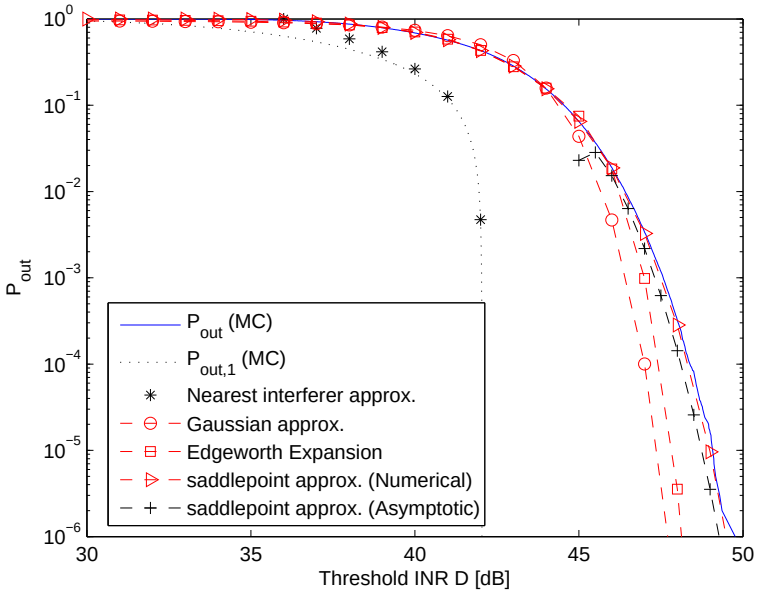

Fig. 3.18 Outage probability for $D_{\max} = D_1$ ($R_s = R_1$). The simulation parameters are $\nu = 4$, $R_s = 18m$, $R_1 = 18m$, $R_{\max} = 10^3 m$, $\lambda = 10^{-3}$ [nodes/m^2], $D_1 = 42$dB, $D_{\max} = 42$dB.

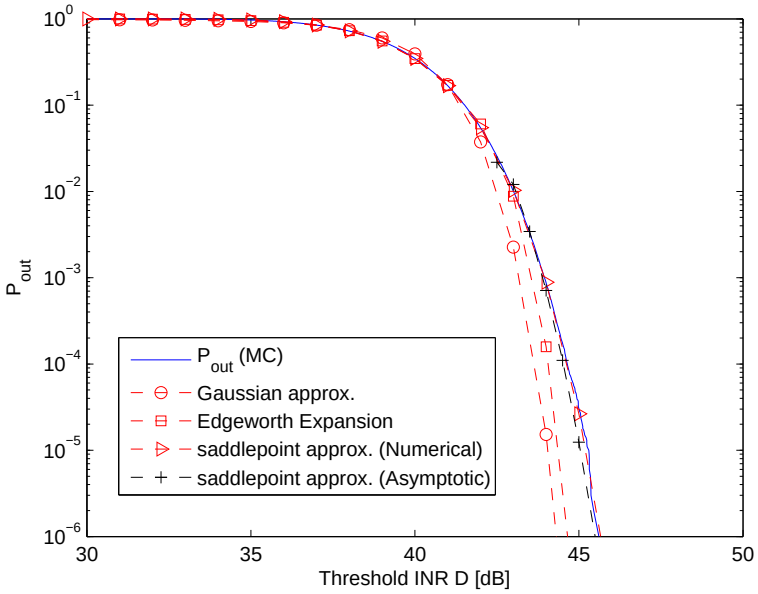

Fig. 3.19 Outage probability for $D_1 > D_{\max}$ ($R_s > R_1$, i.e., large forbidden region). The simulation parameters are $\nu = 4$, $R_s = 24m$, $R_1 = 18m$, $R_{\max} = 10^3 m$, $\lambda = 10^{-3}[\text{nodes/m}^2]$, $D_1 = 42\text{dB}$, $D_{\max} = 37\text{dB}$.

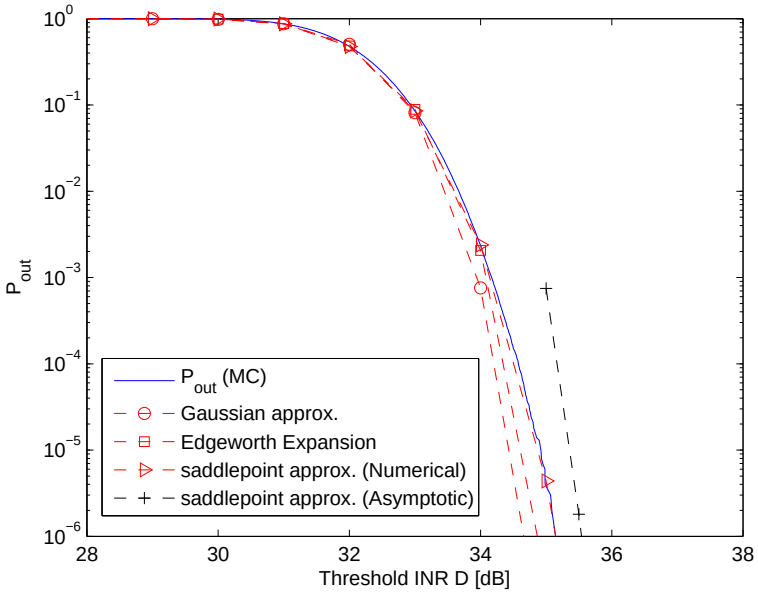

Fig. 3.20 Outage probability for $D_1 > D_{\max}$ ($R_s > R_1$, i.e., large forbidden region). The simulation parameters are $\nu = 4$, $R_s = 56m$, $R_1 = 18m$, $R_{\max} = 10^3 m$, $\lambda = 10^{-3}[\text{nodes/m}^2]$, $D_1 = 42\text{dB}$, $D_{\max} = 22\text{dB}$.

Fig. 3.5 and 3.15-3.20 show the outage probability with fixed $R_1 = 18m$ and varied R_s scenarios. Since R_1 is fixed, D_1 is also fixed. when R_s increases and becomes closer to R_1, the heavy tail regime is getting smaller, and the nearest node approximation becomes less accurate. When $R_s \geq R_1$, the heavy tail regime disappears. Only high-outage regime and super-exponential tail regime remain. Gaussian type approximation becomes accurate in those scenarios. The saddle point approximation (numerical solution) is the most accurate one among all approximations.

3.6 Summary

In this chapter, the distribution of aggregate interference and the outage probability in CR networks for non-fading scenarios have been studied. Based on an asymptotic technique, saddle point theory and the typical outage event, the outage region can be divided into three parts:

◇ *High-outage regime*: $D < D_1$ so that $P_{out} \approx 1$. Nearest node dominates.

◇ *Below-critical (heavy tail) regime*: $D_1 < D < D_{\max}$ so that $P_{out} \approx P_{out,1} \approx (1 - d^{2/\nu})N_0 D^{-2/\nu}$. Nearest node dominates.

◇ *Above-critical (super-exponential tail) regime*: $D > D_{\max}$ so that P_{out} is as in (3.19) and (3.26). Several nodes contribute to typical outage events.

Rigorous analysis is given based on an asymptotic technique and saddle point theory. Theorem 1 and 2 provide the conditions for heavy tail regime and super-exponential tail regime separately. The rigorous foundation has been established for earlier empirical observation in the literature. All results and conclusions are validated via extensive Monte-Carlo simulations.

Chapter 4

Impact of Interference Cancelation

In a CR network and a location-based protocol, some form of protection to the PU receiver is provided by not allowing the SUs in the forbidden region (FR) to transmit. Clearly, the larger the FR, the smaller the interference generated by the remaining (active) SUs, but also the lower the SU spectral efficiency as fewer SUs are allowed to transmit. A compromise solution is to reduce the FR (so that more SUs are allowed to transmit) and to implement an interference cancelation scheme[1] in the PU receiver (so that its quality of service is maintained). PU is willing to do that since it can get some rewards from that by implementing the spectrum trading [19, 60–62], i.e., SUs pay the price for the spectrum which they are using. On the other hand, an interference cancelation can also be implemented at SU transmitter, such as transmit beamforming. In this section, we analyze this scenario using the asymptotic tools developed above.

[1] e.g., null forming by an antenna array as in [80] or any other suitable technique.

4.1 Asymptotic results

Theorem 3: Consider the scenario where, in an addition to the forbidden region, $(k-1)$ nearest (to the PU receiver) interferers located outside the FR are canceled. When $d = D/D_{\max} < 1$ and $D \to \infty$, the CR outage probability $P_{out} = \Pr\{\sum_{i=k}^{N} I_i > DP_0\}$ is still dominated by the nearest active (k-th) node and can be expressed as:

$$\begin{aligned} P_{out} &= P_{out,k}(1+o(1)) = \frac{1}{k!}\left(P_{out,1}\right)^k (1+o(1)) \\ &= \frac{1}{k!}\left[N_0 D^{-2/\nu}(1-d^{2/\nu})\right]^k (1+o(1)) \end{aligned} \tag{4.1}$$

where $P_{out,k} = \Pr\{I_k > DP_0\}$ is the probability that k-th nearest node's interferer exceeds the threshold, and $P_{out,1}$ is that without interference cancelation ($k=1$). The lower bound $P_{out} \geq P_{out,k}$ holds for any D and is tight at high ($D \to \infty$) as well as low ($D \to 0$) INR.

Proof: see the Appendix A.2. ■

Note from (4.1) that P_{out} scales down faster than exponentially in k, so that canceling nearest active interferers pays off well, allowing to maintain low P_{out} for the PU receiver and to increase the spectral efficiency of the SUs. To see this effect in more details, consider the ratio:

$$\frac{P_{out,(k+1)}}{P_{out,k}} = \frac{N_0 D^{-2/\nu}(1-d^{2/\nu})}{k+1} \cdot (1+o(1))$$

Clearly, canceling an extra nearest interferer has a significant beneficial effect for large D. Compared to the conventional network ($d=0$), the impact of the forbidden region on the outage probability is captured by the $(1-d^{2/\nu})^k$ term in (4.1).

Corollary 1 can now be seen as a special case of Theorem 3 with $k=1$.

4.2 Non-asymptotic outage probability and simulation results

Similarly to the no interference cancelation case ($k = 1$), (4.1) can serve as an approximation (without $o(1)$ term) when $D < D_{\max}$,

$$P_{out} \approx P_{out,k} \approx \min\{1, (N_0 D^{-2/\nu}(1 - d^{2/\nu}))^k/k!\} \tag{4.2}$$

where we have used the fact that $1 \geq P_{out} \geq P_{out,k}$, i.e., that P_{out} is at least as large as that due to k-th nearest node and can not exceed one.

We use Matlab to run the Monte Carlo (MC) simulations. The sample code is given in Appendix B.1. We use the system model given in Chapter 3.1. In all simulations, we generate random geometry of the CR network based on Poisson point process for each run, and the parameters given in the figure captions. We fixed $R_{\max} = 1000m$, and the noise power after normalization is 200^{-4}, so $R_0 = 200^{4/\nu}$. The path loss ν, the radius of the forbidden region R_s and the density of active SU nodes λ are variables for different cases. The results are based on 10^6 runs.

To validate this approximation, Fig. 4.1 - 4.8 show the outage probability under interference cancelation when $R_s < R_1$ (small forbidden region). Since $D_{\max}$ is a constant in all figures separately, $d = D/D_{\max}$ becomes a variable along with D. Note that the approximation in (4.2) is quite accurate when $D < D_{\max}$. It is also clear that canceling nearest active node reduces significantly P_{out} in this below-critical regime. For both $k = 1$ and $k = 2$ case, when $D_1 < D \ll D_{\max}$, $P_{out} \sim D^{-2k/\nu}$, since $d = D/D_{\max} \approx 0$. When D close to $D_{\max}$, the affect of the term $(1 - d^{2/\nu})^k$ can not be ignored, and it becomes the dominant parts in (4.2). The outage probability has a transition from the heavy tail region (polynomially decrease in P_{out} as in (4.2)) to the

steep decrease region (super-exponential, as in (3.29)) around the $D = D_{\max}$ point. With k increases, the affect of the term $(1 - d^{2/\nu})^k$ is larger with the same d. So the transition point of $k = 2$ case is a bit smaller than that of $k = 1$ from the simulations.

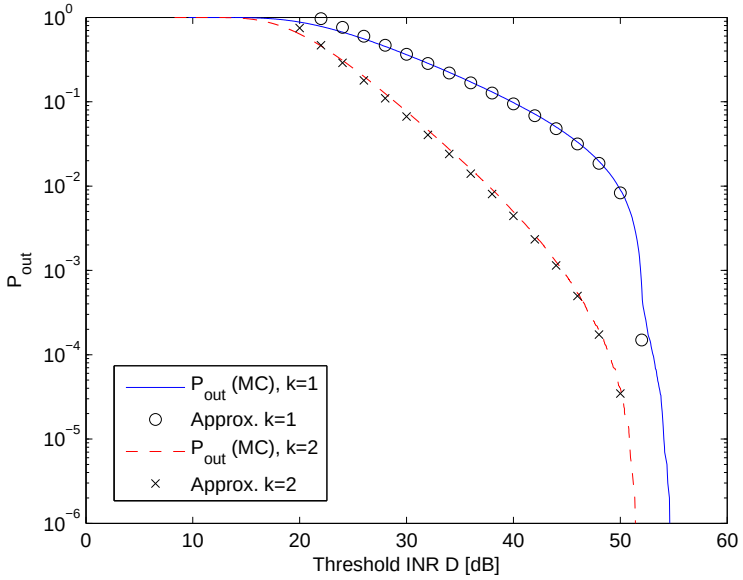

Fig. 4.1 Outage probability with interference cancelation for $D_{\max} > D_1$ in non-fading scenarios ($R_s < R_1$). The simulation parameters are $\nu = 4$, $R_s = 10m$, $R_1 = 56m$, $R_{\max} = 10^3 m$, $\lambda = 10^{-4}[\text{nodes/m}^2]$, $D_1 = 22\text{dB}$, $D_{\max} = 52\text{dB}$.

Fig. 4.1 - 4.3 show the outage probability under interference cancelation with varied R_s, R_1 and λ. The approximation in (4.2) is quite accurate when $D < D_{\max}$ for different $D_{\max}$. Since $\nu = 4$ is fixed for Fig. 4.1- 4.3, the scale of the curves is the same for $k = 1$ and $k = 2$ separately, and $P_{out} \sim D^{-k/2}$.

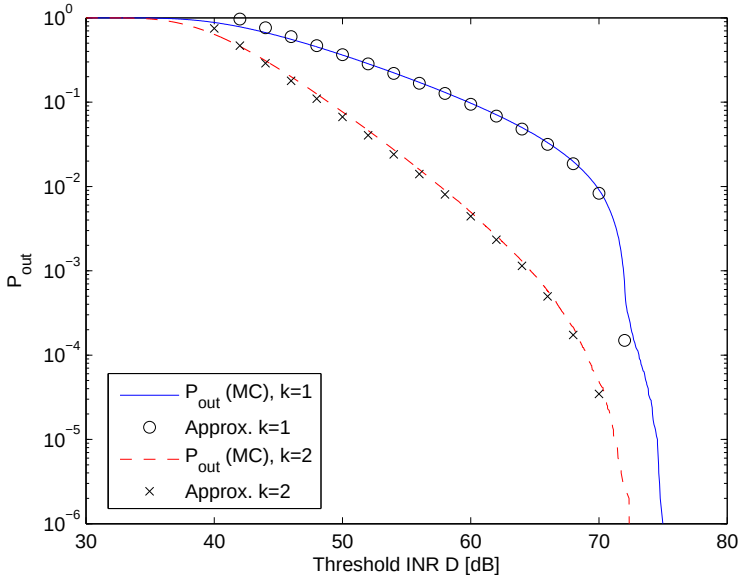

Fig. 4.2 Outage probability with interference cancelation for $D_{\max} > D_1$ in non-fading scenarios ($R_s < R_1$). The simulation parameters are $\nu = 4$, $R_s = 3m$, $R_1 = 18m$, $R_{\max} = 10^3 m$, $\lambda = 10^{-3}$ [nodes/m^2], $D_1 = 42$dB, $D_{\max} = 72$dB.

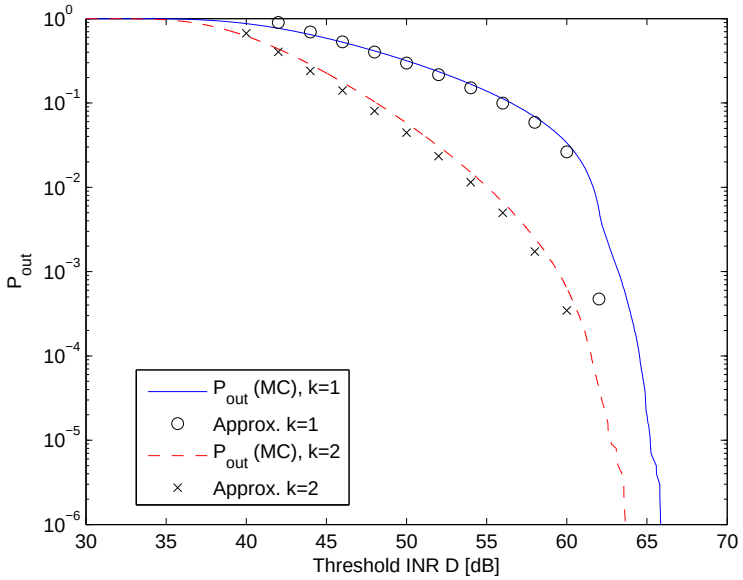

Fig. 4.3 Outage probability with interference cancelation for $D_{\max} > D_1$ in non-fading scenarios ($R_s < R_1$). The simulation parameters are $\nu = 4$, $R_s = 6m$, $R_1 = 18m$, $R_{\max} = 10^3 m$, $\lambda = 10^{-3}$ [nodes/m^2], $D_1 = 42$dB, $D_{\max} = 62$dB.

Fig. 4.1 and Fig. 4.4- 4.8 show the outage probability under interference cancelation with path loss ν from 8 to 2 when $R_s < R_1$ (small forbidden region). With larger ν, $P_{out} \sim D^{-2k/\nu}$ decays slower.

For $\nu = 2$ scenario, the convergence from P_{out} to $P_{out,k}$ is quite slower than that in larger ν scenarios. The reason is that when ν is small, nearest node dominating happens in very low outage region. $I = R^{-\nu}$, so the difference between the nearest node interference and the second or third nearest node interference is not as big as the large ν scenarios when $D_1 < D < D_{\max}$. On the other hand, the gap between D_1 and $D_{\max}$ is smaller, so the room for convergence is smaller. If we let $D_{\max} \to \infty$, i.e., no forbidden region, P_{out} will converge to $P_{out,k}$ in low outage region for sure. See Fig. 4.9.

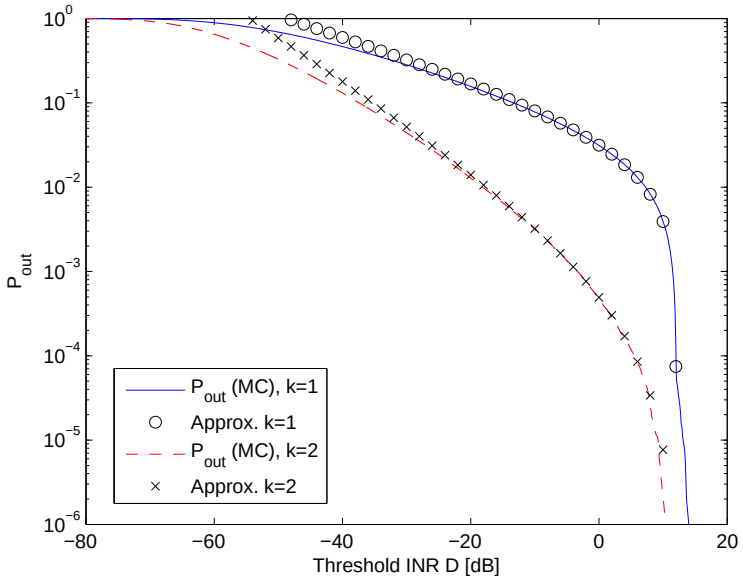

Fig. 4.4 Outage probability with interference cancelation for $D_{\max} > D_1$ in non-fading scenarios ($R_s < R_1$). The simulation parameters are $\nu = 8$, $R_s = 10m$, $R_1 = 56m$, $R_{\max} = 10^3 m$, $\lambda = 10^{-4}$[nodes/m^2], $D_1 = -48$dB, $D_{\max} = 12$dB.

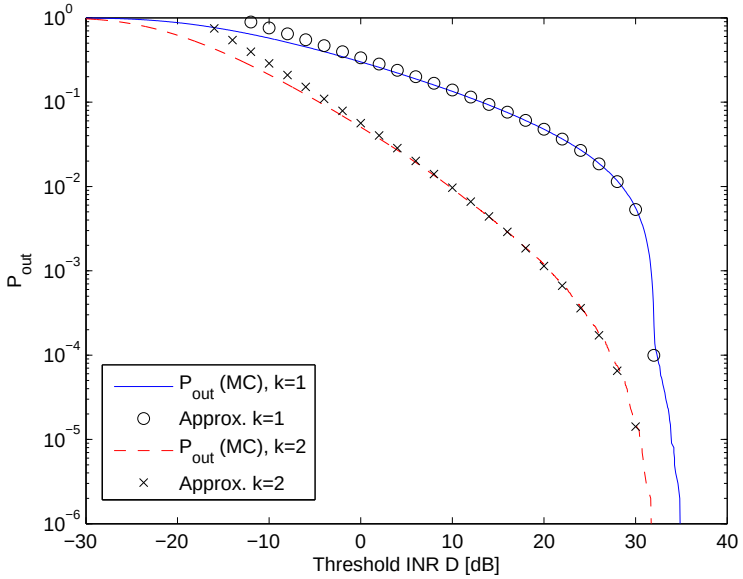

Fig. 4.5 Outage probability with interference cancelation for $D_{\max} > D_1$ in non-fading scenarios ($R_s < R_1$). The simulation parameters are $\nu = 6$, $R_s = 10m$, $R_1 = 56m$, $R_{\max} = 10^3 m$, $\lambda = 10^{-4}[\text{nodes/m}^2]$, $D_1 = -13\text{dB}$, $D_{\max} = 32\text{dB}$.

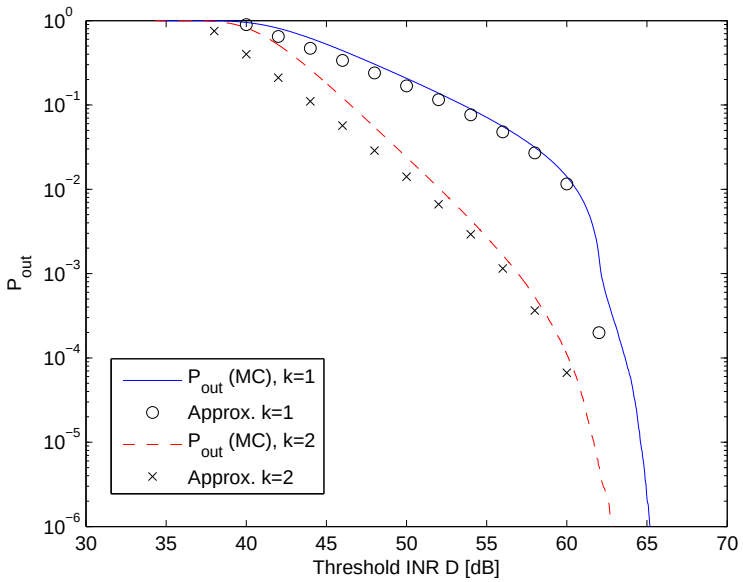

Fig. 4.6 Outage probability with interference cancelation for $D_{\max} > D_1$ in non-fading scenarios ($R_s < R_1$). The simulation parameters are $\nu = 3$, $R_s = 10m$, $R_1 = 56m$, $R_{\max} = 10^3 m$, $\lambda = 10^{-4}[\text{nodes/m}^2]$, $D_1 = 39\text{dB}$, $D_{\max} = 62\text{dB}$.

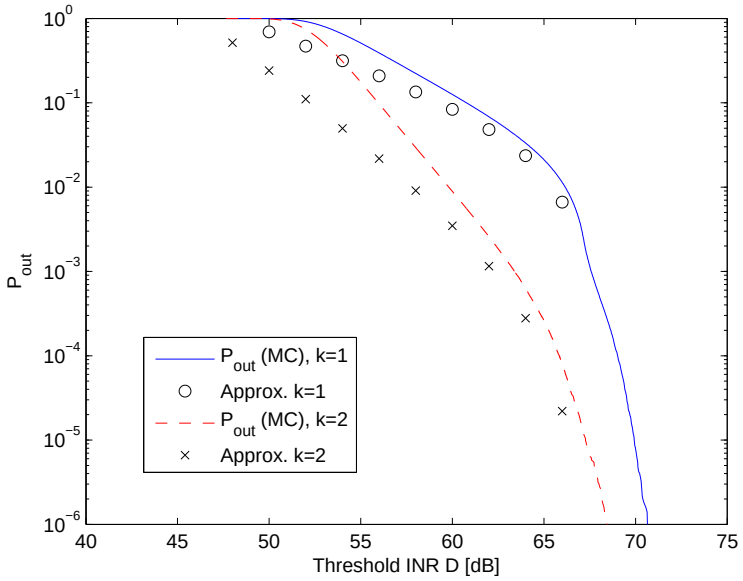

Fig. 4.7 Outage probability with interference cancelation for $D_{\max} > D_1$ in non-fading scenarios ($R_s < R_1$). The simulation parameters are $\nu = 2.5$, $R_s = 10m$, $R_1 = 56m$, $R_{\max} = 10^3 m$, $\lambda = 10^{-4}[\text{nodes/m}^2]$, $D_1 = 48\text{dB}$, $D_{\max} = 67\text{dB}$.

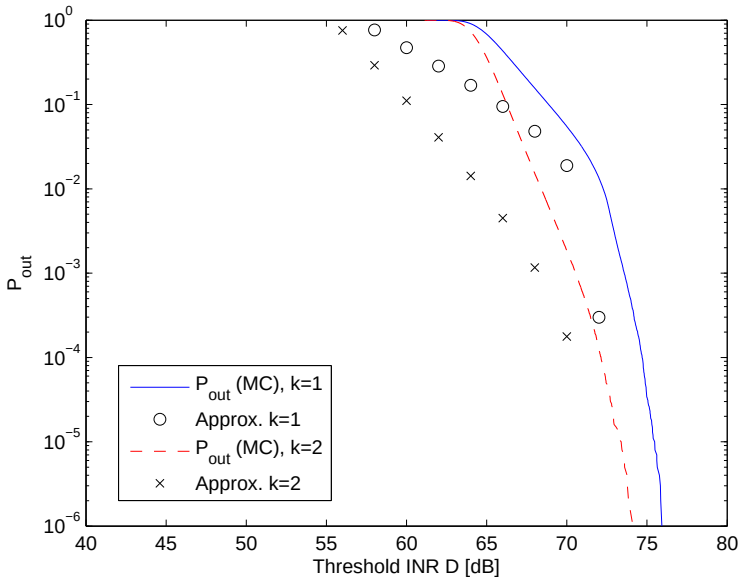

Fig. 4.8 Outage probability with interference cancelation for $D_{\max} > D_1$ in non-fading scenarios ($R_s < R_1$). The simulation parameters are $\nu = 2$, $R_s = 10m$, $R_1 = 56m$, $R_0 = 200m$, $R_{\max} = 10^3 m$, $\lambda = 10^{-4}[\text{nodes/m}^2]$, $D_1 = 57\text{dB}$, $D_{\max} = 72\text{dB}$.

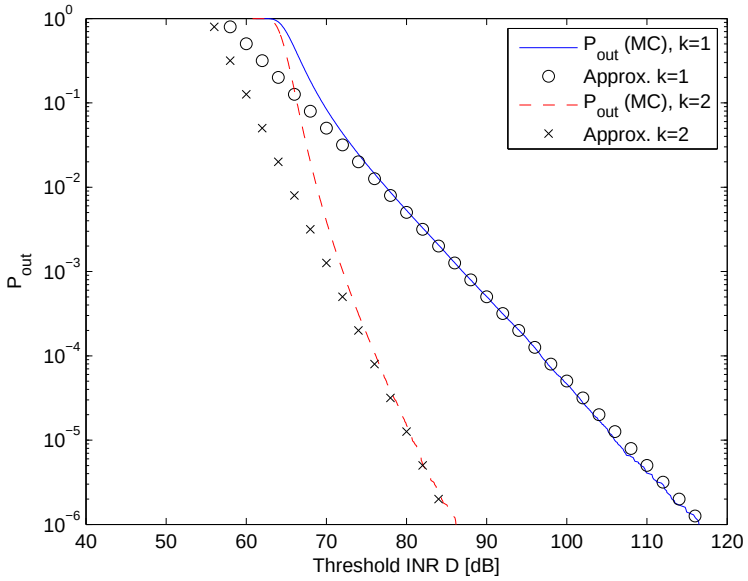

Fig. 4.9 Outage probability with interference cancelation without forbidden region. The simulation parameters are $\nu = 2$, $R_{\max} = 10^3 m$, $\lambda = 10^{-4}$ [nodes/m^2], $D_1 = 57$dB .

4.3 Summary

In this chapter, the outage probability in CR networks under interference cancelation for non-fading scenario has been studied. Due to spectrum trading, PUs may be willing to implement interference cancelation in their receivers with a small forbidden region for the SU network. With this implementation, SUs' spectrum efficiency increases significantly. From Theorem 3, when $(k-1)$ nearest interferers located outside the FR are canceled, and $d = D/D_{\max} < 1$ and $D \to \infty$, the CR outage probability $P_{out} = \Pr\{\sum_{i=k}^{N} I_i > DP_0\}$ is still dominated by the nearest active (k-th) node. The P_{out} is given in (4.1). The simulations show that the approximation in (4.2) based on Theorem 3 is quite accurate when $D < D_{\max}$ for different system parameters. By implementing interference cancelation, the outage probability decreases significantly at PU side with the same system parameters, so SUs can gain some spectrum efficiency without causing more harm to the PUs.

Chapter 5

Impact of Fading

In this section, we study the impact of fading on the aggregate interference distribution. Let us consider the ordered average interference powers $I_{a1} \geq I_{a2} \geq \cdots \geq I_{aN}$ which are further subjected to fading so that the fading received powers are $I_{gi} = g_i I_{ai}$, where g_i are the fading power gains, assumed to be i.i.d. with the PDF $f_g(x)$ and the CDF $F_g(x)$[1].

5.1 Asymptotic results

The theorem and corollary below characterize the asymptotic outage probability under fading (from a broad class of distributions) alone and both fading and interference cancelation simultaneously.

Theorem 4: Let $d = D/D_{\max} < 1$ and the fading distribution tail decays faster than polynomially, i.e.,

$$\lim_{x\to\infty} (1 - F_g(x))x^p = 0 \ \forall p < \infty,$$

[1]Here we tacitly assume that the PU signal is not fading, e.g., due to line-of-sight propagation. Alternatively, our results represent the CCDF of the aggregate interference.

where $F_g(x)$ is the CDF of the fading factor. When $D \to \infty$, the outage probability $P_{out} = \Pr\{\sum_i I_{gi} > DP_0\}$ is dominated by the nearest node interference:

$$P_{out} = \Pr\{I_{g1} > DP_0\}(1 + o(1)) = N_0 D^{-2/\nu} M_1(d) \cdot (1 + o(1)) \tag{5.1}$$

where $M_k(d) = \int_d^\infty \left(g^{2/\nu} - d^{2/\nu}\right)^k f_g(g)dg$ is a biased moment of g of order $2k/\nu$ (when $d = 0$, it is the moment of g of order $2k/\nu$.).

Proof:

The nearest-node INR under fading is $d_s = g_1 I_1/P_0$. The probability of it exceeding the threshold D (and thus causing an outage event) is

$$\begin{aligned} P_{out,1} &= \Pr\{d_s > D\} = \int_0^\infty f_g(g)\overline{F}(D/g)dg \\ &= \underbrace{\int_0^{D/D_{\max}} f_g(g)\overline{F}(D/g)dg}_{J_1} + \underbrace{\int_{D/D_{\max}}^{(D/D_1)^\varepsilon} f_g(g)\overline{F}(D/g)dg}_{J_2} + \underbrace{\int_{(D/D_1)^\varepsilon}^\infty f_g(g)\overline{F}(D/g)dg}_{J_3} \end{aligned} \tag{5.2}$$

where $\overline{F}(x) = \Pr\{I_1 > DP_0\}$ is the CCDF of the nearest-node non-fading INR I_1/P_0, and $0 < \varepsilon < 1$ is a constant. When $g \in [0, D/D_{\max})$, $D/g > D_{\max}$, so that $\overline{F}(D/g) = 0$ and thus $J_1 = 0$. When $D \to \infty$,

$$\begin{aligned} J_2 &= \int_{D/D_{\max}}^{(D/D_1)^\varepsilon} \left[1 - \exp\left(N_0 D_{\max}^{-2/\nu} - N_0 (D/g)^{-2/\nu}\right)\right] f_g(g)dg \\ &= \int_d^{(D/D_1)^\varepsilon} \left[1 - \exp\left(-N_0\left(g^{2/\nu} - d^{2/\nu}\right) D^{-2/\nu}\right)\right] f_g(g)dg \\ &= \int_d^{(D/D_1)^\varepsilon} \left[N_0\left(g^{2/\nu} - d^{2/\nu}\right) D^{-2/\nu}(1 + o(1))\right] f_g(g)dg \\ &= N_0 D^{-2/\nu} \int_d^\infty \left(g^{2/\nu} - d^{2/\nu}\right) f_g(g)dg \cdot (1 + o(1)) \\ &= N_0 D^{-2/\nu} M_1(d) \cdot (1 + o(1)) \end{aligned} \tag{5.3}$$

where $d = D/D_{\max}$. On the other hand,

$$\begin{aligned} J_3 &= \int_{(D/D_1)^{\varepsilon}}^{\infty} f_g(g)\overline{F}(D/g)dg \\ &\leq \int_{(D/D_1)^{\varepsilon}}^{\infty} f_g(g)dg = 1 - F_g((D/D_1)^{\varepsilon}) = o(J_2) \end{aligned} \tag{5.4}$$

since $1 - F_g(x)$ decays faster than polynomially, and thus J_3 can be neglected, so that

$$P_{out,1} = J_2(1 + o(1)) = N_0 D^{-2/\nu} M_1(d) \cdot (1 + o(1)) \tag{5.5}$$

In a similar way, using (A.20), one obtains $P_{out,k} = \Pr\{g_k I_k > DP_0\}$:

$$P_{out,k} = \frac{1}{k!} \left(N_0 D^{-2/\nu}\right)^k M_k(d) \cdot (1 + o(1)) \tag{5.6}$$

Observe further that $P_{out,k}$ has regularly-varying tails and that the tail of $g_1 I_1$ dominates that of $g_2 I_2$, so that Lemma 2 applies and thus (5.1) follows. ■

Note that $M_1(d)$ includes the impact of both the forbidden region and fading. The impact of fading alone is quantified, via comparison of (3.13) and (5.1), by $M_1(d)(1 - d^{2/\nu})^{-1}$: if the latter is greater than 1, the impact is negative (higher P_{out} due to fading), and positive otherwise.

Based on Theorem 4, the impact of fading and interference cancelation can now be quantified.

Proposition 4: Under the conditions of Theorem 4 and when $(k-1)$ nearest nodes are canceled, the outage probability is dominated by the nearest active (k-th)

node:

$$P_{out} = \Pr\{g_k I_k > D P_0\}(1 + o(1)) = \frac{1}{k!}\left(N_0 D^{-2/\nu}\right)^k M_k\left(d\right)\left(1 + o\left(1\right)\right). \qquad (5.7)$$

Proof:

The outage probability caused by the k-th nearest node alone under fading is given by (5.6). Using Lemma 2 and a reasoning similar to that in the proofs of Theorems 3 and 4, (5.7) follows, i.e., the nearest active node dominates the outage probability for a broad class of fading distributions whose tails decay faster than polynomially. ■

Note that $(N_0 D^{-2/\nu})^k/k!$ represents the conventional outage probability, i.e., no forbidden region and fading, and $M_k\left(d\right)$ quantifies the impact of the latter two.

It should be emphasized that Theorem 4 and Proposition 4 allow for a broad class of fading distributions, encompassing all popular models such as Rayleigh, Rice, Nakagami, Weibull and log-normal (also in combination with each other), whose tail decays faster than polynomially.

Theorem 4 can be considered as a generalization of Theorem 1: the latter can be recovered from the former using $f_g(x) = \delta(x-1)$. It can also be considered as a generalization of Theorem 4 in [9]: the latter can be recovered by using $d = 0$, i.e., no forbidden region.

Let us now specify the results above to the two popular fading models.

Rayleigh fading (small scale): The small scale fading gains g_{si} are modeled as independent Rayleigh random variables. The ordered average interference power I_{ai} are further subjected to Rayleigh fading so that the fading received powers are $I_{si} = g_{si} I_{ai}$, where g_{si} are the Rayleigh fading factors, assumed to be i.i.d, with the standard

pdf

$$f_{gs}(x) = e^{-x}. \tag{5.8}$$

The outage probability is as in Theorem 4 and Proposition 4 with,

$$M_k(d) = \sum_{i=0}^{k} C_k^i (-1)^i d^{2i/\nu} \Gamma\left(2(k-i)/\nu + 1, d\right) \tag{5.9}$$

where $C_k^i = k!/(i!(k-i)!)$ is the binomial coefficient; $\Gamma(a,x) = \int_x^\infty t^{a-1}e^{-t}dt$ is incomplete Gamma function. In particular, when $k = 1$, i.e., no interference cancelation,

$$M_1(d) = \Gamma\left(2/\nu + 1, d\right) - d^{2/\nu}e^{-d} \tag{5.10}$$

Derivation of (5.9)**:**

From Theorem 4,

$$M_k(d) = \int_d^\infty \left(g^{2/\nu} - d^{2/\nu}\right)^k f_g(g)dg.$$

For Rayleigh fading, the power gain PDF is

$$f_g(x) = \exp(-x).$$

So that

$$\begin{aligned} M_k(d) &= \int_d^\infty \left(g^{2/\nu} - d^{2/\nu}\right)^k f_g(g)dg \\ &= \int_d^\infty \sum_{i=0}^{k} C_k^i g^{2(k-i)/\nu} \cdot (-1)^i d^{2i/\nu} \cdot e^{-g}dg \end{aligned}$$

$$= \sum_{i=0}^{k} C_k^i \cdot (-1)^i d^{2i/\nu} \int_d^\infty g^{2(k-i)/\nu} \cdot e^{-g} dg$$
$$= \sum_{i=0}^{k} C_k^i (-1)^i d^{2i/\nu} \Gamma\left(2(k-i)/\nu + 1, d\right) \tag{5.11}$$

where $C_k^i = k!/(i!(k-i)!)$ is the binomial coefficient; $\Gamma(a,x) = \int_x^\infty t^{a-1}e^{-t}dt$ is incomplete Gamma function. ■

Log-normal fading (large scale): The large scale fading gains g_{li} are modeled as independent log-normal random variables [74]. The ordered average interference powers I_{ai} are further subjected to log-normal fading so that the received powers are $I_{li} = g_{li} I_{ai}$, where g_{li} are the log-normal fading factors, assumed to be i.i.d, with the pdf

$$f_{gl}(x) = \frac{1}{\sqrt{2\pi} x \sigma} \exp\left[\frac{-\ln^2 x}{2\sigma^2}\right], \tag{5.12}$$

where σ is the standard deviation of $\ln x$ in natural units.

The impact of fading and forbidden region is given by

$$M_k(d) = \sum_{i=0}^{k} C_k^i (-1)^i d^{\frac{2i}{\nu}} \cdot \exp\left(\frac{2\sigma^2(k-i)^2}{\nu^2}\right) Q\left(\frac{\ln d}{\sigma} - \frac{2\sigma(k-i)}{\nu}\right) \tag{5.13}$$

When $k = 1$, i.e., no interference cancelation,

$$M_1(d) = \exp\left(\frac{2\sigma^2}{\nu^2}\right) Q\left(\frac{\ln d}{\sigma} - \frac{2\sigma}{\nu}\right) - d^{\frac{2}{\nu}} Q\left(\frac{\ln d}{\sigma}\right) \tag{5.14}$$

Derivation of (5.13)**:**

From Theorem 4,

$$M_k(d) = \int_d^\infty \left(g^{2/\nu} - d^{2/\nu}\right)^k f_g(g) dg.$$

For log-normal fading, the power gain PDF is

$$f_{gl}(x) = \frac{1}{\sqrt{2\pi}x\sigma} \exp\left[\frac{-\ln^2 x}{2\sigma^2}\right],$$

where σ is the standard deviation of $\ln x$ in natural units. So that

$$\begin{aligned} M_k(d) &= \int_d^\infty \left(g^{2/\nu} - d^{2/\nu}\right)^k f_{gl}(g)dg \\ &= \int_d^\infty \sum_{i=0}^{k} C_k^i g^{2(k-i)/\nu} \cdot (-1)^i d^{2i/\nu} \cdot \frac{1}{\sqrt{2\pi}g\sigma} \exp\left[\frac{-\ln^2 g}{2\sigma^2}\right] dg \\ &= \sum_{i=0}^{k} C_k^i \cdot (-1)^i d^{2i/\nu} \int_d^\infty g^{2(k-i)/\nu} \cdot \frac{1}{\sqrt{2\pi}g\sigma} \exp\left[\frac{-\ln^2 g}{2\sigma^2}\right] dg \end{aligned} \tag{5.15}$$

where $C_k^i = k!/(i!(k-i)!)$ is the binomial coefficient. Let $g = e^x$, so that $x = \ln g$. (5.15) can be expressed as:

$$\begin{aligned} &\int_d^\infty g^{2(k-i)/\nu} \cdot \frac{1}{\sqrt{2\pi}g\sigma} \exp\left[\frac{-\ln^2 g}{2\sigma^2}\right] dg \\ =&\frac{1}{\sqrt{2\pi}\sigma} \int_{\ln d}^\infty \exp\left[-\frac{x^2}{2\sigma^2} + \frac{2x(k-i)}{\nu}\right] dx \\ =&\exp\left(\frac{2\sigma^2(k-i)^2}{\nu^2}\right) \frac{1}{\sqrt{2\pi}\sigma} \int_{\ln d}^\infty \exp\left[-\left(\frac{x}{\sqrt{2}\sigma} - \frac{\sqrt{2}\sigma(k-i)}{\nu}\right)^2\right] dx \\ =&\exp\left(\frac{2\sigma^2(k-i)^2}{\nu^2}\right) Q\left(\frac{\ln d}{\sigma} - \frac{2\sigma(k-i)}{\nu}\right) \end{aligned} \tag{5.16}$$

From (5.15) and (5.16),

$$M_k(d) = \sum_{i=0}^{k} C_k^i (-1)^i d^{\frac{2i}{\nu}} \cdot \exp\left(\frac{2\sigma^2(k-i)^2}{\nu^2}\right) Q\left(\frac{\ln d}{\sigma} - \frac{2\sigma(k-i)}{\nu}\right) \tag{5.17}$$

■

5.2 Non-asymptotic outage probability

Similarly to the non-fading scenario, the asymptotic results above can be used as approximations (without $o(1)$ terms) for finite but large D under certain conditions. We summarize this below based on the concept of typical outage events by considering 3 typical cases depending on the size of the forbidden region.

• **Case 1**: $R_s < R_1$ (small forbidden region).

From Theorem 4 and Proposition 4, for finite but large $D < D_{\max}$, the outage probability is dominated by the k-th nearest node after the cancelation, and thus can be approximated by (5.7) without the $o(1)$ term,

$$P_{out} \approx \left(N_0 D^{-2/\nu}\right)^k M_k\left(d\right)/k! \tag{5.18}$$

Similar to the non-fading case, this approximation holds when $D_1 < D < D_{\max}$, which implies $D_1 < D_{\max}$, which is equivalent to $R_s < R_1$, i.e., a small forbidden region. The condition $D_1 < D$ can be relaxed by noting that $P_{out,k} \leq P_{out} \leq 1$, i.e., via the combined approximation/lower bound,

$$P_{out} \approx \min\{1, \left(N_0 D^{-2/\nu}\right)^k M_k\left(d\right)/k!\} \tag{5.19}$$

Extensive simulation experiments for a wide range of system parameters are given in the next section.

• **Case 2**: $R_s > R_1$ (large forbidden region).

Because of the effect of fading, single node INR can exceed $D_{\max}$ when it is in a positive fading state ($g > 1$), so that single node can still cause an outage even when $D > D_{\max}$. The typical outage event is when the combined interference from a few nearest nodes in positive fading states exceed the threshold, so the approximation in

(5.19) is also suitable for this case.

5.3 Simulation details and results

In this section, simulation details and more results will be demonstrated.

5.3.1 Simulation details

We use Matlab to run the Monte Carlo (MC) simulations. The sample code is given in Appendix B.1. We use the system model given in Chapter 3.1. Rayleigh and log-normal fading are considered. In all simulations, we generate random geometry of the CR network based on Poisson point process for each run, and the parameters given in the figure captions. We fixed $R_{\max} = 1000m$, and the noise power after normalization is 200^{-4}, so $R_0 = 200^{4/\nu}$. The path loss ν, the radius of the forbidden region R_s and the density of active SU nodes λ are variables for different cases. The results are based on 10^6 runs.

To evaluate the cumulants of the aggregate interference needed for the Gaussian approximation and Edgeworth Expansion, we consider unordered fading interference $I_s = I \cdot g_s$, where I is the average interference coming from a randomly-selected node. For Rayleigh fading, the standard pdf of g_s is $f_{gs}(x) = e^{-x}$. Since I and g_s are independent of each other, the n^{th} moment of I_f is $\mu_n = E[I_f^n] = E[I^n]\, E[g_s^n]$. Since $E[g_s^n] = n!$ and $\kappa_n = \mu_n - \sum_{k=1}^{n-1} \binom{n-1}{k-1} \kappa_k \mu_{n-k}$ ($\kappa_1 = \mu_1$), from (3.42), the cumulants of I_{ag} can be expressed as:

$$\kappa_n = \begin{cases} \frac{2\pi\lambda n!(R_s^{2-n\nu} - R_{\max}^{2-n\nu})}{n\nu - 2} & \nu > 0 \text{ and } \nu \neq \frac{2}{n} \\ 2\pi\lambda n!(\ln R_{\max} - \ln R_s) & \nu = \frac{2}{n} \end{cases} \tag{5.20}$$

Similar as for the Rayleigh fading scenario, for log-normal fading, with the pdf

given in (5.12), the cumulants of I_{ag} can be expressed as:

$$\kappa_n = \begin{cases} \exp\left(\frac{n^2\sigma^2}{2}\right) \frac{2\pi\lambda(R_s^{2-n\nu} - R_{\max}^{2-n\nu})}{n\nu-2} & \nu > 0 \text{ and } \nu \neq \frac{2}{n} \\ 2\pi\lambda \exp\left(\frac{n^2\sigma^2}{2}\right) (\ln R_{\max} - \ln R_s) & \nu = \frac{2}{n} \end{cases} \tag{5.21}$$

5.3.2 Simulation results

In this section, extensive simulation results with a wide range of system parameters are given.

To evaluate the approximation accuracy for $D_{\max} > D_1$, Fig. 5.1- 5.10 illustrate this case under Rayleigh and log-normal fading distributions. As expected, when $D < D_{\max}$, P_{out} is well approximated by the contribution of the nearest active node as in (5.18), which is a lower bound in the general case.

Extensive simulation results show that the approximation in (5.18), (5.19) holds even when $D > D_{\max}$. We attribute this to the fact that when fading is present, the nearest node contribution can exceed $D_{\max}$, and the outage probability is dominated by the nearest node in a positive fading state ($g > 1$). Comparing log-normal and Rayleigh fading in this case, the former has more impact on the outage probability than the latter, which is explained by the longer tail of the log-normal distribution ($\exp(-(\ln x)^2)$ vs. $\exp(-x)$). The simulations show that the nearest neighbor approximation in (5.18), (5.19) is much more accurate than the Gaussian type approximations over the whole INR range with different system parameters. It is also able to predict accurately the outage probability in all three distinct regions (high outage ($D < D_1$), heavy (polynomial) tail ($D_1 < D < D_{\max}$) and exponential ($D > D_{\max}$)).

Fig 5.1-5.7 show the outage probabilities with interference cancelation and fading for $D_{\max} > D_1$, i.e., small forbidden region, with same R_s and R_1, different path loss ν from 8 to 2. For the fading cases, with larger path loss ν, P_{out} decays slower in heavy

tail region, i.e., $D < D_{\max}$, since $P_{out} \sim D^{-2k/\nu} M_k(d)$, and $M_k(d)$ is almost a constant when d is small. But P_{out} decay rates are almost the same in super-exponential tail region, i.e., $D > D_{\max}$, from the simulations.

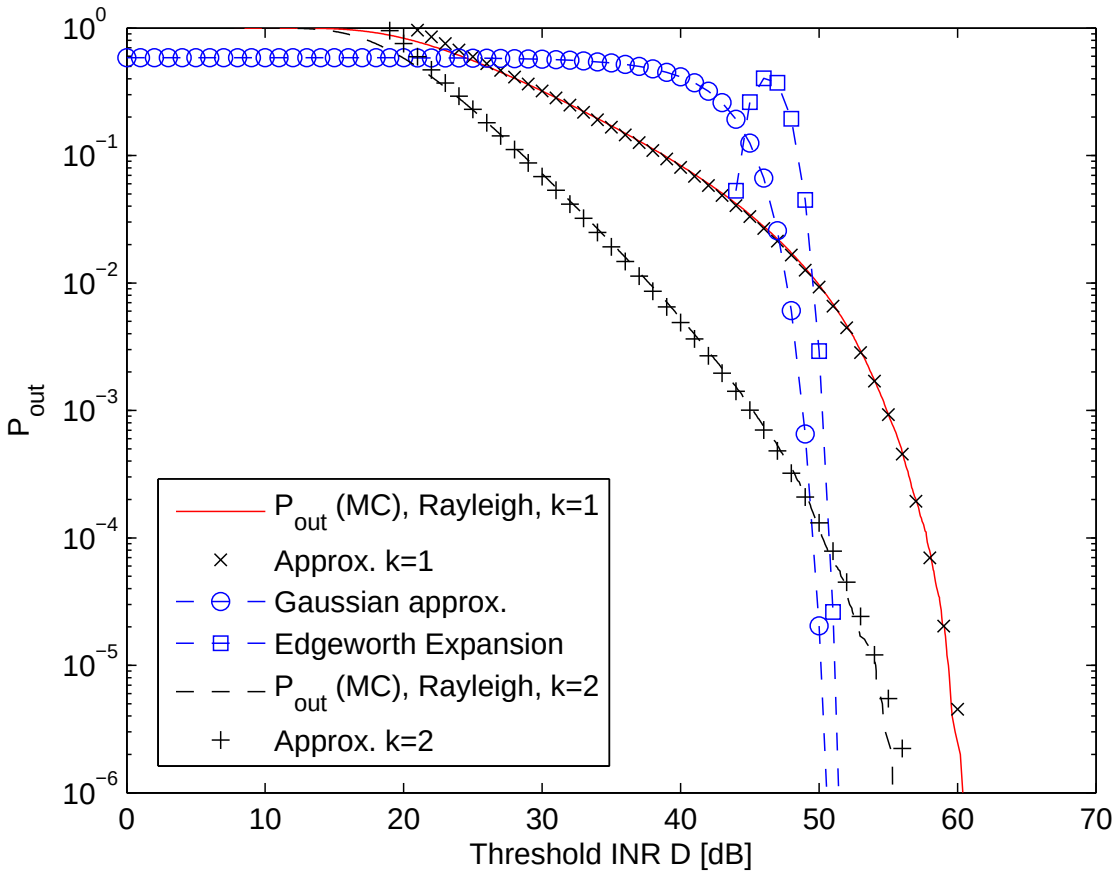

Fig. 5.1 Outage probability with interference cancelation under Rayleigh fading for $D_{\max} > D_1$ ($R_s < R_1$). The simulation parameters are $\nu = 4$, $R_s = 10m$, $R_1 = 56m$, $R_{\max} = 10^3 m$, $\lambda = 10^{-4}$ [nodes/m^2], $D_1 = 22$dB, $D_{\max} = 52$dB.

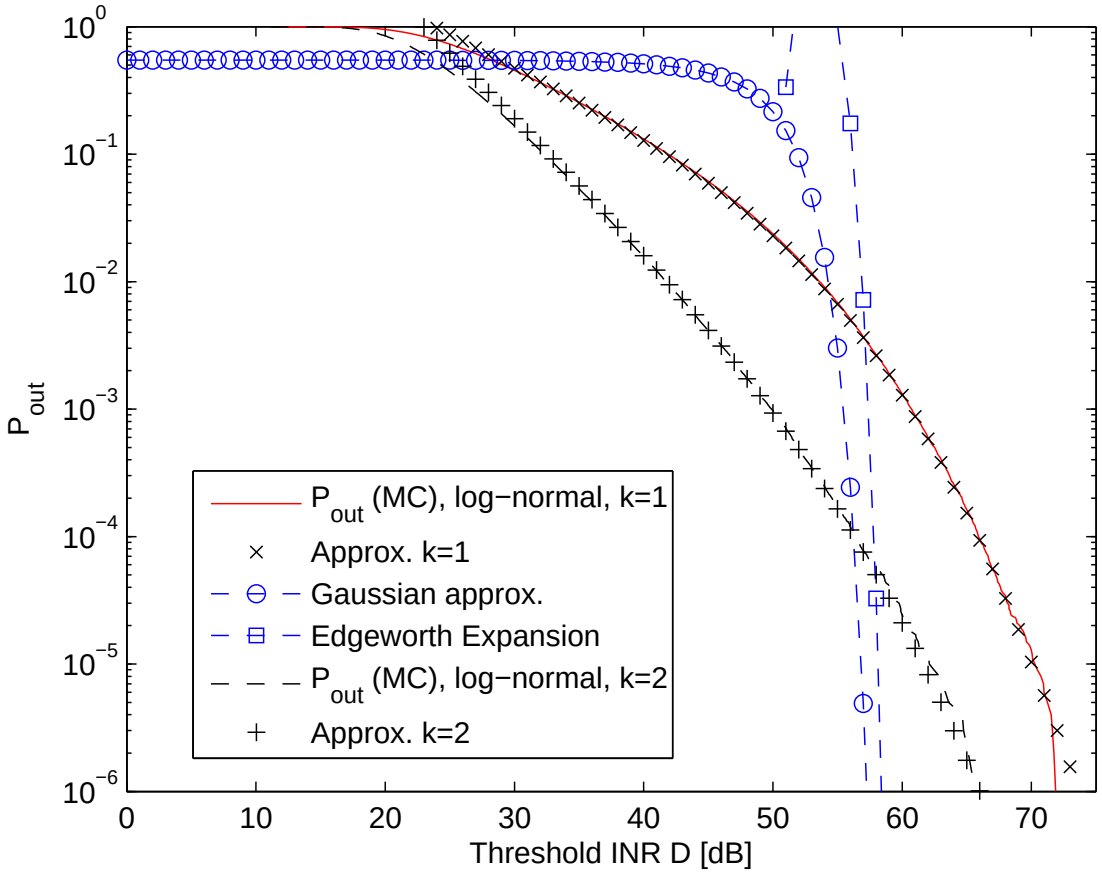

Fig. 5.2 Outage probability with interference cancelation under log-normal fading for $D_{\max} > D_1$ ($R_s < R_1$). The simulation parameters are $\nu = 4$, $R_s = 10m$, $R_1 = 56m$, $R_{\max} = 10^3 m$, $\lambda = 10^{-4}$ [nodes/m^2], $D_1 = 22$dB, $D_{\max} = 52$dB; $\sigma = 6$ dB.

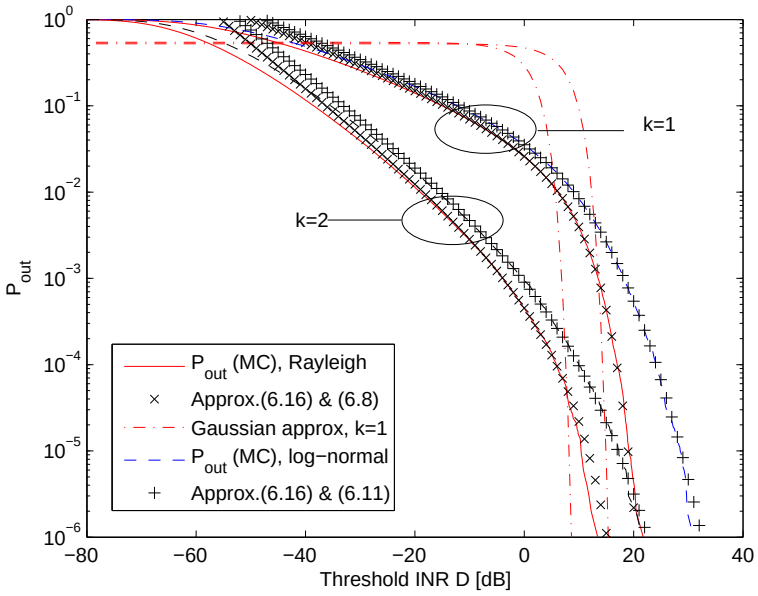

Fig. 5.3 Outage probability with interference cancelation and fading for $D_{\max} > D_1$ ($R_s < R_1$). The simulation parameters are $\nu = 8$, $R_s = 10m$, $R_1 = 56m$, $R_{\max} = 10^3 m$, $\lambda = 10^{-4}$ [nodes/m^2], $D_1 = -48$dB, $D_{\max} = 12$dB; $\sigma = 6$ dB.

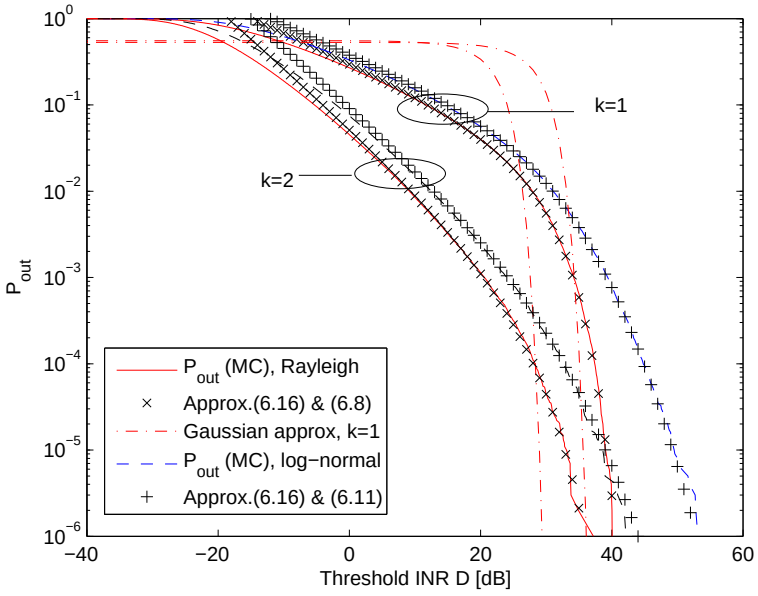

Fig. 5.4 Outage probability with interference cancelation and fading for $D_{\max} > D_1$ ($R_s < R_1$). The simulation parameters are $\nu = 6$, $R_s = 10m$, $R_1 = 56m$, $R_{\max} = 10^3 m$, $\lambda = 10^{-4}$ [nodes/m^2], $D_1 = -13$dB, $D_{\max} = 32$dB; $\sigma = 6$ dB.

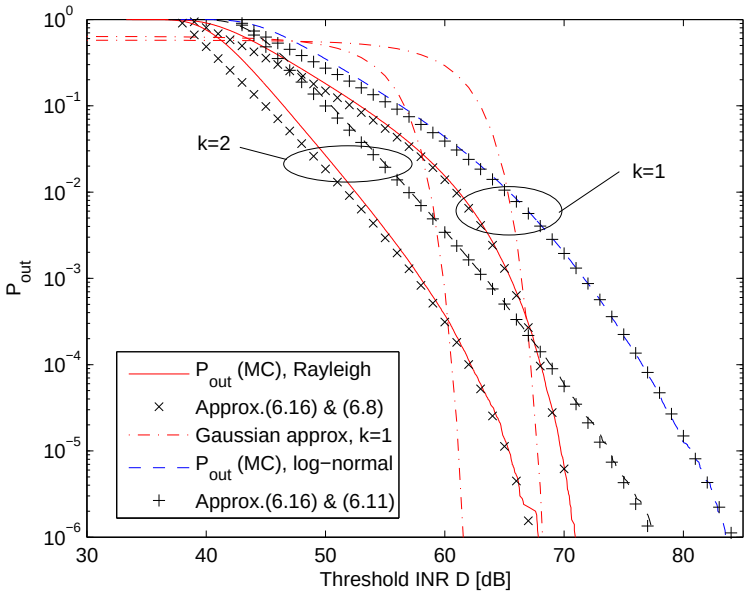

Fig. 5.5 Outage probability with interference cancelation and fading for $D_{\max} > D_1$ ($R_s < R_1$). The simulation parameters are $\nu = 3$, $R_s = 10m$, $R_1 = 56m$, $R_{\max} = 10^3 m$, $\lambda = 10^{-4}[\text{nodes/m}^2]$, $D_1 = 39\text{dB}$, $D_{\max} = 62\text{dB}$; $\sigma = 6$ dB.

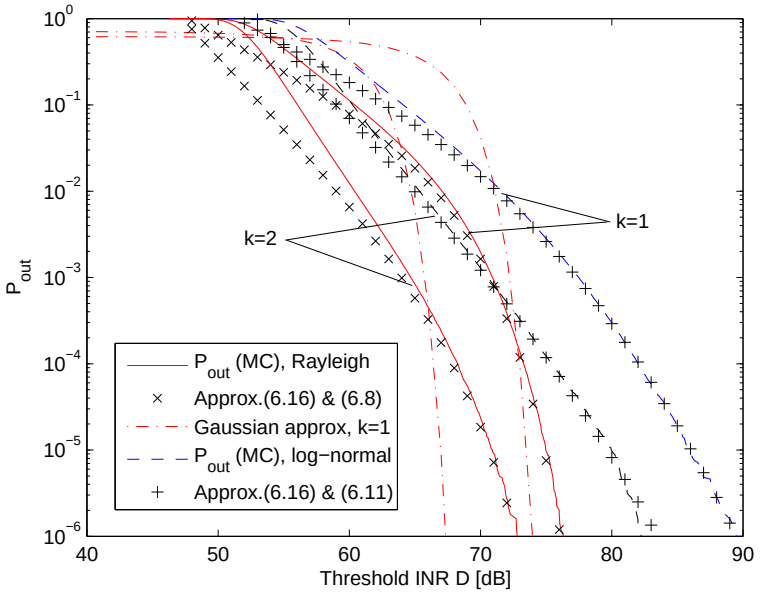

Fig. 5.6 Outage probability with interference cancelation and fading for $D_{\max} > D_1$ ($R_s < R_1$). The simulation parameters are $\nu = 2.5$, $R_s = 10m$, $R_1 = 56m$, $R_{\max} = 10^3 m$, $\lambda = 10^{-4}[\text{nodes/m}^2]$, $D_1 = 48\text{dB}$, $D_{\max} = 67\text{dB}$; $\sigma = 6$ dB.

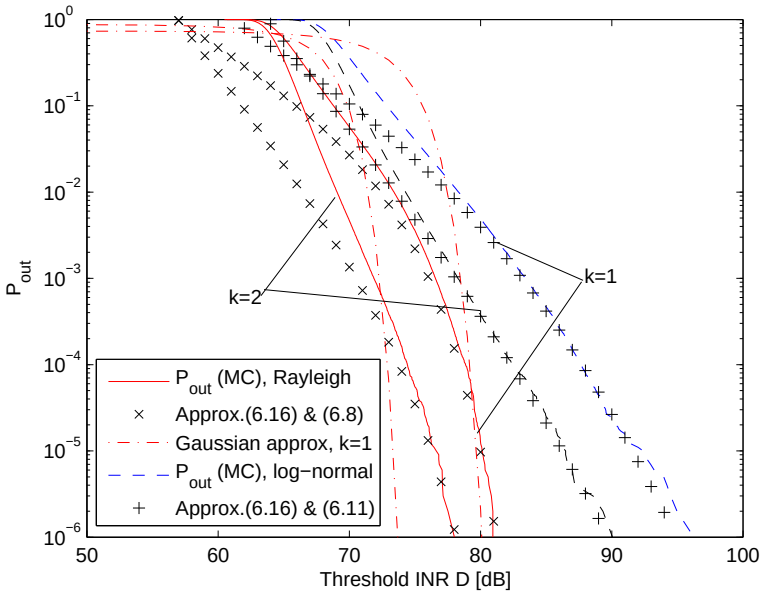

Fig. 5.7 Outage probability with interference cancelation and fading for $D_{\max} > D_1$ ($R_s < R_1$). The simulation parameters are $\nu = 2$, $R_s = 10m$, $R_1 = 56m$, $R_{\max} = 10^3 m$, $\lambda = 10^{-4}$ [nodes/m^2], $D_1 = 57$dB, $D_{\max} = 72$dB; $\sigma = 6$ dB.

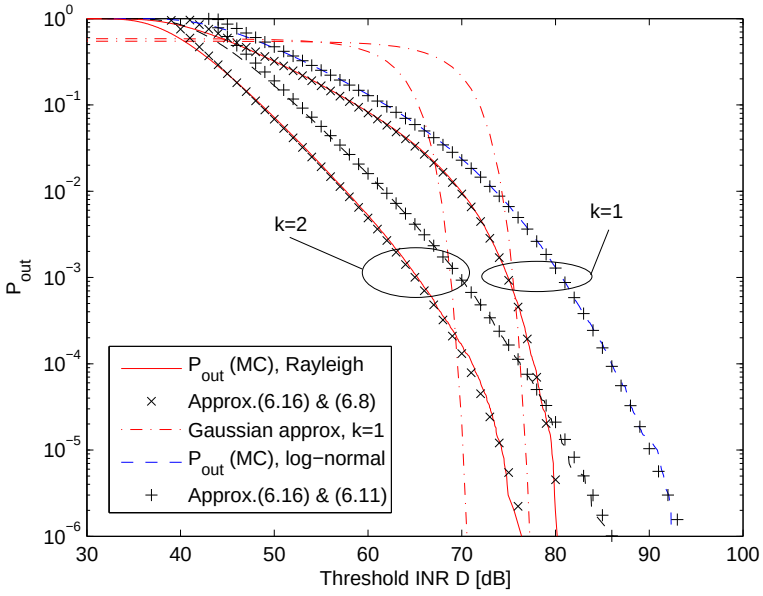

Fig. 5.8 Outage probability with interference cancelation and fading for $D_{\max} > D_1$ ($R_s < R_1$). The simulation parameters are $\nu = 4$, $R_s = 3m$, $R_1 = 18m$, $R_{\max} = 10^3 m$, $\lambda = 10^{-3}$ [nodes/m^2], $D_1 = 42$dB, $D_{\max} = 72$dB; $\sigma = 6$ dB.

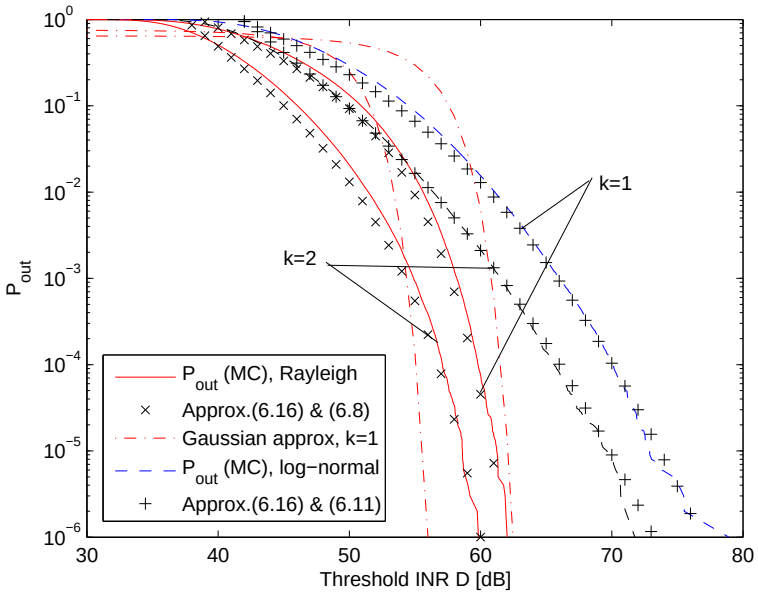

Fig. 5.9 Outage probability with interference cancelation and fading for $D_{\max} > D_1$ ($R_s < R_1$). The simulation parameters are $\nu = 4$, $R_s = 10m$, $R_1 = 18m$, $R_{\max} = 10^3 m$, $\lambda = 10^{-3}$ [nodes/m^2], $D_1 = 42$dB, $D_{\max} = 52$dB; $\sigma = 6$ dB.

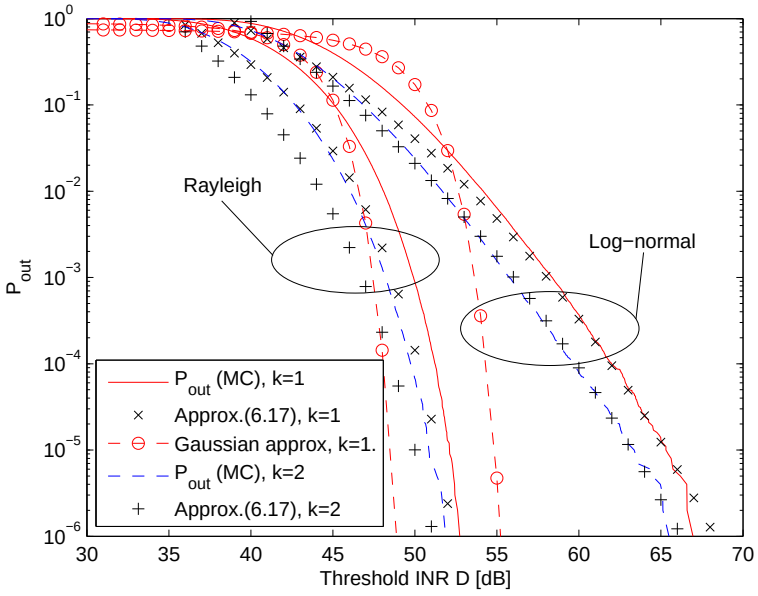

Fig. 5.10 Outage probability with interference cancelation and fading for $D_{\max} = D_1$ ($R_s = R_1$). The simulation parameters are $\nu = 4$, $R_s = 18m$, $R_1 = 18m$, $R_{\max} = 10^3 m$, $\lambda = 10^{-3}$ [nodes/m^2], $D_1 = 42$dB, $D_{\max} = 42$dB; $\sigma = 6$ dB.

Fig 5.11-5.15 show the outage probabilities with interference cancelation and fading for $R_s > R_1$ (large forbidden region), with different system parameters. The approximation in (5.19) is still reasonably accurate, especially for the log-normal fading. We attribute this to the fact that, while many nodes contribute to the typical outage event in the high-outage region (before the steep transition region) so that the Gaussian approximation is appropriate, it is a few nearest nodes plus positive fading that is dominant in the steep transition low-outage region, where the Gaussian approximation is remarkably less accurate. Also note that interference cancelation does not bring significant advantage in this case: since there is no dominant node, canceling the nearest one does not help much. As far as the approximation in (5.18) is concerned, the $M_k(d)$ term provides a dominant contribution in this case, which explains why P_{out} is not reduced significantly by going from $k = 1$ to $k = 2$.

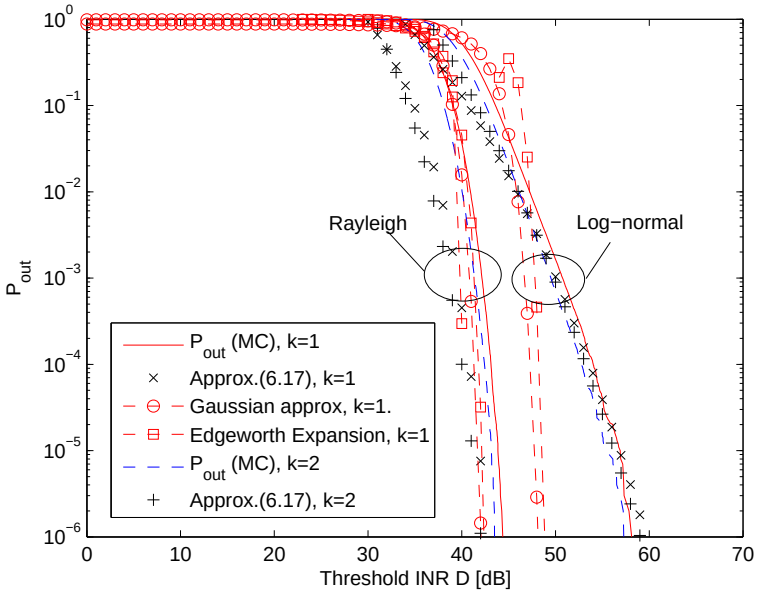

Fig. 5.11 Outage probability with interference cancelation and fading when $R_s > R_1$ ($D_1 > D_{\max}$). The simulation parameters are $\nu = 4$, $R_s = 32m$, $R_1 = 18m$, $R_{\max} = 10^3 m$, $\lambda = 10^{-3}$[nodes/m^2], $D_1 = 42$dB, $D_{\max} = 32$dB; $\sigma = 6$ dB.

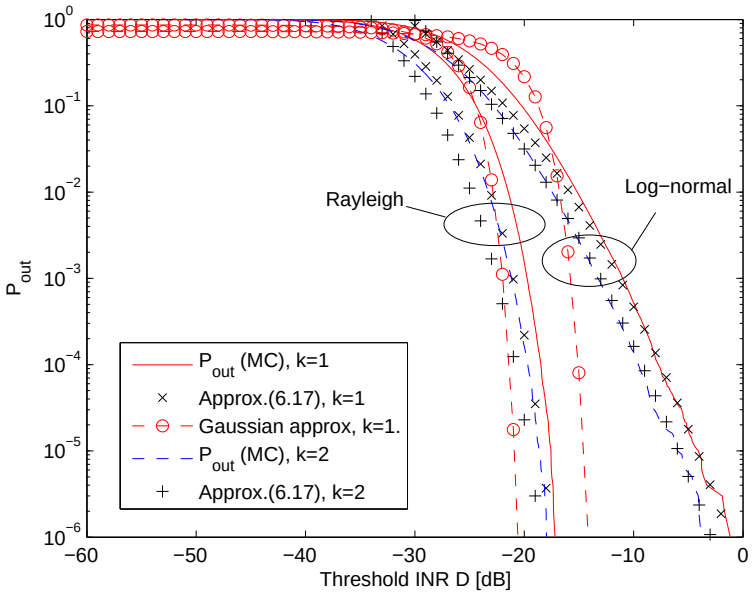

Fig. 5.12 Outage probability with interference cancelation and fading when $R_s > R_1$ ($D_1 > D_{\max}$). The simulation parameters are $\nu = 8$, $R_s = 32m$, $R_1 = 18m$, $R_{\max} = 10^3 m$, $\lambda = 10^{-3}[\text{nodes/m}^2]$, $D_1 = -8\text{dB}$, $D_{\max} = -28\text{dB}$; $\sigma = 6$ dB.

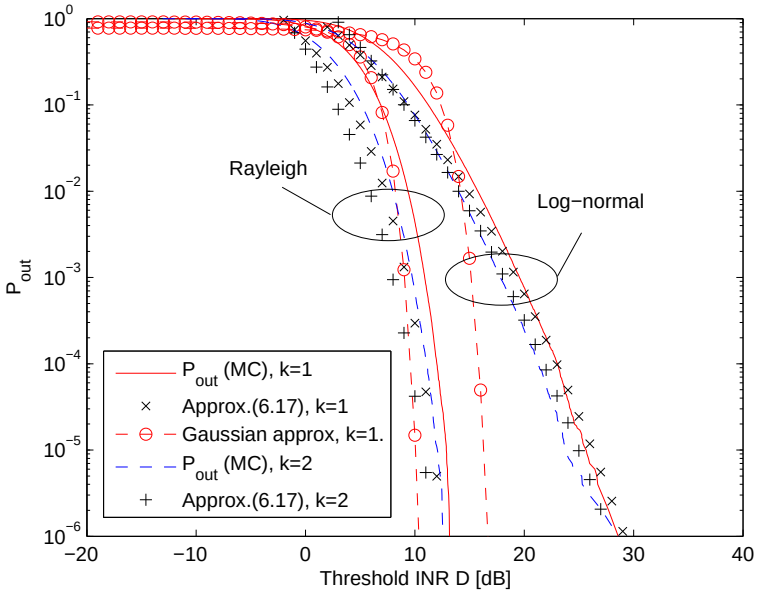

Fig. 5.13 Outage probability with interference cancelation and fading when $R_s > R_1$ ($D_1 > D_{\max}$). The simulation parameters are $\nu = 6$, $R_s = 32m$, $R_1 = 18m$, $R_{\max} = 10^3 m$, $\lambda = 10^{-3}[\text{nodes/m}^2]$, $D_1 = 17\text{dB}$, $D_{\max} = 2\text{dB}$; $\sigma = 6$ dB.

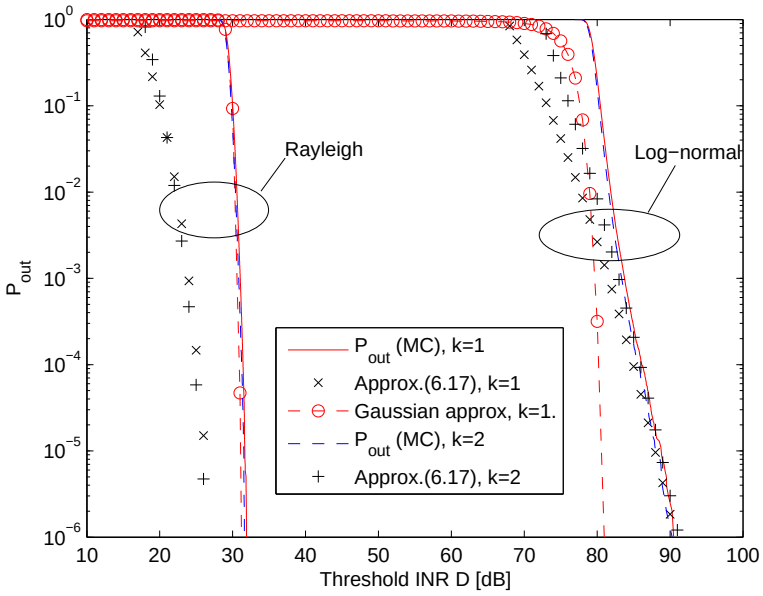

Fig. 5.14 Outage probability with interference cancelation and fading when $R_s > R_1$ ($D_1 > D_{\max}$). The simulation parameters are $\nu = 2$, $R_s = 32m$, $R_1 = 18m$, $R_{\max} = 10^3 m$, $\lambda = 10^{-3}[\text{nodes/m}^2]$, $D_1 = 67\text{dB}$, $D_{\max} = 62\text{dB}$; $\sigma = 6$ dB.

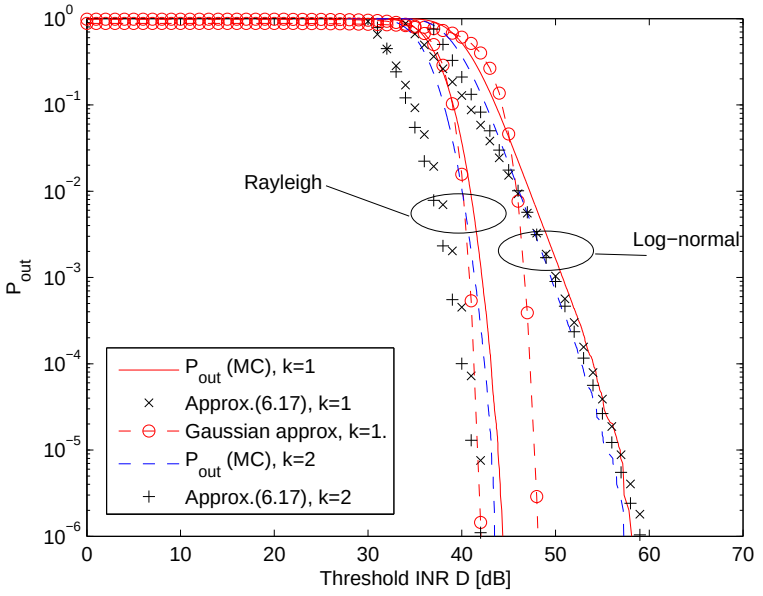

Fig. 5.15 Outage probability with interference cancelation and fading when $R_s > R_1$ ($D_1 > D_{\max}$). The simulation parameters are $\nu = 4$, $R_s = 56m$, $R_1 = 18m$, $R_{\max} = 10^3 m$, $\lambda = 10^{-3}[\text{nodes/m}^2]$, $D_1 = 42\text{dB}$, $D_{\max} = 22\text{dB}$; $\sigma = 6$ dB.

5.4 Summary

In this chapter, the outage probability in CR networks with fading and interference cancelation has been studied. The outage probability under fading is given in 5.1 using asymptotic techniques with condition that is $d = D/D_{\max} < 1$ and $D \to \infty$. Further more, the outage probability under fading including interference cancelation effects are given in 5.7 with the same condition. Theorem 4 and Proposition 4 show that when $(k-1)$ nearest nodes are canceled, the outage probability is dominated by the nearest active (k-th) node. A broad class of fading distributions is considered in the analysis. Rayleigh and log-normal fading scenarios are specifically studied and simulated. Extensive simulation results show that the approximation in (5.18), (5.19) is accurate over the whole INR range with different system parameters.

Chapter 6

Conclusions

6.1 Conclusions of the thesis

This thesis has provided the accurate, closed-form outage approximations for CR networks, which are based on the asymptotic analysis of interference and the saddle-point theory. These approximations can serve as an important evaluation tool in the deployment of the future CR networks since they provide insights into the interference-generating mechanism and suggest ways to combat it, and include the system and network parameters in a clear way. Unlike the prior results, these expressions are accurate in the low-outage region. The asymptotic analysis revealed the qualitative transition in the outage probability behavior around the critical point, when the decay changes from polynomial to super-exponential, thus providing a rigorous analytical foundation for the earlier empirical observations in the literature. Typical outage events have been identified, which further facilitate a reduction in the outage probability via e.g., interference cancelation. The impacts of fading and interference cancelation, either alone or in combination with each other, have also been included in the analysis. In particular, the outage probability is shown to scale down exponen-

tially in the number of canceled nearest interferers in the below-critical region. All results and conclusions are validated via extensive Monte-Carlo simulations.

Our model can be applied to single-band or multi-band RF wireless networks (such as WLAN). In a wireless system design, there are two kind of system parameters. One is unadjustable parameters, such as path loss exponent, fading factors and so on, and they are decided by the environment. The other is adjustable parameters, such as the size of the FR, SU transmitter node density. Our model considers both kind of system parameters, and use the outage probability as a performance metric to modify the adjustable parameters, so the wireless system meets the design requirement. The outage probability is an important performance metric for a system design. The definition is given in 3.2. It can be related with other performance metrics, such as frame error rate.

We summarize the main contributions of this thesis below:

- We develop a direct approach to the outage probability analysis based on the heavy tail and saddle-point approximation theories. The closed-form outage probability expressions were derived based on this combined approach with a guaranteed level of percentage accuracy. Additionally, this analysis provides a number of insights and the expressions are also accurate in the non-asymptotic regime.

- High-outage regime, heavy tail regime and super-exponential tail regime represent the whole picture of the outage behavior in CR networks. There is a critical point below which the outage probability decays polynomially (i.e., slowly) but above which it decays super-exponentially (i.e., very fast), as a function of the threshold INR, thus revealing a qualitative transition around this point. The main analytical tools are the heavy tail distribution theory for the below-critical

region and the saddle-point approximation theory for the above-critical one. The analysis also reveals the outage-forming mechanism that is responsible for such behavior: the polynomial (heavy tail) decay is due to a dominant contribution of the nearest active interferer (this also holds under interference cancelation and fading) and the super-exponential decay is due to the aggregate effect of many interferers, none of which is able to cause an outage alone.

- Due to spectrum trading, PU may be willing to implement the interference cancelation in PU receivers, so that PU keeps the same QoS with smaller FR (SUs gain more spectrum efficiency). The nearest active node is shown to provide the dominant contribution to the outage probability under interference cancelation as well, which scales down exponentially in the number of canceled nodes thus demonstrating significant potential of this approach, at the below-critical level. On the contrary, this approach gives little improvement in the above-critical region as well.

- The obtained results are extended to include the effect of fading from a broad class of fading distributions whose tails decay faster than polynomially. In particular, Rayleigh fading is shown to have a negligible impact on the outage probability in the below-critical region and significantly increases it in the above-critical region, while the log-normal fading induces a slight increase in the former and a significantly higher increase in the latter region. The random CR network geometry and fading dominate the outage probability in the below-critical region and the above-critical region separately.

6.2 Future work

6.2.1 Outage probability in fading scenarios using the saddlepoint approximation

In Chapter 3, we found the numerical and asymptotic solutions of the outage probability using the saddlepoint approximation in non-fading channels. It is a natural way to follow this direction to find the outage probability in fading scenarios using the saddlepoint approximation, but it is hard to find the right approach to solve it. In Chapter 5, we derived the outage probability of aggregate interference under fading. In the large forbidden region case under Rayleigh fading, the outage probability is dominant by a few or many nodes, and the approximations in Chapter 5 are based on nearest node dominant case, so that our approximation is not as accurate as in the small forbidden region case. The saddlepoint approximation should be a good solution since it requires a few or many contributors. It will unveil a full picture for the fading scenario.

6.2.2 The tradeoff between the outage probability and the size of forbidden region under interference cancelation

In CR networks, when the forbidden region increases, the outage probability decreases and the PUs have better QoS, but the spectrum efficiency for SUs decreases since many SUs in forbidden region can not transmit. If the IC techniques are used in CR networks, the QoS of the PUs can be kept in the same level with a smaller forbidden region, and the exact cost is that of the implementing IC, but the spectrum efficiency for SUs increases. When we design CR networks, those questions may be asked: Should we use the IC techniques or increase the forbidden region? How many interferers should be canceled to gain the same QoS as by increasing the forbidden region? What is the gain of the spectrum efficiency by using IC techniques? There is

a tradeoff between the outage probability and the spectrum efficiency.

In the future research, we can fix the outage probability, i.e., QoS level, and study this tradeoff and answer the above questions.

6.2.3 Different CR protocols

In the thesis, we consider a typical location-based CR protocol: all SUs which are inside of a forbidden region, i.e., the circle of the radius R_s centered on the PU, cease their transmissions. In the future research, we may consider other CR protocols, such as using beacon signals to do the spectrum sensing or cooperative spectrum sensing [48]. In the first cognitive radio wireless regional area network standard, IEEE 802.22 [37], not only the standard gives a location requirement, but also the working group develops a standard for a self-organizing network of beacon devices (IEEE 802.22.1).

Ghasemi and Sousa [12] considered the out-of-band sensing where the primary received send a beacon signal through an out-of-band control channel. They considered the energy detector based spectrum sensing. The probability of detection is a function of SNR. When the beacon signal SNR is less than certain threshold, the probability of detection is zero. When the beacon signal SNR is greater than certain threshold, the probability of detection is unity. This CR protocol assumes that any SUs which detect the beacon signal cease their transmission. For the non-fading scenarios, using beacon signals to do the spectrum sensing gives us a circle of forbidden region which is the same as the protocol used in this proposal. For the fading scenarios, the forbidden region is not a disk any more due to fading factors, and the distributions of the strongest interference and unordered single interference have to be derived. Based on those, the outage probability using saddlepoint approximation or typical outage events may be derived.

Appendix A

Proofs and Derivations

A.1 Proof of Theorem 2

The proof is essentially based on Lemma 1 and properties of Poisson point processes. One important property of a Poisson point process is that the number of nodes in the region S is independent with that in any other disjoint region. Based on that, the distances between randomly-selected nodes and the origin are independent of each other, so that the interference powers coming from individual nodes without ordering are i.i.d random variables. The PDF of the interference power I coming from a single node (without ordering) is:

$$f(I) = \begin{cases} \frac{2}{\nu}(R_{\max}^2 - R_s^2)^{-1} I^{-1-2/\nu} & R_{\max}^{-\nu} \leq I \leq R_s^{-\nu} \\ 0 & \text{otherwise} \end{cases} \tag{A.1}$$

Let $x_1, \cdots, x_N$ be the INRs coming from individual nodes without ordering after normalizing by D_1, where $D_1 = 1/R_1^{\nu} P_0 = (\pi\lambda)^{\nu/2}/P_0$, so that the PDF of $x =$

$I/(P_0 D_1)$ is

$$f(x) = \begin{cases} \frac{2}{\nu N_r} x^{-1-2/\nu} & N_{\max}^{-\nu/2} \leq x \leq N_s^{-\nu/2} \\ 0 & \text{otherwise} \end{cases} \tag{A.2}$$

where $N_r = \pi\lambda(R_{\max}^2 - R_s^2)$ is the average number of nodes in the ring between the circles of radii $R_{\max}$ and R_s; $N_{\max} = \pi\lambda R_{\max}^2$ is the average number of nodes in the disk of the radius $R_{\max}$; $N_s = \pi\lambda R_s^2$ is the average number of nodes in the disk of the radius R_s. The MGF of x is

$$M_x(\theta) = \frac{2}{\nu N_r} \int_{N_{\max}^{-\nu/2}}^{N_s^{-\nu/2}} \exp(\theta x)\ x^{-1-2/\nu} dx \tag{A.3}$$

When $D_{\max} < \infty$, $0 < N_s^{-\nu/2} < \infty$. Since $0 < N_{\max}^{-\nu/2} < \infty$, $0 < N_s^{-\nu/2} < \infty$, and $0 < \exp(\theta x)\ x^{-1-2/\nu} < \infty$ when $N_{\max}^{-\nu/2} < x < N_s^{-\nu/2}$ and $\theta < \infty$, it follows that $0 < M_x(\theta) < \infty$, and

$$\sup\{\theta : M_x(\theta) < \infty\} = \infty \tag{A.4}$$

Since the conditions of Lemma 1 are satisfied, the saddlepoint approximation can now be used.

The saddle point $\hat{\theta}$ can be found by solving the stationarity condition $N_r M_x'(\hat{\theta}) = d_1$, where $d_1 = D/D_1$ is the normalized threshold INR. After changing the variables, the saddle-point equation becomes

$$d_1 = p \int_a^b \exp(\hat{\theta} x)\ x^{-p} dx \tag{A.5}$$

where $p = 2/\nu$; $a = N_{\max}^{-\nu/2}$ and $b = N_s^{-\nu/2}$. Unfortunately, this is a transcendental equation for which an analytical solution is not known. It can be solved numerically. Below we give an analytical asymptotic solution to obtain some insights. When $d_1 \to \infty$, it follows that $\hat{\theta} \to \infty$. Using the integration by parts [75], (A.5) can be further

reduced to

$$
\begin{aligned}
d_1 &= p\int_a^b \exp(\hat{\theta}x)\; x^{-p}dx = \frac{p}{\hat{\theta}}\int_a^b x^{-p}d\left(\exp(\hat{\theta}x)\right) \\
&= \frac{p}{\hat{\theta}}\left(\frac{\exp(\hat{\theta}b)}{b^p} - \frac{\exp(\hat{\theta}a)}{a^p}\right) + \frac{p^2}{\hat{\theta}}\int_a^b \exp(\hat{\theta}x)\; x^{-p-1}dx \\
&= \frac{p\exp(\hat{\theta}b)}{\hat{\theta}b^p}\left(1+O\left(e^{-\hat{\theta}(b-a)}\right)\right) + \frac{p^2\exp(\hat{\theta}b)}{\hat{\theta}^2b^{p+1}}\left(1+O\left(e^{-\hat{\theta}(b-a)}\right)\right) \\
&\quad + \frac{p^2(p+1)}{\hat{\theta}^2}\int_a^b \exp(\hat{\theta}x)\; x^{-p-2}dx \\
&= \frac{p\exp(\hat{\theta}b)}{\hat{\theta}b^p}\left(1+o(1)\right) + \frac{p^2\exp(\hat{\theta}b)}{\hat{\theta}^2b^{p+1}}\left(1+o(1)\right) + \exp(\hat{\theta}b)\cdot o(\hat{\theta}^{-2}) \\
&= \frac{p\exp(\hat{\theta}b)}{\hat{\theta}b^p}\left[1+o(1)\right]
\end{aligned}
\tag{A.6}
$$

as $d_1 \to \infty$. Let $\alpha = \hat{\theta}b$ and $\mu = d_1 b^{p-1}/p$, so (A.6) can be expressed as:

$$
\mu = \frac{\exp(\alpha)}{\alpha}\left[1+o(1)\right] \tag{A.7}
$$

Since $d_1 \to \infty$, $\mu \to \infty$. Using the standard tools of asymptotic analysis (see e.g., [75, 78]), we have

$$
\ln\mu = \alpha - \ln\alpha + o(1) = \alpha\left[1+o(1)\right] \tag{A.8}
$$

so,

$$
\alpha = \ln\mu\left[1+o(1)\right] \tag{A.9}
$$

From (A.7) and (A.9),

$$
\alpha = \ln\mu + \ln\alpha + o(1) = \ln\mu + \ln\ln\mu + o(1) \tag{A.10}
$$

Hence, an asymptotic solution for $\hat{\theta}$ (keeping the two leading terms):

$$\begin{aligned}\hat{\theta} &= \frac{1}{b}\ln\left(\frac{d_1 b^{p-1}}{p}\right) + \frac{1}{b}\ln\ln\left(\frac{d_1 b^{p-1}}{p}\right)(1+o(1)) \\ &= N_s^{\nu/2}\left(\ln w + \ln\ln w\right) + o(\ln\ln w)\end{aligned} \tag{A.11}$$

where $w = \nu d_1 N_s^{\nu/2-1}/2$.

Let us now evaluate z_2 and z_3. From Lemma 1, z_2 can be expressed as:

$$z_2 = \mathrm{sgn}(\hat{\theta})(2\hat{\theta}d_1 - 2N_r(M_x(\hat{\theta})-1))^{1/2} \tag{A.12}$$

and

$$\begin{aligned}N_r(M_x(\hat{\theta})-1) &= p\int_a^b \exp(\hat{\theta}x)\; x^{-1-p}dx - N_r \\ &= \frac{p}{\hat{\theta}}\int_a^b x^{-1-p}d\left(\exp(\hat{\theta}x)\right) - N_r \\ &= \frac{p\exp(\hat{\theta}b)}{\hat{\theta}b^{p+1}}\left(1+O\left(e^{-\hat{\theta}(b-a)}\right)\right) \\ &\quad + \frac{p(p+1)}{\hat{\theta}}\int_a^b \exp(\hat{\theta}x)\; x^{-p-2}dx - N_r \\ &= \frac{p\exp(\hat{\theta}b)}{\hat{\theta}b^{p+1}}\left(1+o(1)\right) \\ &= d_1 b^{-1}\left(1+o(1)\right)\end{aligned} \tag{A.13}$$

Alternatively:

$$\begin{aligned}N_r(M_x(\hat{\theta})-1) &= p\int_a^b \exp(\hat{\theta}x)\; x^{-1-p}dx - N_r \\ &= -\int_a^b \exp(\hat{\theta}x)d\left(x^{-p}\right) - N_r \\ &= \hat{\theta}\int_a^b \exp(\hat{\theta}x)x^{-p}dx + \exp\left(\hat{\theta}a\right)a^{-p} - \exp\left(\hat{\theta}b\right)b^{-p} - \left(a^{-p}-b^{-p}\right)\end{aligned} \tag{A.14}$$

$$= \hat{\theta} \int_a^b \exp(\hat{\theta}x) x^{-p} dx + a^{-p} \left(\exp\left(\hat{\theta}a\right) - 1 \right) + b^{-p} \left(1 - \exp\left(\hat{\theta}b\right) \right)$$

If we let $N_{\max} \to \infty$, $a^{-p} \left(\exp\left(\hat{\theta}a\right) - 1 \right) \to 0$, and from (A.6),

$$\hat{\theta} \int_a^b \exp(\hat{\theta}x) x^{-p} dx = \frac{\exp(\hat{\theta}b)}{b^p} + \frac{p \exp(\hat{\theta}b)}{\hat{\theta} b^{p+1}} (1 + o(1))$$

so that

$$\begin{aligned} N_r(M_x(\hat{\theta}) - 1) &= \frac{p \exp(\hat{\theta}b)}{\hat{\theta} b^{p+1}} (1 + o(1)) + b^{-p} + o(1) \\ &= \left(\frac{p \exp(\hat{\theta}b)}{\hat{\theta} b^p} (1 + o(1)) b^{-1} + b^{-p} \right) (1 + o(1)) \\ &= (d_1 N_s^{\nu/2} + N_s)(1 + o(1)) \end{aligned} \tag{A.15}$$

so (3.24) follows.

When $d_1 \to \infty$, (A.13) and (A.15) are identical. But for large d_1, and $N_{\max} \gg N_s$, based on extensive simulation results, we found (A.15) is more accurate than (A.13), so we adopt (A.15) for this Theorem.

From Lemma 1, z_3 can now be expressed as:

$$\begin{aligned} z_3 &= \hat{\theta} \sqrt{N_r M_x''(\hat{\theta})} \\ &= \hat{\theta} \sqrt{p \int_a^b \exp(\hat{\theta}x)\ x^{1-p} dx} \\ &= \hat{\theta} \sqrt{\frac{p}{\hat{\theta}} \int_a^b x^{1-p} d\left(\exp(\hat{\theta}x) \right)} \\ &= \hat{\theta} \sqrt{\frac{p}{\hat{\theta}} \left(\frac{\exp(\hat{\theta}b)}{b^{p-1}} - \frac{\exp(\hat{\theta}a)}{a^{p-1}} \right) - \frac{p(1-p)}{\hat{\theta}} \int_a^b \exp(\hat{\theta}x)\ x^{-p} dx} \end{aligned} \tag{A.16}$$

$$
\begin{aligned}
&= \hat{\theta}\sqrt{\frac{p\exp(\hat{\theta}b)}{\hat{\theta}b^{p-1}}\left(1+o(1)\right) - \frac{p(p-1)\exp(\hat{\theta}b)}{\hat{\theta}^2 b^p}\left(1+o(1)\right)} \\
&= \hat{\theta}\sqrt{\frac{p\exp(\hat{\theta}b)}{\hat{\theta}b^{p-1}}\left(1+o(1)\right)} \\
&= \hat{\theta}\sqrt{d_1 b}\left(1+o(1)\right)
\end{aligned}
$$

Since the PDF $f(x)$ in (A.2) is a log-concave function, so the error term is $O\left(\rho_{c4}(\hat{\theta})\right)$.

An asymptotic solution for $\rho_{c4}(\hat{\theta})$ can be expressed as

$$
\begin{aligned}
\rho_{c4}(\hat{\theta}) &= \frac{\nu}{2}\frac{\int_{N_{\max}^{-\nu/2}}^{N_s^{-\nu/2}} \exp(\hat{\theta}x)\; x^{3-2/\nu}dx}{\left[\int_{N_{\max}^{-\nu/2}}^{N_s^{-\nu/2}} \exp(\hat{\theta}x)\; x^{1-2/\nu}dx\right]^2} \\
&= \frac{\nu}{2}\frac{\frac{\exp(\hat{\theta}b)}{\hat{\theta}b^{p-3}}\left[1+o(1)\right]}{\left\{\frac{\exp(\hat{\theta}b)}{\hat{\theta}b^{p-1}}\left[1+o(1)\right]\right\}^2} \\
&= \frac{\nu b}{2}\frac{\hat{\theta}b^{2/\nu}}{\exp(\hat{\theta}b)}\left[1+o\left(1\right)\right] \qquad \text{(A.17)}
\end{aligned}
$$

and using (A.6),

$$
\rho_{c4}(\hat{\theta}) = bd_1^{-1}\left[1+o\left(1\right)\right] \qquad \text{(A.18)}
$$

Finally, using (A.18) in (3.18), one obtains (3.19). ■

A.2 Proof of Theorem 3

From the system model, the SUs are randomly located according to a Poisson point process, so that the CDF of the distance between k_{th} nearest node and the origin is

$$\begin{aligned} F_{r_k}(R_D) &= \Pr\{r_k < R_D\} \\ &= \begin{cases} 1 - \sum_{i=0}^{k-1} \frac{1}{i!} \exp\left[-\pi\lambda(R_D^2 - R_s^2)\right] \left[\pi\lambda(R_D^2 - R_s^2)\right]^i & R_D > R_s \\ 0 & R_D < R_s \end{cases} \end{aligned} \tag{A.19}$$

Let $d = D/D_{\max} < 1$. After canceling interference from $(k-1)$ nearest nodes, the probability of the k_{th} nearest node alone causing an outage is

$$\begin{aligned} \Pr\{I_k > DP_0\} &= P_{out,k} \\ &= 1 - \sum_{i=0}^{k-1} \frac{1}{i!} \exp\left[-N_0 D^{\frac{-2}{\nu}}(1 - d^{\frac{2}{\nu}})\right] \left[N_0 D^{\frac{-2}{\nu}}(1 - d^{\frac{2}{\nu}})\right]^i \end{aligned} \tag{A.20}$$

where $I_1 \geq I_2 \geq ... \geq I_N$ are ordered interference powers. When $D \to \infty$, (A.20) simplifies to

$$P_{out,k} = \frac{1}{k!} \left[N_0 D^{-2/\nu}(1 - d^{2/\nu})\right]^k \cdot (1 + o(1)) \tag{A.21}$$

We further need the following technical lemma, which is a generalization of Lemma 4.4.2 in [66].

Lemma 2: Let X be a positive random variable with a regularly varying tail, i.e., there is a constant $b > 0$ such that $\forall a > 1$,

$$\lim_{x \to \infty} \frac{\Pr\{X > a \cdot x\}}{\Pr\{X > x\}} = a^{-b} \tag{A.22}$$

and let the tail of X dominate the tail of another positive random variables Y_1, i.e.,

$$\lim_{x\to\infty} \frac{\Pr\{Y_1 > x\}}{\Pr\{X > x\}} = 0 \tag{A.23}$$

Then

$$\lim_{x\to\infty} \frac{\Pr\{X + \sum_{i=1}^{n} Y_i > x\}}{\Pr\{X > x\}} = 1 \tag{A.24}$$

where $Y_1 \geq Y_2 \geq \cdots \geq Y_n$ are ordered positive random variables and $n < \infty$. ■

Proof of Lemma 2: It follows from Lemma 4.4.2 in [66] applied to X and Y_1 that

$$\lim_{x\to\infty} \frac{\Pr\{X + Y_1 > x\}}{\Pr\{X > x\}} = 1 \tag{A.25}$$

Using (A.25), it is straight forward to verify that

$$\lim_{x\to\infty} \frac{\Pr\{X + Y_1 > x\}}{\Pr\{X > x\}} = \lim_{x\to\infty} \frac{\Pr\{X + n \cdot Y_1 > x\}}{\Pr\{X > x\}} = 1 \tag{A.26}$$

Consider now the following bounds

$$\Pr\{X + Y_1 > x\} \leq \Pr\left\{X + \sum_{i=1}^{n} Y_i > x\right\} \leq \Pr\{X + n \cdot Y_1 > x\} \tag{A.27}$$

and use (A.26) to obtain (A.24). ■

Using (A.20), it is straightforward to verify that

$$\lim_{x\to\infty} \frac{\Pr\{I_{k+1} > x\}}{\Pr\{I_k > x\}} = 0$$

Now, observe that N is finite with probability one and use Lemma 2 with $X = I_k$,

$Y_i = I_{k+i}, i = 1...N-k$, so that

$$\lim_{x\to\infty} \frac{\Pr\left\{\sum_{i=k}^{N} I_i > x\right\}}{\Pr\{I_k > x\}} = 1 \tag{A.28}$$

Thus, the outage probability is dominated by the nearest active (k-th) node and 1st equality in (4.1) follows. 2nd and 3rd equalities follow from (A.21). ■

Appendix B

Sample Codes

B.1 Matlab codes

The function generating a Poisson point process in a plane.

```
%number of nodes is a Poisson random variable.
%Points are randomly put in plane.
function [R,th]=ppp2(lambda,r)
R=[];
th=[];
n= poissrnd(lambda*4*r*r);%number of points.
po=(rand(2,n)-0.5)*2*r;
i=1;
for j=1:n
    R1=sqrt(po(1,j)^2+po(2,j)^2);
    if R1<=r
        R(i)=R1;
        th(i)=atan(po(2,j)/po(1,j));
        i=i+1;
    end
end
R=sort(R);
```

The function reducing some points generated by ecdf function.

```
%There are too many points generated by ecdf function
%this function reduces some points in the figure with enough accuracy.
function [xi_sh,f_sh]=short_length(xi,f,rate)
a=length(xi);
xi_sh=ones(1,rate);
f_sh=xi_sh;
xi_max=max(xi);
```

```
xi_min=min(xi);
xi_step=(xi_max-xi_min)/(rate-1);
for i=1:rate
    xi_sh(i)=xi_min+xi_step*(i-1);
end
i=1;
for j=1:a
    if(xi(j)>=xi_sh(i))
        xi_sh(i)=xi(j);
        f_sh(i)=f(j);
        i=i+1;
    end
end
```

Simulating aggregate interference in a CR network for non-fading and Rayleigh fading Scenarios.

```
% Simulate aggregate interference in a CR network
% for non-fading and Rayleigh fading Scenarios
close all
clear all
N_ave=314;
r=10^3; %the radius of the circle (plane) (potential interference zone)
N_run=1*10^6; %running times
alpha=4; %exponent path loss
thr=10^(-4); %interference power threshold
Rs=thr^(-1/4); %sensing range
lambda=N_ave/(pi*(r^2)); %SU node's density
Rd=1/sqrt(pi*lambda); %R_1
Noise_l=(200)^(-4); %noise level, R_0=200
I_max=thr;
D_max=I_max/Noise_l;
D_0=(pi*lambda)^(alpha/2)/Noise_l;
I_n=zeros(1,N_run); %the nearest interference
I_ag=I_n; %aggregate interference
I_n_f=I_n; %the nearest interference considering fading
I_ag_f=I_n; %aggregate interference considering fading
I_n_s=I_n; %the nearest interference with spectrum sensing
I_n_s_c2=I_n; %second node interference with spectrum sensing
I_ag_s=I_n; %aggregate interference with spectrum sensing
%aggregate interference with spectrum sensing.
%Canceling the nearest interference
I_ag_s_c2=I_n;
%the nearest interference considering fading with spectrum sensing
I_n_f_s=I_n;
%aggregate interference considering fading with spectrum sensing
I_ag_f_s=I_n;
%the nearest interference considering fading with spectrum sensing,
%Canceling the nearest interference
I_n_f_s_c2=I_n;
%aggregate interference considering fading with spectrum sensing,
%Canceling the nearest interference
```

```
I_ag_f_s_c2=I_n;
%the strongest interference considering fading
%with spectrum sensing
I_str_f_s=I_n;
%main parts
for i=1:N_run
     %generate poisson point process in the plane
    [R,th]=ppp2(lambda,r);
    if(isempty(R))
    else
        Len_R=length(R);
      %without spectrum sensing
        %non-fading
        I_n(i)=(min(R))^(-alpha);
        I=R.^(-alpha);
        I_ag(i)=sum(I);
        %fading
        x=randn(1,Len_R)+sqrt(-1)*randn(1,Len_R); %Rayleigh
        x=x.*conj(x)/2;
        I_n_f(i)=I_n(i)*x(1);
        I_ag_f(i)=I*x';
      %with spectrum sensing
        if (R(end)<Rs)
        else
            %non-fading
            j=1;
            while R(j)<Rs
                j=j+1;
            end
            Rm=R(j:end);
            I_n_s(i)=(min(Rm))^(-alpha);
            I_s=Rm.^(-alpha);
            I_ag_s(i)=sum(I_s);
            %fading
            I_n_f_s(i)=I_n_s(i)*x(1);
            I_ag_f_s(i)=I_s*x(1:length(I_s))';
            I_str_f_s(i)=max(I_s.*x(1:length(I_s)));
            %interference cancelation, cancel the nearest node
            Rm2=R(j+1:end);
            I_n_s_c2(i)=(min(Rm2))^(-alpha);
            I_s2=Rm2.^(-alpha);
            I_ag_s_c2(i)=sum(I_s2);
            %fading
            I_n_f_s_c2(i)=I_n_s_c2(i)*x(2);
            I_ag_f_s_c2(i)=I_s2*x(2:length(I_s2)+1)';
        end
    end
end
I_n=10*log10(I_n/Noise_l);
I_ag=10*log10(I_ag/Noise_l);
I_n_f=10*log10(I_n_f/Noise_l);
```

```
I_ag_f=10*log10(I_ag_f/Noise_l);
I_n_s=10*log10(I_n_s/Noise_l);
I_ag_s=10*log10(I_ag_s/Noise_l);
I_n_f_s=10*log10(I_n_f_s/Noise_l);
I_ag_f_s=10*log10(I_ag_f_s/Noise_l);
I_str_f_s=10*log10(I_str_f_s/Noise_l);
I_n_s_c2=10*log10(I_n_s_c2/Noise_l);
I_ag_s_c2=10*log10(I_ag_s_c2/Noise_l);
I_n_f_s_c2=10*log10(I_n_f_s_c2/Noise_l);
I_ag_f_s_c2=10*log10(I_ag_f_s_c2/Noise_l);
%save the simulation data
save thesisSimu_R4_1000_10_56_200_1e_04_c1.mat
```

Simulating aggregate interference in a CR network for non-fading and log-normal fading Scenarios.

```
% Simulate aggregate interference in a CR network
% for non-fading and log-normal fading Scenarios
close all
clear all
% initialize
N_ave=3140;
r=10^3; %the radius of the circle (plane) (potential interference zone)
N_run=1*10^3; %running times
alpha=4; %exponent path loss
thr=10^(-6); %threshold
Rs=thr^(-1/alpha); %sensing range
lambda=N_ave/(pi*(r^2)); %SU node's density
Rd=1/sqrt(pi*lambda); %R_1
Noise_l=(200)^(-4); %noise level, R_0=200
I_max=thr;
D_max=I_max/Noise_l;
D_0=(pi*lambda)^(alpha/2)/Noise_l;
sigma_db=6; %log-normal standard deviation in dB
%log-normal standard deviation in natural units
sigma_log=0.1*log(10)*sigma_db;
I_n=zeros(1,N_run); %the nearest interference
I_ag=I_n; %aggregate interference
I_n_f=I_n; %the nearest interference considering fading
I_ag_f=I_n; %aggregate interference considering fading
I_n_s=I_n; %the nearest interference with spectrum sensing
I_n_s_c2=I_n; %second node interference with spectrum sensing
I_ag_s=I_n; %aggregate interference with spectrum sensing
%aggregate interference with spectrum sensing.
%Canceling the nearest interference
I_ag_s_c2=I_n;
%the nearest interference considering fading with spectrum sensing
I_n_f_s=I_n;
%aggregate interference considering fading with spectrum sensing
I_ag_f_s=I_n;
%the nearest interference considering fading with spectrum sensing,
%Canceling the nearest interference
```

```
I_n_f_s_c2=I_n;
%aggregate interference considering fading with spectrum sensing,
%Canceling the nearest interference
I_ag_f_s_c2=I_n;
%the strongest interference considering fading
%with spectrum sensing
I_str_f_s=I_n;
%main parts
for i=1:N_run
    %generate poisson point process in the plane
    [R,th]=ppp2(lambda,r);
    if(isempty(R))
    else
        Len_R=length(R);
        %without spectrum sensing
        %non-fading
        I_n(i)=(min(R))^(-alpha);
        I=R.^(-alpha);
        I_ag(i)=sum(I);
        %fading
        x=randn(1,Len_R);
        x=exp(sigma_log*x);
        I_n_f(i)=I_n(i)*x(1);
        I_ag_f(i)=I*x';
        %with spectrum sensing
        if (R(end)<Rs)
        else
            %non-fading
            j=1;
            while R(j)<Rs
                j=j+1;
            end
            Rm=R(j:end);
            I_n_s(i)=(min(Rm))^(-alpha);
            I_s=Rm.^(-alpha);
            I_ag_s(i)=sum(I_s);
            %fading
            I_n_f_s(i)=I_n_s(i)*x(1);
            I_ag_f_s(i)=I_s*x(1:length(I_s))';
            I_str_f_s(i)=max(I_s.*x(1:length(I_s)));
            %interference cancelation
            Rm2=R(j+1:end);
            I_n_s_c2(i)=(min(Rm2))^(-alpha);
            I_s2=Rm2.^(-alpha);
            I_ag_s_c2(i)=sum(I_s2);
            %fading
            I_n_f_s_c2(i)=I_n_s_c2(i)*x(2);
            I_ag_f_s_c2(i)=I_s2*x(2:length(I_s2)+1)';
        end
    end
end
```

```
I_n=10*log10(I_n/Noise_l);
I_ag=10*log10(I_ag/Noise_l);
I_n_f=10*log10(I_n_f/Noise_l);
I_ag_f=10*log10(I_ag_f/Noise_l);
I_n_s=10*log10(I_n_s/Noise_l);
I_ag_s=10*log10(I_ag_s/Noise_l);
I_n_f_s=10*log10(I_n_f_s/Noise_l);
I_ag_f_s=10*log10(I_ag_f_s/Noise_l);
I_str_f_s=10*log10(I_str_f_s/Noise_l);
I_n_s_c2=10*log10(I_n_s_c2/Noise_l);
I_ag_s_c2=10*log10(I_ag_s_c2/Noise_l);
I_n_f_s_c2=10*log10(I_n_f_s_c2/Noise_l);
I_ag_f_s_c2=10*log10(I_ag_f_s_c2/Noise_l);
save thesisSimu_L4_1000_32_18_200_1e_03_c2.mat
```

Displaying non-fading scenario.

```
close all
clear all
load thesisSimu_L4_1000_32_18_200_1e_03_c2.mat
figure (1)
%non fading cumulants
for i=1:3
    kappa_n(i)=2*pi*lambda*Rs^(2-i*alpha)/(i*alpha-2);
end
k3z=kappa_n(3)/kappa_n(2)^(3/2);
R0=(Noise_l)^(-1/alpha)
N_0=pi*lambda*R0^2
thr=Rs^(-alpha)
I_max=thr;
D_max=I_max/Noise_l
for i=0:1:100
    ii=(i-0)/1+1;
    xx(ii)=i;
    I_t=10^(i/10)*Noise_l;
    D_t=10^(i/10);
    I_z=(I_t-kappa_n(1))/sqrt(kappa_n(2));
    %Edgeworth expansion
    E_yy(ii)=qfunc(I_z)+(k3z/6)*(I_z^2-1)*(1/sqrt(2*pi))*exp(-I_z^2/2);
    yy(ii)=qfunc(I_z); %gaussian approx
    y_n(ii)=N_0*D_t^(-2/alpha)*(1-(D_t/D_max)^(2/alpha)); %nearest approx
    y_n_c2(ii)=y_n(ii)^2/2; %IC
end
%saddle point approx
N_max=pi*lambda*r^2;
N_s=pi*lambda*Rs^2;
p=2/alpha;
b=N_s^(-1/p);
for i=0:0.5:100
    ii=(i-0)*2+1;
    x_sp(ii)=i;
    D_t=10^(i/10)/D_0;
```

```
    sp=log(D_t*b^(p-1)/p)/b+log(log(D_t*b^(p-1)/p))/b;
    if (2*D_t*(sp-1/b)-2*N_s >0)
        R_sp=sign(sp)*sqrt(abs(2*D_t*(sp-1/b)-2*N_s));
        U_sp=sp*sqrt(D_t*b);
        RL=R_sp+log(U_sp/R_sp)/R_sp;
        y_sp(ii)=qfunc(RL);
    else
        y_sp(ii)=0;
    end
end
clear I_ag
clear I_n
clear I_n_f
clear I_ag_f
clear I_str_f_s
rate=1000;
[f,xi] = ecdf(I_ag_s);
[xi,f]=short_length(xi,f,rate);
clear I_ag_s
semilogy(xi,1-f,'b-');
hold on
semilogy(xx,yy,'r--o')
hold on
semilogy(xx,E_yy,'r--s')
hold on
load saddle_c2_32_18_4.mat
semilogy(data_x,data,'r-->')
hold on
semilogy(x_sp,y_sp,'k+--')
xlabel('Threshold INR D [dB]');
ylabel('P_{out}');
legend('P_{out} (MC)','Gaussian approx.','Edgeworth Expansion',...
'saddlepoint approx. (Numerical)','saddlepoint approx. (Asymptotic)');
AXIS([25 45 0.000001 1])
```

Displaying interference cancelation scenario.

```
close all
clear all
load thesisSimu_R4_1000_10_56_200_1e_04_c1.mat
figure (1)
R0=(Noise_l)^(-1/alpha);
N_0=pi*lambda*R0^2;
thr=Rs^(-alpha);
I_max=thr;
D_max=I_max/Noise_l;
for i=0:2:52
    ii=(i-0)/2+1;
    xx(ii)=i;
    I_t=10^(i/10)*Noise_l;
    D_t=10^(i/10);
    y_n(ii)=N_0*D_t^(-2/alpha)*(1-(D_t/D_max)^(2/alpha));
```

```
    y_n_c2(ii)=y_n(ii)^2/2;
end
clear I_ag
clear I_n
clear I_n_f
clear I_ag_f
clear I_str_f_s
rate=1000;
[f,xi] = ecdf(I_ag_s);
[xi,f]=short_length(xi,f,rate);
semilogy(xi,1-f,'b-');
hold on
semilogy(xx,y_n,'ko')
hold on
[f,xi] = ecdf(I_ag_s_c2);
semilogy(xi,1-f,'r--');
hold on
semilogy(xx,y_n_c2,'kx')
xlabel('Threshold INR D [dB]');
ylabel('P_{out}');
legend('P_{out} (MC), k=1','Approx. k=1','P_{out} (MC), ...
k=2','Approx. k=2');
AXIS([0 60 0.000001 1])
```

Displaying Rayleigh fading scenario.

```
close all
clear all
load thesisSimu_R4_1000_10_56_200_1e_04_c1.mat
figure (1)
for i=1:3
    kappa(i)=2*pi*lambda*(Rs^(2-i*alpha)/(i*alpha-2)-...
            r^(2-i*alpha)/(i*alpha-2))*factorial(i);
end
k3z=kappa(3)/kappa(2)^(3/2);
rate=1000;
[f,xi] = ecdf(I_ag_f_s);
[xi,f]=short_length(xi,f,rate);
semilogy(xi,1-f,'r-');
hold on
N_0=D_0^(2/alpha);
for i=0:1:70
    ii=(i-0)+1;
    xx(ii)=i;
    I_t=10^(i/10)*Noise_l;
    D_t=10^(i/10);
    I_z=(I_t-kappa(1))/sqrt(kappa(2));
    E_yy(ii)=qfunc(I_z)+(k3z/6)*(I_z^2-1)*(1/sqrt(2*pi))*exp(-I_z^2/2);
    yy(ii)=qfunc(I_z);
    y_n(ii)=N_0*D_t^(-2/alpha)*(gamma(2/alpha+1)*...
            gammainc(D_t/D_max,2/alpha+1,'upper')-...
            (D_t/D_max)^(2/alpha)*exp(-D_t/D_max));
```

```
    y_n_c2(ii)=(N_0*D_t^(-2/alpha))^2/2*(gamma(4/alpha+1)*...
                gammainc(D_t/D_max,4/alpha+1,'upper')-...
                2*(D_t/D_max)^(2/alpha)*gamma(2/alpha+1)*...
                gammainc(D_t/D_max,2/alpha+1,'upper')+...
                (D_t/D_max)^(4/alpha)*exp(-D_t/D_max));
end
semilogy(xx,y_n,'kx')
hold on
semilogy(xx,yy,'b--o')
hold on
semilogy(xx,E_yy,'b--s')
hold on
[f,xi] = ecdf(I_ag_f_s_c2);
[xi,f]=short_length(xi,f,rate);
semilogy(xi,1-f,'k--');
hold on
semilogy(xx,y_n_c2,'k+')
xlabel('Threshold INR D [dB]');
ylabel('P_{out}');
legend('P_{out} (MC), Rayleigh, k=1','Approx. k=1','Gaussian approx.',...
'Edgeworth Expansion', 'P_{out} (MC), Rayleigh, k=2','Approx. k=2');
AXIS([0 70 0.000001 1])
```

Displaying log-normal fading scenario.

```
close all
clear all
load thesisSimu_L4_1000_32_18_200_1e_03_c2.mat
figure (1)
for i=1:3
    kappa(i)=2*pi*lambda*(Rs^(2-i*alpha)/(i*alpha-2)-...
            r^(2-i*alpha)/(i*alpha-2))*exp(0.5*sigma_log^2*i^2);
end
k3z=kappa(3)/kappa(2)^(3/2);
rate=1000;
[f,xi] = ecdf(I_ag_f_s);
[xi,f]=short_length(xi,f,rate);
semilogy(xi,1-f,'r-');
hold on
N_0=D_0^(2/alpha);
for i=0:1:80
    ii=i+1;
    xx(ii)=i;
    I_t=10^(i/10)*Noise_l;
    D_t=10^(i/10);
    I_z=(I_t-kappa(1))/sqrt(kappa(2));
    E_yy(ii)=qfunc(I_z)+(k3z/6)*(I_z^2-1)*(1/sqrt(2*pi))*exp(-I_z^2/2);
    yy(ii)=qfunc(I_z);
    yyx(ii)=-N_0*D_max^(-2/alpha)*(qfunc(log(D_t/D_max)/sigma_log))+...
            N_0*D_t^(-2/alpha)*(qfunc(log(D_t/D_max)/sigma_log-...
            2*sigma_log/alpha))*exp(2*sigma_log^2/alpha^2);
    d=D_t/D_max;
```

```
    yyx_c2(ii)=(N_0*D_t^(-2/alpha))^2/2*(exp(8*sigma_log^2/alpha^2)*...
            qfunc(log(d)/sigma_log-4*sigma_log/alpha)-...
            2*d^(2/alpha)*(qfunc(log(d)/sigma_log-2*sigma_log/alpha))*...
            exp(2*sigma_log^2/alpha^2)+...
            qfunc(log(D_t/D_max)/sigma_log)*d^(4/alpha));
end
semilogy(xx,yyx,'kx')
hold on
semilogy(xx,yy,'b--o')
hold on
semilogy(xx,E_yy,'b--s')
hold on
[f,xi] = ecdf(I_ag_f_s_c2);
[xi,f]=short_length(xi,f,rate);
semilogy(xi,1-f,'k--');
hold on
semilogy(xx,yyx_c2,'k+')
xlabel('Threshold INR D [dB]');
ylabel('P_{out}');
legend('P_{out} (MC), log-normal, k=1','Approx. k=1','Gaussian approx.',...
'Edgeworth Expansion', 'P_{out} (MC), log-normal, k=2','Approx. k=2');
AXIS([0 75 0.000001 1])
```

Appendix C

Background of the Saddlepoint Approximation

C.1 Edgeworth expansion

Let $Y_1, \cdots, Y_n$ be independent and identically distributed (i.i.d) random variables, with $E(Y) = \mu, var(Y) = \sigma_Y^2$. Their moment generating functions (MGF) $M(\theta) = E(\exp(\theta Y))$; Their cumulant generating functions (CGF) $\mathrm{K}(\theta) = \ln(M(\theta))$; Their cumulants are $\kappa_r = (d/d\theta)^r \mathrm{K}(\theta)$; $\rho_r = \kappa_r/\sigma_Y^r$ are the standardized cumulants.

Let $S_n = Y_1 + \cdots + Y_n$, $S_n^* = (S_n - n\mu)/(\sigma_Y\sqrt{n})$, the Edgeworth expansion of pdf of S_n^* is [77]:

$$f(S_n^*; x) = \phi(x)\left\{1 + \rho_3\frac{H_3(x)}{6\sqrt{n}} + \rho_4\frac{H_4(x)}{24n} + \rho_3^2\frac{H_6(x)}{72n}\right\} + O(n^{-3/2}) \qquad \text{(C.1)}$$

where $\phi(x) = \exp(-x^2/2)/\sqrt{2\pi}$ is the pdf of $\mathcal{N}(0,1)$, $H_r(x)$ is the Hermite polynomial of degree r, $(d/dx)^r\phi(x) = (-1)^r H_r(x)\phi(x)$. The first few Hermite polynomials are:

$$H_0(x) = 1$$

$$H_1(x) = x$$

$$H_2(x) = x^2 - 1$$

$$H_3(x) = x^3 - 3x,$$

$$H_4(x) = x^4 - 6x^2 + 3$$

$$H_5(x) = x^5 - 10x^3 + 15x$$

$$H_6(x) = x^6 - 15x^4 + 45x^2 - 15.$$

The Edgeworth expansion of CDF of S_n^* is [77]:

$$F(S_n^*; x) = \Phi(x) - \phi(x)\left\{\rho_3 \frac{H_2(x)}{6\sqrt{n}} + \rho_4 \frac{H_3(x)}{24n} + \rho_3^2 \frac{H_5(x)}{72n}\right\} + O(n^{-3/2}) \qquad \text{(C.2)}$$

where $\Phi(x) = \int_{-\infty}^{x} \phi(x)dx$.

C.2 Tilted Edgeworth expansion

When $\rho_3 \neq 0$, (C.1) and (C.2) show that the error of the leading term of the Edgeworth expansion is $O(1/\sqrt{n})$ in general [77]. The convergence of Edgeworth expansion to Gaussian is relatively slow, especially in the tails of the distribution where the value of $H_3(x)$ can not be ignored.

When the argument is the mean $x = 0$, the coefficient of $1/\sqrt{n}$ vanishes due to $H_3(0) = 0$, and the error of the standard normal approximation is $O(1/n)$ rather than $O(1/\sqrt{n})$. If one shifts the density of S_n or S_n^* in such a way that the argument equals to the mean under the new distribution, the relative approximation error is $O(1/n)$.

More specifically, we consider the exponential family of pdf $f(y)$ [77]:

$$f(y;\theta) = \frac{\exp(\theta y) f(y)}{M(\theta)} = \exp[\theta y - \mathrm{K}(\theta)] f(y) \qquad \text{(C.3)}$$

The operation of forming $f(y;\theta)$ is called exponential tilting. For S_n, we have

$$f(S_n;s;\theta) = \exp[\theta y - n\mathrm{K}(\theta)]f(S_n;s;0) \tag{C.4}$$

so that $f(S_n;s;0) = \exp[-\theta y + n\mathrm{K}(\theta)]f(S_n;s;\theta)$. We choose θ, so that let s be the mean of the modified distribution of S_n under that θ. Let $\hat{\theta}$ be the solution of

$$E(S_n;\theta) = n\mathrm{K}'(\theta) = s \tag{C.5}$$

where $E(S_n;\theta)$ is the expectation of S_n according to the tilted pdf $f(S_n;\theta)$. We approximate $f(S_n;s;\hat{\theta})$ using the Edgeworth expansion

$$f(S_n;s;\hat{\theta}) = \frac{1}{\sqrt{2\pi n\mathrm{K}''(\hat{\theta})}}\left[1 + O\left(\frac{1}{n}\right)\right] \tag{C.6}$$

where we use $var(S_n;\hat{\theta}) = n\mathrm{K}''(\hat{\theta})$.

Thus, the tilted Edgeworth expansion is:

$$f(S_n;s;0) = \frac{\exp[-\hat{\theta}y + n\mathrm{K}(\hat{\theta})]}{\sqrt{2\pi n\mathrm{K}''(\hat{\theta})}}\left[1 + O\left(\frac{1}{n}\right)\right] \tag{C.7}$$

and the normalized tilted Edgeworth expansion is :

$$f(S_n;s;0) = c_n\frac{\exp[-\hat{\theta}y + n\mathrm{K}(\hat{\theta})]}{\sqrt{2\pi n\mathrm{K}''(\hat{\theta})}}\left[1 + O\left(\frac{1}{n}\right)\right] \tag{C.8}$$

where c_n is chosen to normalize the leading term. It makes integration of $f(S_n;s;0)$ is unity over the support range of S_n.

Comparing (C.1) and (C.7) or (C.8), we find that the tilted Edgeworth expansion

has a relative error $O(1/n)$ over a wide range of values of S_n, and the direct Edgeworth expansion has an absolute error $O(1/\sqrt{n})$, which makes that the convergence to Gaussian for the latter is much slower than that for the former. This property is due to the fact that the Hermite polynomials are bounded when the particular argument is the mean.

Since $\hat{\theta}(s)$ is the saddle point of the function $f(\theta) = \theta s - n\mathrm{K}(\theta)$, the tilted Edgeworth expansion is also called the saddlepoint approximation [76].

References

[1] S. Haykin, "Cognitive radio: brain-empowered wireless communications," *IEEE Journal on Selected Areas in Communications*, vol. 23, pp. 201 – 220, Feb 2005.

[2] *Spectrum policy task force report*. Washington DC: Federal Communication Commission, FCC 02-135, Nov 2002.

[3] M. Haenggi and R. K. Ganti, "Interference in large wireless networks," *Foundations and Trends in Networking*, vol. 3, no. 2, pp. 127 – 248, 2009.

[4] D. Stoyan, W. S. Kendal, and J. Mecke, *Stochastic Geometry and Its Applications, 2nd ed*. New York: Wiley, 1995.

[5] J. F. C. Kingman, *Poisson Processes*. Oxford: Oxford University Press, 1993.

[6] E. Sousa and J. Silvester, "Optimum transmission ranges in a direct-sequence spread-spectrum multihop packet radio network," *IEEE Journal on Selected Areas in Communications*, vol. 8, pp. 762 – 771, Jun 1990.

[7] J. Ilow and D. Hatzinakos, "Analytic alpha-stable noise modeling in a Poisson field of interferers or scatterers," *IEEE Transactions on Signal Processing*, vol. 46, pp. 1601 – 1611, Jun 1998.

[8] S. Weber, J. Andrews, X. Yang, and G. de Veciana, "Transmission capacity of wireless ad hoc networks with successive interference cancellation," *IEEE Transactions on Information Theory*, vol. 53, pp. 2799 – 2814, Aug 2007.

[9] V. Mordachev and S. Loyka, "On node density - outage probability tradeoff in wireless networks," *IEEE Journal on Selected Areas in Communications*, vol. 27, pp. 1120 – 1131, Sep 2009.

[10] O. Ben Sik Ali, C. Cardinal, and F. Gagnon, "On the performance of interference cancellation in wireless ad hoc networks," *IEEE Transactions on Communications*, vol. 58, pp. 433 – 437, Feb 2010.

[11] M. Aljuaid and H. Yanikomeroglu, "Investigating the gaussian convergence of the distribution of the aggregate interference power in large wireless networks," *IEEE Transactions on Vehicular Technology*, vol. 59, pp. 4418 – 4424, Nov 2010.

[12] A. Ghasemi and E. Sousa, "Interference aggregation in spectrum-sensing cognitive wireless networks," *IEEE Journal of Selected Topics in Signal Processing*, vol. 2, pp. 41 – 56, Feb 2008.

[13] A. Rabbachin, T. Quek, H. Shin, and M. Win, "Cognitive network interference," *Selected Areas in Communications, IEEE Journal on*, vol. 29, pp. 480 – 493, Feb 2011.

[14] A. J. Ganesh and G. L. Torrisi, "Large deviations of the interference in a wireless communication model," *IEEE Transactions on Information Theory*, vol. 54, pp. 3505 – 3517, Aug 2008.

[15] X. Hong, C.-X. Wang, and J. Thompson, "Interference modeling of cognitive radio networks," in *Vehicular Technology Conference, 2008. VTC Spring 2008. IEEE*, pp. 1851 – 1855, May 2008.

[16] Y.Wen, S. Loyka, and A. Yongacoglu, "The impact of fading on the outage probability in cognitive radio networks," in *2010 IEEE 72nd Vehicular Technology Conference: VTC2010-Fall*, Sep 2010.

[17] Y.Wen, S. Loyka, and A. Yongacoglu, "On distribution of aggregate interference in cognitive radio networks," in *25th Biennial Symposium on Communications (QBSC)*, pp. 265 – 268, May 2010.

[18] R. N. Mantegna and H. E. Stanley, "Stochastic process with ultraslow convergence to a gaussian: the truncated levy flight," *Physical Review Letters*, vol. 73, pp. 2946 – 2949, Nov 1994.

[19] D. Niyato and E. Hossain, "Spectrum trading in cognitive radio networks: A market-equilibrium-based approach," *IEEE Wireless Communications*, vol. 15, pp. 71 – 80, Dec 2008.

[20] P. Gupta and P. R. Kumar, "The capacity of wireless networks," *IEEE Transactions on Information Theory*, vol. 46, pp. 388 – 404, Mar 2000.

[21] L. L. Xie and P. R. Kumar, "A network information theory for wireless communication: scaling laws and optimal operation," *IEEE Transactions on Information Theory*, vol. 50, pp. 748 – 767, May 2004.

[22] O. Leveque and I. Telatar, "Information-theoretic upper bounds on the capacity of large extended ad hoc wireless networks," *IEEE Transactions on Information Theory*, vol. 51, pp. 858 – 865, Mar 2005.

[23] M. Grossglauser and D. Tse, "Mobility increases the capacity of ad hoc wireless networks," *IEEE/ACM Transactions on Networking*, vol. 10, pp. 477 – 486, Aug 2002.

[24] S. Jafar, "Too much mobility limits the capacity of wireless ad hoc networks," *IEEE Transactions on Information Theory*, vol. 51, pp. 3954 – 3965, Nov 2005.

[25] A. Nosratinia, T. Hunter, and A. Hedayat, "Cooperative communication in wireless networks," *IEEE Communications Magazine*, vol. 42, pp. 74 – 80, Oct 2004.

[26] J. Laneman, D. Tse, and G. Wornell, "Cooperative diversity in wireless networks: Efficient protocols and outage behavior," *IEEE Transactions on Information Theory*, vol. 50, pp. 3062 – 3080, Dec 2004.

[27] "Special issue on stochastic geometry and random graphs for the analysis and design of wireless networks," *IEEE Journal on Selected Areas in Communications*, vol. 27, Sep 2009.

[28] M. Haenggi, J. Andrews, F. Baccelli, O. Dousse, and M. Franceschetti, "Stochastic geometry and random graphs for the analysis and design of wireless networks," *IEEE Journal on Selected Areas in Communications*, vol. 27, pp. 1029 – 1046, Sep 2009.

[29] J. Mitola and G. Maguire, "Cognitive radio: making software radios more personal," *IEEE Personal Communications*, vol. 6, pp. 13 – 18, Aug 1999.

[30] E. Hossain and V. Bhargava(Eds.), *Cognitive Wireless Communication Networks*. Springer, 2007.

[31] Y. Xiao and F. Hu(Eds.), *Cognitive Radio Networks*. New York: CRC press, 2009.

[32] H. Arslan(Ed), *Cognitive Radio, Software Defined Radio, and Adaptive Wireless Systems*. Springer, 2007.

[33] "Special issue on adaptive, spectrum agile, and cognitive wireless networks," *IEEE Journal on Selected Areas in Communications*, vol. 25, Apr 2007.

[34] "Special issue on cognitive radio: Theory and applications," *IEEE Journal on Selected Areas in Communications*, vol. 26, Jan 2008.

[35] "Special issue on signal processing and networking for dynamic spectrum access," *IEEE Journal of Selected Topics in Signal Processing*, vol. 2, Feb 2008.

[36] "Special issue on cognitive radio technology," *IEEE Signal Processing Magazine*, vol. 25, Nov 2008.

[37] C. Stevenson, Z. L. G. Chouinard, W. Hu, S. Shellhammer, and W. Caldwell, "IEEE 802.22: The first cognitive radio wireless regional area network standard," *IEEE Communications Magazine*, vol. 47, pp. 130 – 138, Jan 2009.

[38] M. Sherman, A. Mody, R. Martinez, C. Rodriguez, and R.Reddy, "IEEE standards supporting cognitive radio and networks, dynamic spectrum access, and coexistence," *IEEE Communications Magazine*, vol. 46, pp. 72 – 79, Jul 2008.

[39] T. Yucek and H. Arslan, "A survey of spectrum sensing algorithms for cognitive radio applications," *IEEE Communications Surveys Tutorials*, vol. 11, pp. 116 – 130, Feb 2009.

[40] I. Akyildiz, W.-Y. Lee, M. Vuran, and S. Mohanty, "A survey on spectrum management in cognitive radio networks," *IEEE Communications Magazine*, vol. 46, pp. 40 – 48, Apr 2008.

[41] N. Shankar, C. Cordeiro, and K. Challapali, "Spectrum agile radios: utilization and sensing architectures," in *2005 First IEEE International Symposium on New Frontiers in Dynamic Spectrum Access Networks, 2005. DySPAN 2005*, pp. 160 – 169, Nov 2005.

[42] Y. Yuan, P. Bahl, R. Chandra, P. Chou, J. Ferrell, T. Moscibroda, S. Narlanka, and Y. Wu, "Knows: Cognitive radio networks over white spaces," in *2nd IEEE International Symposium on New Frontiers in Dynamic Spectrum Access Networks, 2007. DySPAN 2007*, pp. 416 – 427, Apr 2007.

[43] H. Tang, "Some physical layer issues of wide-band cognitive radio systems," in *2005 First IEEE International Symposium on New Frontiers in Dynamic Spectrum Access Networks, 2005. DySPAN 2005*, pp. 151 – 159, Nov 2005.

[44] R. Tandra and A. Sahai, "SNR walls for signal detection," *IEEE Journal of Selected Topics in Signal Processing*, vol. 2, pp. 4 – 17, Feb 2008.

[45] W. Gardner, "Exploitation of spectral redundancy in cyclostationary signals," *IEEE Signal Processing Magazine*, vol. 8, pp. 14 – 36, Apr 1991.

[46] J. Lunden, V. Koivunen, A. Huttunen, and H. V. Poor, "Spectrum sensing in cognitive radios based on multiple cyclic frequencies," in *2nd International Conference on Cognitive Radio Oriented Wireless Networks and Communications, 2007. CrownCom 2007*, pp. 37 – 43, Aug 2007.

[47] R. Tandra and A. Sahai, "Fundamental limits on detection in low snr under noise uncertainty," in *2005 International Conference on Wireless Networks, Communications and Mobile Computing*, vol. 1, pp. 464 – 469, Jun 2005.

[48] G. Ganesan and Y. Li, "Cooperative spectrum sensing in cognitive radio, part i: Two user networks, part ii: Multiuser networks," *IEEE Transactions on Wireless Communications*, vol. 6, pp. 2204 – 2222, Jun 2007.

[49] A. Ghasemi and E. Sousa, "Spectrum sensing in cognitive radio networks: the cooperation-processing tradeoff," *Wireless Communications and Mobile Computing*, vol. 7, no. 9, pp. 1049 – 1060, 2007.

[50] Z. Quan, S. Cui, H. Poor, and A. Sayed, "Collaborative wideband sensing for cognitive radios," *IEEE Signal Processing Magazine*, vol. 25, pp. 60 – 73, Nov 2008.

[51] Z. Quan, S. Cui, A. Sayed, and H. Poor, "Optimal multiband joint detection for spectrum sensing in cognitive radio networks," *IEEE Transactions on Signal Processing*, vol. 57, pp. 1128 – 1140, Mar 2009.

[52] A. Ghasemi and E. Sousa, "Spectrum sensing in cognitive radio networks: requirements, challenges and design trade-offs," *IEEE Communications Magazine*, vol. 46, pp. 32 – 39, Apr 2008.

[53] N. Devroye, P. Mitran, and V. Tarokh, "Achievable rates in cognitive radio channels," *IEEE Transactions on Information Theory*, vol. 52, pp. 1813 – 1827, May 2006.

[54] N. Devroye, M. Vu, and V. Tarokh, "Cognitive radio networks," *IEEE Signal Processing Magazine*, vol. 25, pp. 12 – 23, Nov 2008.

[55] A. Jovicic and P. Viswanath, "Cognitive radio: An information-theoretic perspective," *IEEE Transactions on Information Theory*, vol. 55, pp. 3945 – 3958, Sep 2009.

[56] I. Budiarjo, H. Nikookar, and L. Ligthart, "Cognitive radio modulation techniques," *IEEE Signal Processing Magazine*, vol. 25, pp. 24 – 34, Nov 2008.

[57] B. Farhang-Boroujeny and R. Kempter, "Multicarrier communication techniques for spectrum sensing and communication in cognitive radios," *IEEE Communications Magazine*, vol. 46, pp. 80 – 85, Apr 2008.

[58] B. Wang, Y. Wu, Z. Ji, K. Liu, and T. Clancy, "Game theoretical mechanism design methods," *IEEE Signal Processing Magazine*, vol. 25, pp. 74 – 84, Nov 2008.

[59] Z. Ji and K. Liu, "Cognitive radios for dynamic spectrum access - dynamic spectrum sharing: A game theoretical overview," *IEEE Communications Magazine*, vol. 45, pp. 88 – 94, May 2007.

[60] E. Pasandshanjani and B. Khalaj, "Primary-secondary interaction modelling in cellular cognitive radio networks: A game-theoretic approach," *IET Communications*, vol. 6, pp. 1212 – 1219, Jul 2012.

[61] L. Gao, X. Wang, Y. Xu, and Q. Zhang, "Spectrum trading in cognitive radio networks: A contract-theoretic modeling approach," *IEEE Journal on Selected Areas in Communications*, vol. 29, pp. 843 – 855, Apr 2011.

[62] L. Qian, F. Ye, L. Gao, X. Gan, T. Chu, X. Tian, X. Wang, and M. Guizani, "Spectrum trading in cognitive radio networks: An agent-based model under demand uncertainty," *IEEE Transactions on Communications*, vol. 59, pp. 3192 – 3203, Nov 2011.

[63] S. Al-Rubaye, A. Al-Dulaimi, and J. Cosmas, "Cognitive femtocell," *IEEE Vehicular Technology Magazine*, vol. 6, pp. 44 – 51, Mar 2011.

[64] A. He, K. K. Bae, T. Newman, J. Gaeddert, K. Kim, R. Menon, L. Morales-Tirado, J. Neel, Y. Zhao, J. Reed, and W. Tranter, "A survey of artificial intelligence for cognitive radios," *IEEE Transactions on Vehicular Technology*, vol. 59, pp. 1578 – 1592, May 2010.

[65] C. Nikias and M. Shao, *Signal processing with alpha-stable distributions and applications*. New York: Wiley, 1995.

[66] G. Samorodnitsky and M. S. Taqqu, *Stable Non-Gaussian Random Processes*. New York: Chapman and Hall, 1994.

[67] P. Embrechts, C. Kliippelberg, and T. Mikosch, *Modelling Extremal Events: for Insurance and Finance*. Berlin: Springer, 1997.

[68] E. Sousa, "Performance of a spread spectrum packet radio network link in a Poisson field of interferers," *IEEE Transactions on Information Theory*, vol. 38, pp. 1743 – 1754, Nov 1992.

[69] C. C. Chan and S. Hanly, "Calculating the outage probability in a CDMA network with spatial Poisson traffic," *IEEE Transactions on Vehicular Technology*, vol. 50, pp. 183 – 204, Jan 2001.

[70] X. Yang and A. Petropulu, "Co-channel interference modeling and analysis in a Poisson field of interferers in wireless communications," *IEEE Transactions on Signal Processing*, vol. 51, pp. 64 – 76, Jan 2003.

[71] S. Weber, X. Yang, J. Andrews, and G. de Veciana, "Transmission capacity of wireless ad hoc networks with outage constraints," *Information Theory, IEEE Transactions on*, vol. 51, pp. 4091 – 4102, Dec 2005.

[72] S. Weber, J. Andrews, and N. Jindal, "The effect of fading, channel inversion, and threshold scheduling on ad hoc networks," *IEEE Transactions on Information Theory*, vol. 53, pp. 4127 – 4149, Nov 2007.

[73] E. Salbaroli and A. Zanella, "Interference analysis in a Poisson field of nodes of finite area," *IEEE Transactions on Vehicular Technology*, vol. 58, pp. 1776 – 1783, May 2009.

[74] G. L. Stuber, *Principles of Mobile Communication, 2nd ed.* Boston: Kluwer, 2001.

[75] F. W. J. Olver, *Asymptotics and special functions*. New York: Academic Press, 1997.

[76] J. L. Jensen, *Saddlepoint Approximation*. Oxford: Oxford University Press, 1995.

[77] O. B. Nielsen and D. Cox, *Asymptotic Techniques for use in statistics*. New York: Chapman and Hall, 1989.

[78] M. Efgrafov, *Asymptotic Expansions and Entire Functions*. Moscow: GITTL, 1957.

[79] G. Korn and T. Korn, *Mathematical Handbook for Scientists and Engineers*. New York: Dover, 2000.

[80] H. L. V. Trees, *Optimum Array Processing*. New York: Wiley, 2002.